Packed Bed Condenser for Fresh Water Production

Study of a direct contact ocean thermal water production pilot-plant

Lieke van der Most

Delft University of Technology

TU Delft Delft University of Technology

Challenge the future

PACKED BED CONDENSER FOR FRESH WATER PRODUCTION

STUDY OF A DIRECT CONTACT OCEAN THERMAL WATER PRODUCTION PILOT-PLANT

by

Lieke van der Most

in partial fulfillment of the requirements for the degree of

Master of Science
in Sustainable Energy Technology

at the Delft University of Technology,
to be defended publicly on Tuesday April 9, 2018 at 03:00 PM.

Report number:	2890	
Student number:	4428803	
Supervisor:	Dr. Ir. C. A. Infante Ferreira	
Thesis committee:	Prof. Dr. Ir. T. J. H. Vlugt,	TU Delft
	Dr. Ir. C. A. Infante Ferreira,	TU Delft
	Dr. H. B. Eral,	TU Delft
	Ir. B. J. Kleute,	Bluerise B.V.

This thesis is confidential and cannot be made public until April 09, 2022.

TU Delft Delft University of Technology

PREFACE

This report concludes my work for Masters Degree in Sustainable Energy Technology. In this thesis a competitive new sustainable water production pilot-plant is presented. This was done through the development of two models that predict the rate of atmospheric air condensation and pressure drops in a structured packed bed condenser. The models were validated through experiments and scaled-up to simulate a pilot-plant. The research, development, experiments and writing took place in the P&E department of the 3ME faculty.

I'm thankful for the great guidance from my direct supervisor, Dr. ir. Infante Ferreira and Berend-Jan from Bluerise B.V., who I would like to thank for the learning experience and opportunity to work on such a versatile and interesting project. This project could not have been done without the work by Floris, thanks for the great cooperation in the beginning of my thesis, and for the introduction lessons to atmospheric water condensation, Ludger, for all the experimental work and Kees, for teaching me how to work with the experimental set-up.

But above all I would like to thank my family and friends: Leonie, for the good company in the office, helping me out with Aspen plus and endlessly listening to my out loud thoughts, my boyfriend Manuel, for always supporting and motivating me, Enid, for being the best at keeping my mind off work. And I'm especially grateful to Dorothé, for always being there, without her support I would have never ended up in Delft.

Lieke van der Most
Delft, March 2018

ABSTRACT

To tackle the expected increase in fresh water shortage in the world, alternative water production methods are required. One such a possible method is Ocean Thermal Water Production (OTWP). This thesis continues on the innovative concept of the use of OTEC waste water as a cooling fluid for atmospheric water production introduced in previous work [1–3].

In this thesis, an experimental study on a structured packed bed condenser column is presented. This work was carried out on an experimental OTWP set-up installed in the Process & Energy lab at the Delft University of Technology. Additionally, a numerical Python model was used to investigate the heat transfer and condensation characteristics of the packed bed column. The condenser function of the Python model was used to compare the prediction performances of different mass transfer coefficient and hydraulic correlations. The Python model simulations were compared both to the predictions of Aspen plus, an established chemical process software, and to the experimental results. The correlation by Olujić *et al.* [4] was chosen as the most suitable for the transfer rate and hydraulic behavior predictions for the Python condenser model. A mean average error in the mass transfer predictions of 2.5 % and in the hydraulic predictions of 16.9 % was reached in relation to the experiments. outperforms the Aspen plus model, that has respective mean average errors for the mass and pressure drop predictions of 9.5 % and 35.0 % for the correlation proposed by Rocha *et al.* [5]. The Python model was extended with functions that calculate the pressure drop over the remaining necessary equipment for an OTWP plant.

The aim of the developed model was to predict the processes in the OTWP condenser column and design a pilot-plant. The model was used to perform a sensitivity analysis on a large-scale column. A preliminary economic analysis identified that reducing the diameter of the condenser column reduces the cost of water production but increases the energy requirement. For an OTWP pilot-plant with a production of 25 $m^3\,day^{-1}$, the chosen column diameter of 6.6 m leads to a system energy requirement of 3.5 $kWh\,m^{-3}$ and a levelized cost of water production of 8.08 $\$\,m^{-3}$. Those production costs can be reduced by an optimization study of the full OTWP pilot-plant.

Contents

List of Tables

List of Figures

ACRONYMS

AH absolute humidity

BS-model Billet and Schultes model

DBT dry bulb temperature

DC-HDH Direct Contact Humidifier-DeHumidifier

DC-DH Direct Contact DeHumidifier

DPT dew-point temperature

DR-variable The independent variable to reach a design requirent

ED Electrodialysis

Hanley-model Hanley and Chen model

HDH Humidification-DeHumidification

HETP Height Equivalent To Plate

HEX heat exchanger

LCOWP Levelized cost of water production

MAPE mean absolute percentage error

MED Multi-Effect Distillation

MSF Multi-Stage Flash

OTEC Ocean Thermal Energy Conversion

OTWP Ocean Thermal Water Production

RBFadapt-model adapted Rocha, Bravo Fair model

RBF-model Rocha, Bravo, and Fair model

RH relative humidity

RO Reverse Osmosis

SA-variable An independent variable in the sensitivity analysis

TAG tropical air generator

WBT wet bulb temperature

GLOSSARY

Aspen plus A chemical process optimization software used for the design, operation, and optimization of safe, profitable manufacturing facilities

HETP Height Equivalent to a Theoretical Plate: In a packed fractionating column, a height of packing that makes a separation equivalent to that of a theoretical plate; used in absorption and distillation calculations

mass balance production The production that was calculated from the mass balance over the experiment.

OTEC Ocean Thermal Energy Conversion is the production of energy by using the temperature gradient in the sea to run a heat engine

OTWP Ocean Thermal fresh Water Production is the concept of producing fresh water through the condensation of hot humid air, established through cooling with cold sea water retrieved from 1000 m depth.

scale production The production that was measured by the scale of the experimental set-up, MT-01

NOMENCLATURE

Symbols

f	Friction factor	
a	Packing specific area- surface area per volume	$\mathrm{m^2\,m^{-3}}$
A	Contact area	$\mathrm{m^2}$
A	Packing specific constant (Delft model)	
A_c	Cross-sectional area of the column	$\mathrm{m^2}$
a_h	Hydraulic area (BS-model)	$\mathrm{m^2\,m^{-3}}$
B	Packing specific constant (Delft model)	
c	Molar concentration	$\mathrm{mol\,m^{-3}}$
c_0	Wallis equation fitting parameter	$\mathrm{m^{1/2}\,s^{-1/2}}$
$C_1 ... C_4$	Constants in eq. 2.5	
$c_1 ... c_5$	Correlation constants in eq. 2.73 - 2.74	
C_E	Correction factor for surface renewal RBF-model	
C_Eq	Equipment cost	\$
C_fp	Packing specific constant (BS-model)	
C_G	Packing specific constant (BS-model)	
C_h	Packing specific constant (BS-model)	
C_L	Packing specific constant (BS-model)	
c_p	Thermal capacity	$\mathrm{J\,kg^{-1}\,K^{-1}}$
C_P	Packing specific constant (BS-model)	
C_s	Density corrected superficial vapor velocity	$\mathrm{m\,s^{-1}}$
d	Diameter	m
D	Diffusion coefficient	$\mathrm{m^2\,s^{-1}}$
F_i	Installation factor	
f_L	Fractional approach to flood at constant liquid loading	
F_SE	Constant depending on packing material (RBF-model)	
F_t	Correction factor for hold-up due to a_e (RBF-model)	
g	Gravitational constant	$\mathrm{m\,s^{-2}}$
G	Gaseous mass flux	$\mathrm{kg\,m^{-2}\,s^{-1}}$
gm	Mass transfer conductance	$\mathrm{kg\,m^{-2}\,s^{-1}}$
h	Enthalpy	J
H	Height	m
k	Mass transfer coefficient	$\mathrm{m\,s^{-1}}$
K	Henry constant	$\mathrm{mol\,m^{-3}\,Pa^{-1}}$
K_1	Correlation constant (RBF-model)	
l_v	Specific latent heat of vaporization	$\mathrm{KJ\,kg^{-1}}$
L	Liquid mass flux	$\mathrm{kg\,m^{-2}\,s^{-1}}$
l_0	Generic characteristic length (depends on correlation)	m
m	Mass of component in moist air of volume V	kg
M	Molar mass	$\mathrm{kg\,mol^{-1}}$
m_0	Wallis equation fitting parameter	
$\dot{m}$	Mass flow rate	$\mathrm{kg\,s^{-1}}$
n	Equipment dependent exponent	
P	Pressure	Pa
R	Ideal gas constant	$\mathrm{kg\,kmol^{-1}\,K^{-1}}$

Symbols

RH	Relative humidity	
S	Characteristic length	m
sf	Stripping factor	
t	Time	s
T	Temperature	°C
u	Velocity	$\mathrm{m\,s^{-1}}$
U	Total convective heat transport coefficient	$\mathrm{W\,m^{-2}\,K^{-1}}$
V	Volume	$\mathrm{m^3}$
W	Width	
x	Component mole fraction in the liquid phase	
y	Component mole fraction in the vapor phase	
z	Height	m

Greek letters

α	Convective heat transfer coefficient	$\mathrm{W\,m^{-2}\,K^{-1}}$
β	Relative volatility	
χ	Fraction of flow channels ending at column wall	
δ	Film thickness	m
ϵ	Void fraction	$\mathrm{m^3\,m^{-3}}$
κ_L	Total liquid hold-up	$\mathrm{m^3\,m^{-3}}$
λ	Thermal conductivity	$\mathrm{W\,m^{-1}\,K^{-1}}$
μ	Dynamic viscosity	Pa s
$\mu_{\mathrm{L},0}$	Dynamic viscosity at 20 C	Pa s
ω	Humidity ratio	$\mathrm{kg\,kg^{-1}}$
Ω	void fraction of a_p	$\mathrm{m^2\,m^{-2}}$
π	The number of pi: 3.1416...	
ψ	Flow parameter (BS-model)	
ρ	Density	$\mathrm{kg\,m^{-3}}$
σ	Surface tension	$\mathrm{N\,m^{-1}}$
θ	Corrugation angle	deg
ν	Volume fraction	$\mathrm{m^3\,m^{-3}}$
ξ	Friction/resistance factor	
ζ	Pressure loss factor	

Subscript

a	Dry air component
bulk	In the bulk
c	Column
cg	Corrugation
cond	Condensated component
d	In dry packing
DB	Dry bulb
DC	Direction change
eq	Equivalent
e	Effective
el	Packing element
evap	Evaporated component
fp	Flooding point
fw	Fresh water
G	Gaseous component

Subscript

GD	Gas distributor
h	Hydraulic
i	Property at interface
j	Component j
L	Liquid component
lam	Laminair
LD	Liquid distributor
lp	Loading point
max	Maximum
p	Packing component
par	Particle
rv	Relative velocity
s	Superficial
sat	Property at saturation
sol	Dissolution
sw	Sea water
t	Total
turb	Turbulent
v	Water vapor component
w	Wetted
W	Water component
wall	At the column wall
WB	Wet bulb

Dimensionless	*numbers*	
Bo	$= \frac{\rho_L d_e^2 g}{\sigma}$	Bond number
Fr_L	$= \frac{u_L}{l_0 g}$	Froude number for liquid
Gr	$= \frac{g l_0^3 \left((\rho_G(T_G) - \rho_G(T_L) \right) / \rho_G}{(\mu_G / \rho_G)}$	Grashoff number
G_z	$= Re_L Sc_L \frac{\delta \sin\gamma}{H_{el}}$	Graetz number
K_a	$= \frac{\sigma^3 \rho_L}{\mu_L^4 g}$	Kapitza number
Nu_G	$= \frac{U_G l_0}{\lambda_G}$	Nusselt gas number
Nu_L	$= \frac{U_L l_0}{\lambda_L}$	Nusselt gas number
Pr_G	$= \frac{cp,_G \mu_G}{\lambda_G}$	Prandtl gas number
Pr_L	$= \frac{cp,_L \mu_L}{\lambda_L}$	Prandtl liquid number
Re_L	$= \frac{l_0 u_L \rho_L}{\mu_L}$	Reynolds number for liquid
Re_G	$= \frac{l_0 u_G \rho_G}{\mu_G}$	Reynolds number for gas
Sc_G	$= \frac{\mu_G}{\rho_G D_G}$	Schmidt gas number
Sc_L	$= \frac{\mu_L}{\rho_L D_L}$	Schmidt liquid number
Sh_G	$= k_G \frac{l_0}{D_G}$	Sherwood gas number
Sh_L	$= k_L \frac{l_0}{D_L}$	Sherwood liquid number
WeL	$= \frac{u_L^2 \rho_L l_0}{\sigma g_e}$	Weber number for liquid

1

INTRODUCTION

In many parts of the world, the presence of fresh water is not self-evident, and must either be found or developed. These regions are becoming more widespread, and fresh water scarcity is predicted to rise in the future. There are multiple factors contributing to this increase, including population growth, rise in water demand and climate change [12]. This leads to the conclusion that, to meet the growth in demand, new sources of fresh water must be developed.

Ocean Thermal Water Production (OTWP), is the concept of producing fresh water through the condensation of hot humid air, established through cooling with cold sea water retrieved from 1000 m depth. The conceptual production process runs in connection with an Ocean Thermal Energy Conversion (OTEC), by reusing the cold deep-sea water retrieved for the energy production. This multi-use of service fluid allows for a reduction in production costs. Bluerise B.V. is developing a pilot-plant with a fresh water production of 25 $m^3\,day^{-1}$ in the Caribbean.

Previous works by Van der Drift [1] and Lopez [2] showed that a Direct Contact DeHumidifier (DCDH), consisting of a packed bed and an external heat exchanger would be the most profitable set-up for this pilot-plant. The development of a production plant of that magnitude asks for a numerical model that holds under up-scaling. The formulation of mass and heat transfer in packed bed columns has been described by numerous researchers. Unfortunately, those transfers are usually designed based on coefficients calculated with an empirical approach, resulting in unproven designs when applied outside of the experimental database [13]. Based on the work by Lopez [2] and Van der Drift [1], Noordhoek Hegt [3] has constructed a numerical model in Python for Bluerise B.V..

Bluerise B.V. has developed an experimental OTWP set-up at the Process & Energy department of Delft University of Technology to validate the numerical model. The packed bed condenser column in this set-up is equipped with random packing. However, the current numerical model does not give an accurate prediction of the production and pressure drop. It has not been validated for structured packings and is not designed for system optimization. Structured packing is more suitable for the 25 $m^3\,day^{-1}$ model, since it shows improved hydraulic behavior [14].

The conjecture of this work is that a validated numerical packed bed column modeled in Aspen plus will allow for both up-scaling and variation to structured packings. It can be used as an affir-

mation for a Python model on larger scale simulations, and function as a column design tool. In this chapter the general notion of OTWP is introduced, followed by the most relevant related work, and an outline of the objectives and the approach of this thesis.

1.1. OCEAN THERMAL WATER PRODUCTION

Ocean Thermal Water Production (OTWP) can be considered a type of desalination. Desalination is a widespread technique used in areas where fresh water is not available. Seawater, the feed water source for the majority of desalination facilities, offers a large water supply that is constantly available, and thus very attractive [12, 15].

State of the art desalination techniques are offer a wide variety, with most commonly thermal (distillation and evaporation) and membrane desalination. Thermal desalination is done in single or dual-purpose power plants and requires substantial amounts of heat. Membrane desalination techniques ask for energy in the form of pressure difference. In both cases, energy is most often provided by unsustainable fuels [12].

The application of membrane techniques is more expensive than conventional water production [12]. Because of the high cost and non-sustainability of the process, it is worth considering the development of non-traditional techniques. These should be cost-effective and scalable to reach a large number of people. One of those techniques is the OTWP.

Figure 1.1 shows a dual-purpose fresh water production plant proposed by Bluerise B.V., designed for the Caribbean, that allows for a sustainable desalination process. The proposed plants' main purpose is the generation of energy, Ocean Thermal Energy Conversion (OTEC), with a side production of fresh water, OTWP. The closed heat cycle in the OTEC process is a reversed refrigeration process, and requires a minimum temperature difference of 20 °C, this temperature difference can be observed in tropical regions [1]. Surface water in the Caribbean is around 25 °C, meaning the cold sea water has to be at least 5 °C and thus retrieved from a depth of around 1000 m.

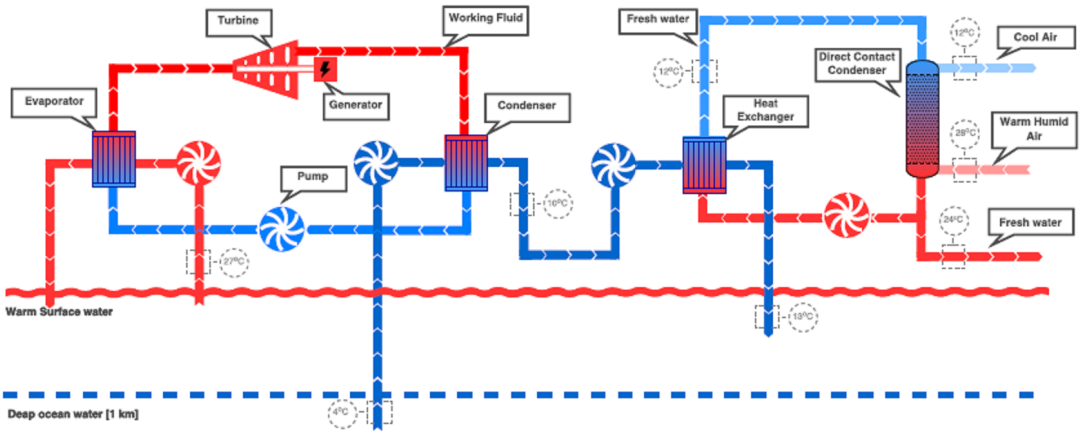

Figure 1.1: The OTEC and OTWP cycle proposed by Bluerise B.V., retrieved from Lopez [2].

Figure 1.1 shows that the cold seawater is led to a heat exchanger that condenses ammonia in the OTEC heat cycle. The water flow that leaves the ammonia condenser has a temperature of around 12 °C [2] [3]. This is still significantly lower than the surrounding air temperature in the Caribbean of

28 °C. Getting the cold sea water to the surface is an energy intensive process and it is thus desirable to exploit this unused temperature gradient.

This thesis aims to utilize the waste heat of the OTEC plant by designing a packed bed condenser column that produces fresh water from atmospheric air through cooling it with the 12 °C seawater. The Caribbean experiences a constant relative humidity (RH) throughout the year of 80 %. Van der Drift [1] assessed various dehumidification methods and selected direct-contact condensation as the most cost effective. Thereafter Lopez [2] explored various direct contact condensation methods and concluded that packed bed columns were the most appropriate method for the contact between water and air in the OTWP system. Figure 1.1 shows that the proposed system has a freshwater cycle that is cooled with the cold seawater. This cooled fresh water is fed to the top of the packed bed column where it is distributed over the content of the column. The hot and humid Caribbean air is fed to the bottom of the column, consequently being cooled by the fresh water, achieving condensation of atmospheric water vapor.

1.2. RELATED WORK

This section describes supporting technologies and research for the present work. It discusses previous work done in cooperation with the Delft University of Technology and Bluerise B.V., related work on similar desalination techniques, how it differs from the current work, and gives examples of packed bed models in Aspen plus.

1.2.1. PREVIOUS WORK

VAN DER DRIFT

Van der Drift [1] made a techno-economic assessment of atmospheric water extraction with deep ocean water for her master thesis research. She performed a technical and economical feasibility study of a direct contact dehumidifier for a 5 $m^3\,day^{-1}$ fresh water production plant. She compared three different dehumidification methods and selected direct contact dehumidification as the most cost effective. With this method she reaches an auxiliary energy requirement of less than 2 $kWh\,m^{-3}$. It should be mentioned that an inlet fresh water temperature of 10 °C is used. Furthermore, her research shows that for a lifetime of 20 years for the process plant, and 10 years for the packing, the water cost will be 4.31 $\$\,m^{-3}$. Her research shows that the heat exchanger will have a significant impact on the performance and component cost of the system. Simultaneously to Van der Drift [1], Lie *et al.* [16] described in the bachelor thesis work a differential control volume model on evaporation and condensation of humid air in a packed bed based on Li *et al.* [17] and Onda *et al.* [18]. This model was used in Van der Drift's analysis.

LOPEZ

Lopez [2] continued this work by developing an OTWP system based on the selected direct contact condenser for her master thesis. She compared different methods of direct contact condensation and selected the 16 mm Pall ring packed bed as most suitable for the experimental set-up. She improved the existing numerical model of the system by creating a Python model that is based on Li *et al.* [17] and uses the Maćkowiak correlations [19] for the mass transfer coefficients. The Python model was

used to compare different packing types and column diameters and make a design proposition. With the selected packing (Montz Pak B2-500Y) and a column diameter of 3 m, the system reached an energy consumption of 0.477 kWh m^{-3}, and a water cost of 5.569 \$ m^{-3} for a production of 25 m^3 day^{-1}.

It should be noted that this design study was done with a model that was incomplete and not yet validated.

NOORDHOEK HEGT

Simultaneous to current work, Noordhoek Hegt [3] has improved and expanded on the theoretical background of the Python model for random packing and validated it with experiments. He examined three different direct contact mass transfer correlations (Billet and Schultes [13], Onda *et al.* [18], Mackowiak [19]) and compared their performance with experimental data. He concluded that the correlations of Billet and Schultes [13] and Mackowiak [19] both provide a relative good profile of the heat transfer in the column, deviations stay within 20 %. However, the pressure drop and the mass transfer (production), two very important parameters in deciding on the feasibility of the OTWP system, showed significant deviations from the experimental data. Furthermore, the experiments showed much larger than expected pressure drop over the packing. It is therefore advised to select a new type of packing.

Current work will expand on previous work by adapting the theory behind the model and extending it to fit structured packing. The following assumptions that were used in previous model are dismissed:

- Inside the column, the bulk air is humidified to 100 % RH before condensation occurs.
- Once the RH in the column reaches unity, the water vapor saturation pressure (driving force) corresponds to the bulk humid air temperature, and not the interphase temperature.
- The heat transfer between the packing and the humid air can be represented by the overall heat transfer coefficient between the humid air and water, which is calculated in analogy to the mass transfer coefficient correlations.

.

1.2.2. RELATED TECHNOLOGIES

To understand why the development of this new technology is valuable it is important to examine related work. Currently conventional, and thus competitive, desalination techniques are: Multi-Stage Flash (MSF), Multi-Effect Distillation (MED), Reverse Osmosis (RO) and Electrodialysis (ED). Based on the 2012 report about desalination with the use of renewable energy, published by the International Energy Agency [20], table 1.1 gives an overview of some of the key data for those technologies.

There are possibilities to make the conventional processes more sustainable: thermal processes can be powered by waste or by-product heat, and electricity by renewables (such as photovoltaics, wind-energy, solar thermal or geothermal). However, the development of new, alternative technologies that are more efficient is required to keep up with the increase in demand. A closer look at the market share shows that only a very small percentage, 0.3 %, is taken up by alternative technologies. One of those alternative technologies is Humidification-DeHumidification (HDH).

Table 1.1: Conventional desalination techniques

		MSF	MED	RO[1]	ED
Type of process		Thermal	Thermal	Membrane	Membrane
Electricity demand	$kWh\,m^{-3}$	2.5-5.0	1.5-2.5	3.5-5.0	1.5-4.0[2]
Thermal energy demand	$kWh\,m^{-3}$	80.6	80.6		
Cost in Curaçao	$\$\,m^{-3}$			7.21[3]	
Market share	%	27	8	60	1
Average plant capacity	$m^3\,day^{-1}$		4.000-5.000		

[1] For spiral wound reverse osmosis [2] For feed water with 1500-3500 ppm solids
[3] retrieved from Lopez [2]

HUMIDIFICATION-DEHUMIDIFICATION

Figure 1.2a shows the regular HDH process. In the process (atmospheric) air is used as a carrier gas for water. It is first heated and humidified until saturation and then cooled down with sea water, resulting in condensation and thus fresh water production. In section 2.1 the theoretical background of this process is discussed.

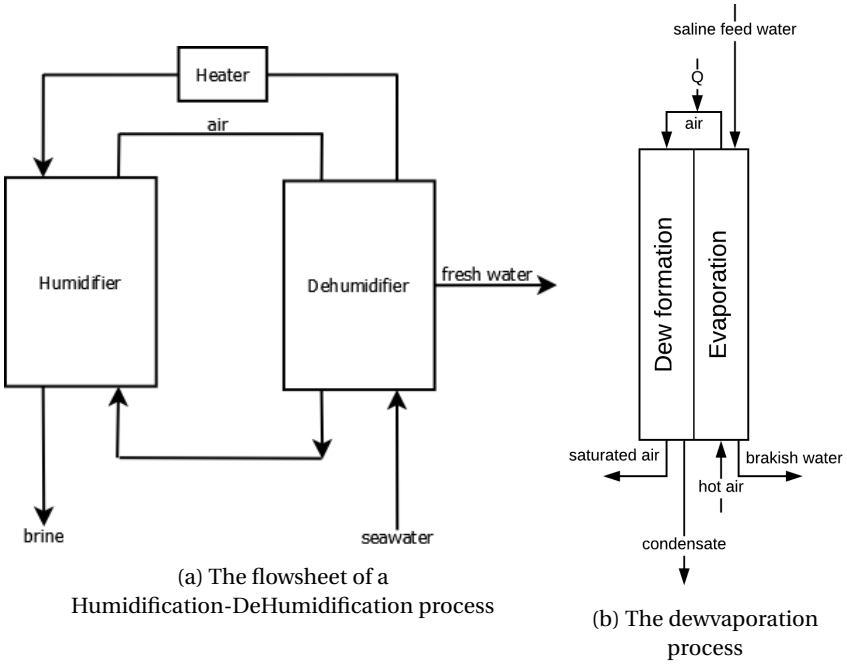

(a) The flowsheet of a Humidification-DeHumidification process

(b) The dewvaporation process

Figure 1.2: Dual and single column Humidification-DeHumidification processes

The use of Humidification-DeHumidification in desalination is not new. Numerous research studies have been performed to study the HDH method, including many efforts to change the energy source of the heater in this process from fossil fuel to renewable ones such as solar [21] and geothermal [22]. The seawater that is used to cool down the air is often surface seawater (around 25 °C in the Caribbean).

The OTWP system that is the topic of this work tries to minimize the energy requirement by cutting out the energy intensive humidification process. Because the system is being developed for locations around the Caribbean, the atmospheric air is already at high temperatures and high humidity, the use

of 12 °C cooling water should still give a sufficient temperature difference for condensation. Although the method of HDH is different, it is valuable to look at past studies, since, like current work, they study the performance evaluation and efficiency improvement [23].

Bourouni *et al.* [24] researched state of the art HDH techniques and mention that current studies are mainly focused on the use of solar and recovery of latent heat from condensation. They mention that, although the coupling of HDH units with solar collectors is very interesting, currently the costs are relatively high. This is caused by the large sums of investment in solar collector that are needed to heat the water stream. Additionally, for continuous operation of such a unit, a heat storage system is required [23]. In connected research, Bourouni *et al.* [22] showed, with an experimental set-up, that by using a geothermal heat source, the cost of water could be reduced to 1.2 $\$\,m^{-3}$, for the lifetime of 10 years. It should be noted that their work shows that the desalination is only competitive when the energy used is less expensive then the capital costs. In that same year Müller-Holst *et al.* [25] described the performance of an optimized HDH system that is connected to a solar collector. Under optimized conditions they estimate a production cost of 13.35 $\$\,m^{-3}$.

In a more recent study, Ahmed *et al.* [26] built a HDH desalination unit to investigate the use of a corrugated aluminum sheeted packing in the humidifier. They use a finned tube condenser as a dehumidifier. They note that the inlet air temperature only has small effect on the productivity of the unit compared to the inlet water temperature of the humidifier. According to their cost analysis, a cost of 10 $\$\,m^{-3}$ is achieved, based on a lifetime of 10 years.

Eslamimanesh and Hatamipour [21] mathematically modeled a HDH system and performed an economic study on it to estimate the benefits. They conclude that HDH is mainly an appropriate choice when costs are not of much interest, or renewable energies are available. Additionally, they conclude that fouling would increase the water production cost with minimal 5 %. They found a specific energy consumption of 40 $kWh\,m^{-3}$ for a system that produces 1.7 $m^3\,day^{-1}$ of fresh water. With the energy cost in Curaçao of 0.27 $\$\,kWh^{-1}$ (based on Aqualectra industrial standard prices of July 2017), this results in a water cost of 10.8 $\$\,m^{-3}$. This is for a system that utilizes natural gas as an energy source. As the capacity of the plant increases, the water production cost decreases. Table 1.2 gives an overview of the cost estimations that have been presented in this section. It shows that the costs for the water production system with the geothermal heat source are estimated significantly lower than the other heat sources.

Table 1.2: Published cost of the HDH process

Heat source	Lifetime	Cost
Geothermal	10 years	1.2 $\$\,m^{-3}$
Solar collector	-	13.35 $\$\,m^{-3}$
Electric heater	10 years	10 $\$\,m^{-3}$
Natural gas	-	10.8 $\$\,m^{-3}$ (only OPEX)

Single Column systems Eslamimanesh and Hatamipour [21] suggested that one of the causes of cost increase in the HDH system compared to other desalination techniques is the energy loss in a system with two separate columns. Some studies have been done on the HDH process in a single column. Hamieh and Beckman [27] use, as described in Beckman [28] a single continuous contacting tower for a process called dewvaporation. Figure 1.2b shows that hot air is fed to the bottom of the

column, on the evaporation side. Saline feed water is fed to the top of the tower, on the evaporation side. The hotter humid air that comes out is fed back into the top of the tower on the dew formation side. The heat needed for evaporation is supplied by heat released from dew condensation.

Based on this, Xiong *et al.* [29] did an experimental investigation of a shell and tube column in which Humidification and Dehumidification are performed simultaneously. The experiment examined the effects of parameters and did not include an efficiency or cost analyses.

COOLING TOWERS

Cooling towers are widely used in industry for cooling circulating water [30]. A cooling tower is essentially the same as the fresh water condenser, except that there is a negative feed temperature difference (the water feed is hotter than the air feed). In these cooling towers the ratio of gas to liquid mass flow rate is one of the main factors effecting the cooling rate in the column [30, 31]. Ramkumar and Ragupathy [31] showed with a study on experimental performance analysis and optimization with the Taguchi method that packing has the most dominant effect on total performance variation of cooling towers, followed by liquid to gas flow ratio and inlet air temperature. Qi *et al.* [30] analyzed the performance of an empty cooling tower for applications in which, due to salt deposition on the packing, the use of tower packing is not practical. They mention many advantages in comparison to the packed bed towers, such as longer lifetime, lower pressure drops and a longer duration of heat transfer.

1.2.3. ASPEN PLUS

Aspen plus [32] is a chemical process optimization software that allows for the design of columns. This process simulator provides several built-in model blocks that can be directly applied in process simulation. The problem with modeling a cooling water network such as the OTWP with a process simulator as Aspen plus, is that there is no standard for setting up the cooling tower block [33]. Numerous investigators such as Sadeghifar and Sadeghifar [34], Ramzan *et al.* [35], Thiels *et al.* [36], describe the use of Aspen plus in modeling packed bed columns.

HYDRAULIC CALCULATIONS

Spiegel and Duss [37] mention that Aspen plus contains built-in proprietary hydraulic correlations from, for example, Sulzer and Koch-Glitsch. These are empirical correlations that are considered reliable because the are designed for specific packing types. Beside the vendors correlations, Aspen plus holds a selection of generic pressure drop correlations, developed specifically for packed beds.

MASS TRANSFER CORRELATIONS

Aspen plus mostly uses the the well-known Onda correlation [18] for the modeling of mass transfer in random packing [34]. Although it is a widely trusted correlation, Sadeghifar and Sadeghifar [34] argue that the Onda method tends to overestimate the vapor mass transfer coefficient. It uses the interphase area estimation and deals directly with flux rather than rate quantities. Table 1.3 gives two examples of packed bed models in Aspen plus and specify the correlations they use for coefficient calculations.

Hanley and Chen [41] reviewed the performance of several packed bed column mass-transfer and interphase area correlations found in Aspen Technology's 'Aspen Rates Based Distillation component'. They stress the importance of the Height Equivalent To Plate (HETP), a packing efficiency measurement that is further explained in section 2.3.1. It ties the equilibrium stages performance expression to

Table 1.3: Packed beds in Aspen plus

Source	Type of packed bed	Coefficient	Correlations
Sadeghifar and Sadeghifar [34]	Randomly packed columns	The entire Mass transfer correlation method	Onda *et al.* [18]
		The entire Mass transfer correlation method	Bravo and Fair [38]
Ramzan *et al.* [35]	Randomly packed column	Liquid holdups - random packing	Stichlmair *et al.* [39]
		Liquid hold-ups - wire-gauze structured packing	Rocha *et al.* [40]

the rate-based differential expression of performance. Their experiments show that the random packing correlations used in Aspen plus, give a 20 % or more deviation in two-thirds of the tested packings, and about 40 % of the structured packings show deviations outside of those limits. This led to the development of new correlations that are now implemented in Aspen plus. Table 1.4 gives an overview of the available correlations for packings in Aspen plus.

Table 1.4: Packed bed correlations in Aspen plus

Type of packed bed	Correlations
random packings	Onda *et al.* [18]
	Bravo and Fair [38]
	Billet and Schultes [42]
	Hanley and Chen [41]
wire gauze structured packings	Bravo, Rocha and Fair (1985)
sheet metal structured packings	Rocha *et al.* [40]
	Hanley and Chen [41]
	Billet and Schultes [42]
	Hanley and Chen [41]

1.3. OBJECTIVES

The main objective of this research is to select (and validate) the most suitable packings and properties for an OTWP plant with a fresh water production of 25 $m^3\,day^{-1}$ in the Caribbean. The production plant should be competitive with current desalination techniques. More specifically, the aim is to stay below an energy consumption of 3.5 $kWh\,m^{-3}$.

To support this main objective, the following topics should be examined.

- What physical phenomena occur in the packed bed section of the condenser column?
- How does an Aspen plus model represent those phenomena in a randomly packed bed column?
- What structured packing would be most appropriate for the experimental set-up, based on the Aspen plus model?
- How does an Aspen plus model represent the transfer phenomena and hydraulics in a structured packed bed column, and how does this compare to the Bluerise B.V. Python model?
- What column design would be appropriate for the 25 $m^3\,day^{-1}$ production pilot-plant?

1.4. APPROACH

An Aspen plus model is constructed, validated and used to select a structured packing for the experimental set-up. Previous work by Van der Drift [1], Noordhoek Hegt [3], and Lopez [2] resulted in a numerical Python model that described the physical phenomena that occur in the randomly packed bed condenser column, and an experimental set-up to validate this model. The theory that was adopted in the Python model is evaluated and improved based on analysis performed with the Aspen plus model. The numerical model is then expanded with new mass transfer correlations to predict performance of structured packings.

Experiments are performed on the newly selected structured packing to validate both the Python and the Aspen plus model. The models are fitted with the best performing correlations and their predictions for large-scale condenser columns are compared. The Python model is used to make a technical and economic analyses of the 25 $m^3\,day^{-1}$ Ocean Thermal Water Production pilot-plant.

2

THEORETICAL BACKGROUND

The focus of the present work is the design of a condenser through the validation of the correlations used to define the heat- and and mass transfer coefficients of the packed bed column in the Ocean Thermal Water Production (OTWP) plant designed by Bluerise B.V.. Before turning to the development of the models and the presentation of the column design we first discuss the necessary background and theory.

The following theoretical background is described in this chapter:

- The thermodynamics of atmospheric air
- The theory and terminology of packed bed columns
- The physical phenomena that take place in the column
- The different mass transfer coefficient correlations that are used in the models
- The corresponding two phase hydraulic models

Throughout this chapter the subscripts L and G represent the liquid an gas properties respectively.

2.1. PSYCHROMETRICS

Psychrometrics is the description of atmospheric thermodynamics. Our atmosphere basically consists of two components: dry air and water. In this work we will refer to the system of water vapor and dry air as "humid air". There are numerous ways to describe the amount of water vapor in humid air. We define the humidity ratio, ω, the absolute humidity, AH, and the relative humidity, RH, as,

$$\omega = \frac{m_\mathrm{v}}{m_\mathrm{a}} \tag{2.1}$$

$$AH = \frac{m_\mathrm{v}}{m} \tag{2.2}$$

$$RH = \frac{m_\mathrm{v}}{m_\mathrm{v}^{sat}} \approx \frac{\omega}{\omega^{sat}} \tag{2.3}$$

Where m is mass in humid air of volume V, the subscripts a and v represent the properties of dry air and water vapor respectively, and sat denotes the property at saturation. $m = m_\mathrm{a} + m_\mathrm{v}$ is the total mass of the mixture.

It can be shown how the humidity ratio and the RH relate by applying the ideal gas law. Since we apply the ideal gas law and thus $\rho_v = P_v M_v/(RT)$ and $\rho_a = P_a M_a/(RT)$ it follows from equation 2.1 that,

$$\omega = \frac{m_v}{m_a} = \frac{0.662 P_v(T)}{P - P_v(T)} = \frac{0.662 RH * P_v^{sat}(T)}{P - RH * P_v^{sat}(T)} \tag{2.4}$$

Where P_v^{sat} is the water vapor saturation pressure, ρ is density, M the molar mass, T is temperature and R the ideal gas constant. The saturation pressure is temperature dependent, and can be empirically represented by the Arden Buck correlation:

$$P_v^{sat}(T) = C_1 \exp(C_2 T - C_3 T^2 + C_4 T^3) \tag{2.5}$$

Here C_1 to C_4 are empirically fitted constants, that are applicable in a temperature range of −80 to 50 °C (table 2.1). It should be noted that equation 2.5 gives the pressure in kPa. For atmospheric air it is most common to express the amount of vapor with a relative humidity. In Curaçao the RH shows little fluctuation and is around 80 % [1].

Table 2.1: Arden Buck constants

C_1	0.61121
C_2	18.678
C_3	234.5
C_4	257.14

The Mollier diagram, displayed in figure 2.1, is a visual equation of state and an alternative display of the psychrometric chart. It is a graph of the thermodynamic properties of moist air and depicts the following parameters: dry bulb temperature (DBT), wet bulb temperature (WBT), dew-point temperature (DPT), relative humidity (RH), humidity ratio, specific enthalpy and the specific volume. Humid air is a single-phase two-components system, that allows for all parameters to be determined if any two are known under constant pressure [43].

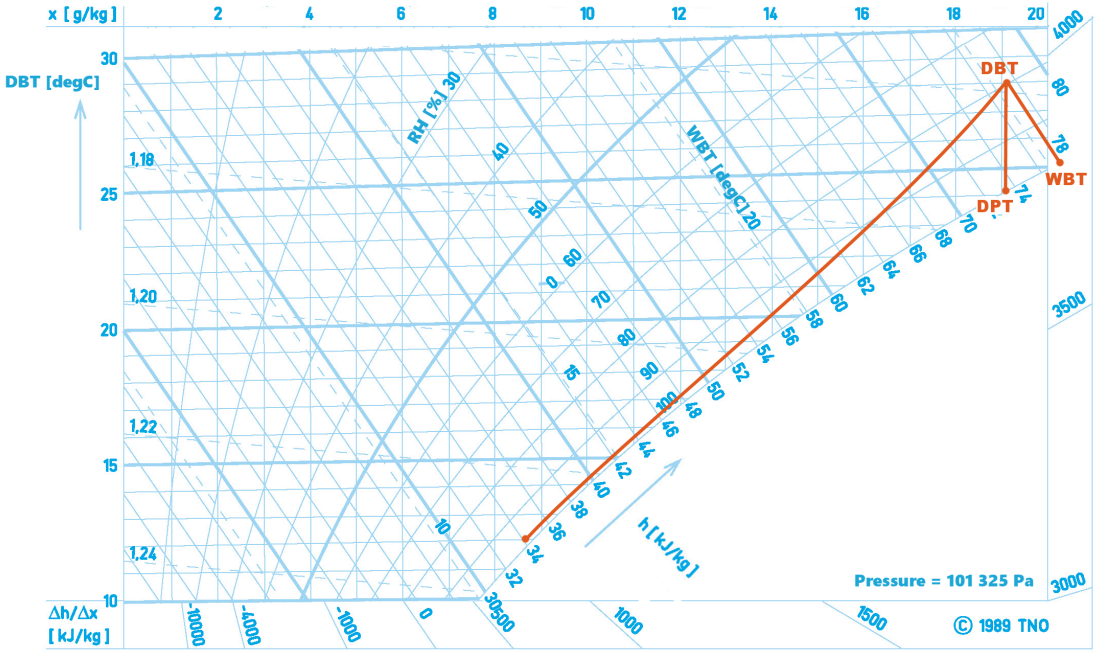

Figure 2.1: Mollier diagram showing the process of the OTWP pilot-plant

2.1.1. TEMPERATURES

The psychrometric chart presented in figure 2.1 depicts three different temperatures: the dry bulb temperature (DBT), the wet bulb temperature (WBT) and the dew-point temperature (DPT). The DBT is the temperature that is measured by a regular (dry) thermometer. It is the temperature, T, of an unsaturated humid air and liquid water system, or in other words the temperature of air at a given humidity.

The WBT is the temperature of adiabatic saturation. It is measured with a wet thermometer bulb: Air that comes in contact with the wet thermometer absorbs some water and gives off some heat, reducing the air temperature to the WBT, it is the temperature reached when humid air is cooled adiabatically until saturation ($m_v = m_{v,s}$). The cooling down of the humid air can happen in two ways: adiabatic / evaporative cooling and regular cooling. Indirect evaporative cooling is a form of adiabatic cooling where the humid air is cooled because of the phase transition from water in the humid air. The specific evaporation energy is the energy that is needed to pass the phase transition. Water can evaporate at much lower temperatures than its boiling point by using energy of the environment for its phase change. The thermal energy needed to evaporate the water, or the specific latent heat, is taken from the hot humid air, cooling it. It means the air is cooled without energy loss or gain.

Equation 2.6 shows how the WBT is related to the DBT:

$$T_{WB} = T_{DB} + \frac{l_v}{c_{p_a}}\omega - \frac{l_v}{c_{p_a}}\omega^{sat}(T_{WB}) \tag{2.6}$$

where l_v is the specific latent heat of vaporization and is dependent on temperature, $\omega^{sat}(T_{WB})$ is the saturation humidity ratio at the wet bulb temperature and c_{p_a} is the thermal capacity of the dry air. In this definition it is assumed, because for temperatures in the ranges of meteorological interest they vary insignificantly, that l_v and c_{p_a} are independent of temperature.

This evaporation in direct contact would only take place if the interface temperature is equal to, or higher than, the DPT. Figure 2.1 shows that for incoming air with a temperature of 28 °C and a relative humidity of 80 %, for evaporation to take place, the interface temperature would have to be higher than 24 °C.

2.1.2. CONDENSATION

The basis of fresh water production through humid air condensation is the ability of air to hold significant quantities of vapor. This ability increases with rising (dry bulk) temperatures of air [24]. Atmospheric water vapor only condenses when air reaches saturation (RH = 100 %). For condensation to happen at temperatures below the saturation point, solid surfaces must be present. Then, air can be saturated at the interface, resulting in condensation. Spontaneous condensation in the absence of surfaces (or nuclei) needs supersaturation (extremely high relative humidities). One way to increase the available surface is in a packed bed column.

2.2. PACKED BED COLUMNS

A packed bed column is a commonly used piece of equipment in the chemical industries, designed to improve contact between two phases, increasing heat and/or mass transfer. Essentially, it is a hollow

vessel that is filled with a packing material. This material can either be randomly distributed small objects, called a random packing, or a specifically arranged or stacked packing, called a structured packing.

A possible application of a packed bed column is direct contact condensation: the condensation through direct-contact between the two phases, such as the mass transfer of water between the liquid fresh water stream and the humid air. In previous work done by Van der Drift [1] and Lopez [2] for Bluerise B.V., the direct-contact condensation in a counter-current flow through a packed bed was selected as the most suitable for the OTWP process.

2.2.1. WORKING PRINCIPLE

Figure 2.2 depicts the packed bed column with a fresh water and humid air feed.

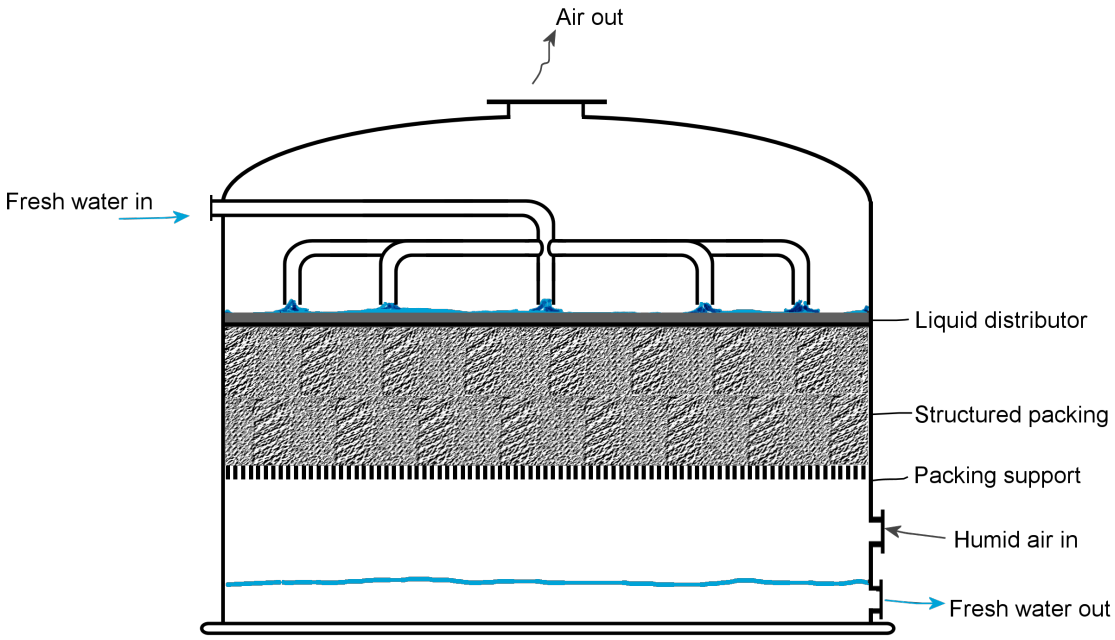

Figure 2.2: A packed Ocean Thermal Water Production column

A very common, and more researched, application of such a column is a cooling tower. In cooling (or evaporative) towers, the cooling power is obtained by the evaporation of a quantity of the process water. Because in cooling towers the process water and air are in direct contact with each other, the cooling tower performance, while cooling a given quantity of water, is only influenced by the wet bulb temperature. In condensation towers heat transfer between water and air takes place, as in evaporative towers, mainly through mass transfer. That quantity of heat that is transferred from water to air is much higher than by conduction and convection [44].

Mass is transferred between water and humid air through diffusion. The concentration gradient between the phases is the driving force for the mass transfer. According to Fick's law, the steady state of mass transfer between the two phases can be described with the mass transfer coefficient,

$$\dot{m}_j = kA\Delta\rho_j \tag{2.7}$$

Where k is the mass transfer coefficient, and $\dot{m}_j$ is the mass transfer of component j per surface area A. For the packed bed column, the gradient of evaporation, $\partial \dot{m}_{v,evap}/\partial z$, could then be expressed as,

$$\frac{\partial \dot{m}_{v,evap}}{\partial z} = kA_c\left[\rho_v(T_G) - \rho_v^{sat}(T_i)\right]a_e \tag{2.8}$$

Where a_e is the effective interface surface area in $m^2\,m^{-3}$, A_c is the cross-sectional surface area of the column and $\rho_v(T_G)$ and $\rho_{v,s}(T_i)$ the water vapor density at the gas phase temperature and the saturated water vapor density at the interface temperature respectively. This shows the driving force behind the mass transfer and thus the working principle of the columns. The density differences between the bulk at the dry air temperature and the saturation density at the interface temperature determine the velocity at which the vapor molecules diffuse.

2.2.2. COLUMN INTERNALS

Figure 2.2 shows an example of what a packed bed column looks like on the inside. The main components that contribute to the efficiency and hydraulic characteristic of the columns are described below. The main internal that this work covers is the packing, although the other internals are as important for optimum column performance [45].

DISTRIBUTORS

A uniform distribution of the two phases is important to ensure maximum driving force. Additionally, the equations that are used to determine the performance characteristics (mass transfer rate and pressure drops) are not reliable in case of maldistribution. Columns often perform at conditions of maldistribution; one possibility of its reduction is the implementation of phase distributors.

Liquid distributor The initial liquid distribution over the columns cross section strongly defines the efficiency of the packed bed. Therefore, their selection is important for the effective column operation [8]. In the VISION 2020, 2000 Separations Roadmap published by AIChE in cooperation with the U.S. Department of Energy [46] the liquid distribution in packed beds is categorized as inadequate and mentioned as a key technical barrier of distillation.

Liquid distributors are characterized in two types: single stream and spray distributors. The single stream distributors distribute the liquid phase in single streams, that are uniformly positioned over the column cross section. Determining the necessary number of irrigation points and the manner of their location is very important [47]. The spray or nozzle distributors are small and therefore do not create additional resistance to gas flow. This type of liquid distribution can be applied to columns with a diameter until 2.5 m [47]. Appendix A gives an overview of the application areas of the liquid distributors as they are listed by Kolev [8]. Spray distributors are preferred in cooling towers since they produce drops and thus a larger surface area for heat exchange. The differential pressure over the spray nozzles is usually around 3 bar [8].

Gas distributor The initial gas flow under the packing will be irregular, due to initial forces and slow dissipation. Until recently, it was presumed that the gas velocity profile in a packed bed quickly becomes uniform because of layer pressure drop. This statement applies only to packings with small

voidage. Modern structured packings have high free volume, but because of their low pressure drop they have poor gas distribution abilities and require special precautions. Placing the gas inlet at a distance of $(0.15-0.18)*d_c$, with d_c the column diameter, from the packing layer significantly improves gas distribution [47]. Furthermore, special cross-section devices are developed to reduce the irregularity of the gas distribution.

One principle is the use of multivane triangular diffusers such as the 'Schoepentoeter'. Figure 2.3a shows this device, which is specifically designed to create an even gas distribution across the column cross section, while maintaining low pressure drops. A device such as the 'Schoepentoeter' is technically designed to improve the gas flow but comes with considerable investment cost. Three lower cost, but surprisingly well performing devices are an orifice baffle (in a column with d_c =3.5 m [48]), a bend inlet (in a column with d_c =1 m [49]) and feeding the gas by a pipe with slit or perforation at the bottom, as presented in figure 2.3b.

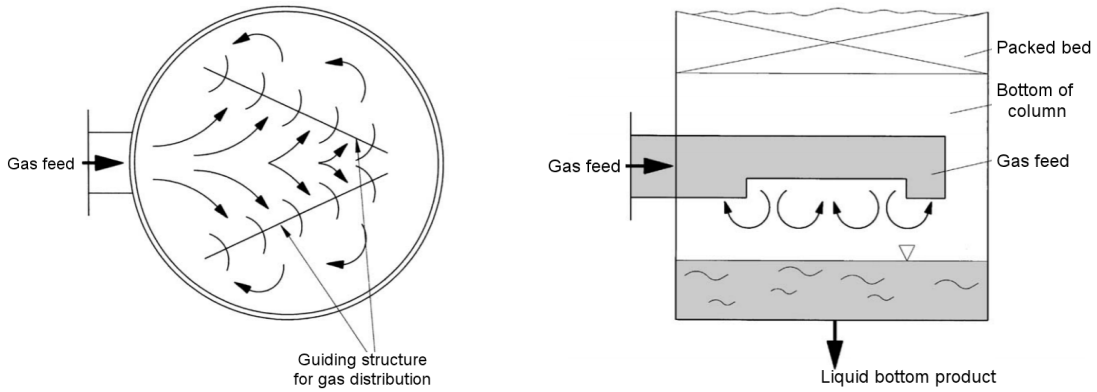

(a) The 'Schoepentoeter' gas distributor

(b) Gas feed with slit at the bottom

Figure 2.3: Two different types of gas distributors

PACKINGS

There are different types of packing available to fill a column. The optimal solution for a column will be determined by economic considerations. There are two main types of packing: random and structured. Random packings are significantly cheaper, since they don't have to be fitted and produced per column, but structured packings show a significantly better performance (lower pressure drop per mass transfer efficiency) and a lower necessary packing height. It is common for processes that operate under atmospheric pressure, to be fitted with random packing, since the price of the column vessel is not high (compared to high pressure operations) and this makes the volume of the packing less important [8].

Random A random packing consists of elements of the same form, that are dumped in a column on top of a grid. Random column packing types are typically described by the diameter of one single packing element and are available in sizes from 10-100 mm. Larger diameter packings have significantly lower efficiency, but as an advantage they have very low pressure drop and high operating range, similar to that of structured packings. To neglect the wall effects in the packed bed, as a rule of thumb the packing size should at least be 6 to 10 times smaller than the column diameter [50].

Most distillation columns use stainless steel packings, but the packing elements can be produced of ceramic, metal and plastic [8].

Structured A significant difference with the random packings is that a structured packing has a well-defined structure, that can be expressed with three factors: the corrugation angle, the base width of the corrugation, and the height of the corrugation. This allows for a more reliable definition of the parameters that influence the pressure drop and mass transfer. The thickness of the material defines the void fraction of the packing. There are three main types of structured packings [37]:

- Gauze packings: The first packing on the market was a metal gauze packing. The gauze maximizes the capillary effect, causing very high wetted areas for low liquid loads. Its main application is in vacuum systems, or laboratory set-ups with very small diameter columns. Gauze packings have high investment costs.
- Sheet packings: Metal sheet packings consists of several corrugated sheets of the same height, that are tightly packed against each other to form a cylindrical body with wall wipers. The wall wipers make sure that the phases don't bypass the packing at the column wall. The corrugation angle is typically 45° (Y-type packing) or 60° (X-type packing). Most structured sheet packing types are also sold in high performance versions, which have a modification of the corrugation angle at the end of the layers.
- Grid packings: Grids are used in applications were fouling is a main concern. They are built up of vertically arranged parallel metal strips and have a much lower specific surface area than the corrugated sheet packings.

2.3. BASIC CONCEPTS

Before discussing the balance and correlations used to predict the efficiency and hydraulics of the atmospheric condenser column, it is necessary to introduce a few basic concepts of the packed bed columns.

2.3.1. HEIGHT EQUIVALENT TO THEORETICAL PLATE

The Height Equivalent To Plate (HETP) is an expression of the mass transfer efficiency, a concept of ideal stages. The concept HETP is still widely used, although there are no real plates or integral steps in a packed distillation column. Although the diffusion in the OTWP column appears only in one direction, it can be considered a distillation process. In a binary system, the HETP is equal for both components.

So, to determine the overall transfer rate, and the packing performance, the HETP is determined. According to the two-film theory, the HETP can be described as [14] [4] [51]:

$$HETP = \frac{\ln sf}{sf-1}\left(\frac{u_{G,s}}{k_G a_e} + sf\frac{u_{L,s}}{k_L a_e}\right) \tag{2.9}$$

u is the velocity with the indexes L and G the liquid and vapor component respectively, and the index

s indicates that it is superficial. sf is the stripping factor as,

$$sf = \frac{m}{(L/G)} = \frac{\beta}{(L/G)} = \frac{\beta}{[1+(\beta-1)x_a]^2}\frac{G}{L} \tag{2.10}$$

With β the relative volatility as,

$$\beta = \frac{y_a/x_a}{y_{fw}/x_{fw}} \tag{2.11}$$

The subscripts a and fw represent dry air and fresh water, with x the mole fraction in the liquid (in equilibrium), and y the mole fraction in the vapor (in equilibrium). G and L are the gas and liquid mass flux, respectively.

Although the transfer of air into the liquid is ignored in the mass balances, the amount of air in water in equilibrium is needed to calculate the relative volatility. This requires the mole fraction of air and water in the liquid (x) and the vapor (y) phase. In a water/air mixture, an ideal gas and liquid phase can be assumed. This allows the application of Henry's law,

$$K = c_j P_j^{sat} \tag{2.12}$$

With K the Henry constant, c_j the molar concentration of component j and P_j^{sat} the vapor saturation pressure. It should be noted that these methods ignore the composition dependency of the equilibrium vapor and liquid mole fraction ratios. The saturation pressure of water vapor in air is calculated according to equation 2.5.

For the solubility of air in water the temperature dependent Henry constant is calculated by applying Van't Hoff equation, with the constants presented in table 2.2, with K^0 the Henry's law constant under standard conditions, and Δh_{sol} the enthalpy of dissolution. We assume the air to have a composition of 78.12 mol% of N_2 and 21.88 mol% of O_2.

Table 2.2: Henry's law constants [6]

	K^0	$\Delta h_{sol}/R$
N_2	6.4×10^{-4}	1300
O_2	1.3×10^{-4}	1700

The accuracy of the packing efficiency calculations depends on the mass and heat transfer correlations and the calculation of the effective interface area.

2.3.2. EFFECTIVE INTERFACE AREA

There are many different definitions of the effective interface area, and although numerous efforts have been made, the problem of defining it has not been solved satisfactorily [14] [52] [4].

Originally, in most models, the effective interface area and the mass transfer coefficients were not determined separately [13, 18], but were empirically defined as one unit. All the definitions that are currently available for the effective interface area, are based on falling film dynamics, but they show considerable differences. In gauze structured packings, it happens that the complete specific packing area is assumed to be wetted, and thus no correlation is required. For sheet structured packings this is somewhat different. Some correlations show overlap between the wetted surface area and the effective interface area [18]. Generally, this does not apply, since the wetted area consists of both dynamic and static fluid [14], and droplets of liquid are formed within the voidage of the packing [53]. Therefore, other correlations [5] include a correction factor for the instable flow behavior between the packing sheets [52].

2.3.3. HYDRAULIC CHARACTERISTICS

To accurately design the performance of a packed bed column it is important to have knowledge of its hydraulic characteristics throughout the operating range. The gas velocity at the flooding point is an important part of this, as it gives information about the maximum loading capacity. When a column has a high loading capacity, the required column diameter is smaller.

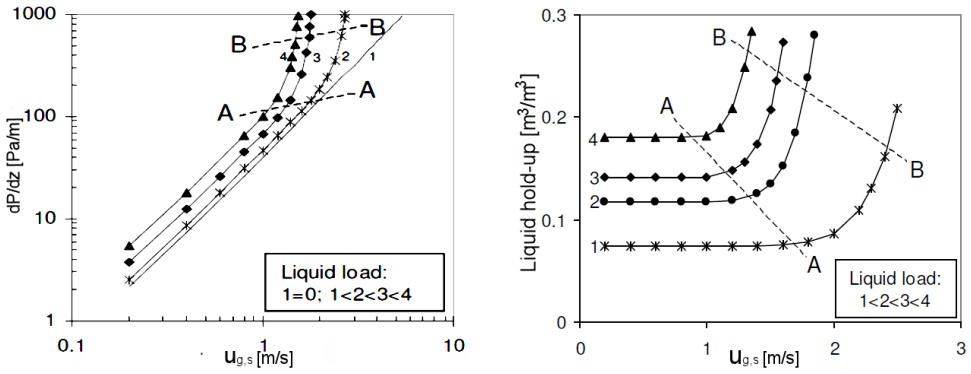

(a) Pressure drop (b) Liquid hold-up

Figure 2.4: Hydraulic column characteristics as a function of superficial gas velocity [11]

The liquid hold-up, κ_L, is the fraction of the liquid that is held up in the column. Because the total free void in the packing (the packing voidage minus the liquid hold-up, $\epsilon - \kappa_L$) reduces with an increase in liquid hold-up, the free cross-section for gas flow reduces. Consequently, an increase in liquid load, with a constant gas load, causes an increase in pressure drop over the packing. The liquid hold-up is also an important parameter in the calculation of the effective interface area (and thus the mass transfer). It can be easily deducted, that for completely wetted packings, the liquid hold-up is the product of the film thickness and the specific packing area.

Until the loading region, the liquid flow has virtually no influence on the gas flow, and the liquid hold-up does not depend on the gas load. In the loading region, the liquid hold-up starts to increase steadily with an increase in gas load. This causes the pressure drop to rise, but also means that more water is held up in the column, leading to an increase in effective interface area [54].

The flooding point is the upper operating limit of the packed bed column. In packings, the constant occurrence of droplets, and their entrainment, defines the flooding point mechanism. At flooding point, the down flowing liquid phase is held back by the up flowing gas phase so much, that it cannot flow down anymore. This causes a strong segregation of the phases, and a rapid increase in the gas phase pressure drop.

Figure 2.4a and figure 2.4b depict those concepts. Figure 2.4a shows how pressure drop increases over superficial vapor velocity. It shows two transfer regions (A-A and B-B) that are the loading point and flooding point respectively. Until the loading point, the pressure drop for different liquid loads is parallel to the pressure drop in a dry column. After the flooding point, the slopes of the pressure drop curves reach infinity. These two regions correspond to the behavior of the liquid hold-up curve in figure 2.4b. Until the loading point (A-A), the liquid-hold up is not influenced by the superficial gas velocity. At the loading point the shearing forces of the gas start to keep liquid, causing a hold-up. At the flooding point, the liquid cannot flow down the column any more, and the hold-up increases

infinitely.

Commonly, the operating area of columns is between the loading point and the flooding point. This is where there is the largest effective interface area (and thus mass transfer), with a relative small increase in pressure drop.

2.4. ENERGY AND MASS BALANCES

The formulation for the mass and heat transfer is presented below and applies one-dimensional mass and energy conservation equations to a differential volume of the packed bed over the height z. The model was initially based on the balance proposed by Alnaimat *et al.* [55], but adapted for a dehumidification system, without humidification. Further in this section it is shown (with eq. 2.18), that it is valid to assume that dehumidification starts the moment gas enters the packed bed column. In the dehumidification model the following assumptions were made:

- The fresh water is assumed to be pure water
  - Thermodynamic properties of pure water are used
  - Evaporation or fouling by other components is not accounted for
- The system is adiabatic
- The system is working under atmospheric pressure
- The system has a controlled volume, thus a constant gas and liquid flow
- There is no transfer of air to the fresh water flow

In the definition of the HETP it was made clear that there is air in the water, but since the solubility changes only little in the temperature gradient of this system, it has very limited influence on the mass transfer process of the water vapor and is assumed constant in the following balance. In the formulation the subscripts a, v, and p describe the properties of dry air, vapor and the packing respectively. The subscripts L and G denote the liquid and gas properties: in this system the fresh water and humid air.

MASS BALANCE

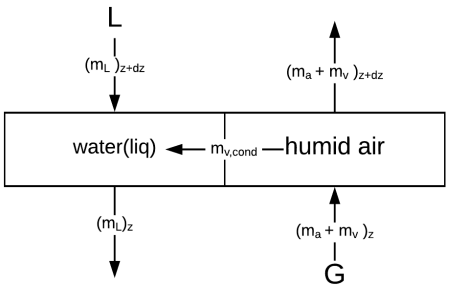

Figure 2.5: Control volume of dehumidification model

Figure 2.5 shows the differential control volume for the water vapor mass transfer between the water and humid air in the counter-current column. Applying the conservation of mass to the liquid phase (fresh water) gives,

$$(\dot{m}_{\mathrm{L}})_{\mathrm{z+dz}} - (\dot{m}_{\mathrm{L}})_{\mathrm{z}} + d\dot{m}_{\mathrm{v,cond}} = \frac{d}{dt}(\rho_{\mathrm{L}} \nu_{\mathrm{L}} A_{\mathrm{c}} dz) \tag{2.13}$$

Where $\dot{m}$ is the mass flow rate, $\dot{m}_{\mathrm{v,cond}}$ is the mass flow rate of the vapor from condensation, ρ represents the density, ν is the volume fraction and A_{c} the cross-sectional area. Because a constant gas and liquid flow are assumed, the liquid volume fraction, or the hold-up, is nearly constant. Density and the cross-sectional area are not time dependent. Therefore, equation 2.13 can be simplified to:

$$\frac{d(\dot{m}_{\mathrm{L}})}{dz} = \frac{d(\dot{m}_{\mathrm{v,cond}})}{dz} \tag{2.14}$$

It shows that the change in mass flow rate of the liquid over the height of the control volume should be equal to the change in portion of liquid condensed from humid air over the height of control volume. In other words: water only comes to the liquid flow through condensation.

Similarly, the conservation of mass can be applied to the gas phase (humid air) in the control volume:

$$(\dot{m}_a + \dot{m}_v)_z - (\dot{m}_a + \dot{m}_v)_{z+dz} - d\dot{m}_{v,cond} = \frac{d(\dot{m}_G)}{dt} \tag{2.15}$$

The mass of the humid air, $\dot{m}_G$ can be expressed as $\dot{m}_G = \rho_G v_G A_c dz$. Because the liquid volume fraction was assumed nearly constant, the volume fraction of the humid air should be too ($v_G + v_p + v_L = 1$). It is assumed that there is no transfer of air to the liquid phase, and thus $\dot{m}_a$ in the vapor phase is constant. The humid air density, ρ_G, can be expressed in humidity ratio and the dry air and vapor density according to,

$$\rho_G = \frac{1}{1+\omega}\rho_a + \frac{\omega}{1+\omega}\rho_v \tag{2.16}$$

Because the densities of dry air and vapor are assumed constant over time, the time derivative of the humid air also disappears, so that equation 2.15 can be simplified to,

$$\frac{d(\dot{m}_v)}{dz} = -\frac{d(\dot{m}_{v,cond})}{dz} \tag{2.17}$$

Combining equation 2.16 and 2.17 shows that, to calculate the liquid and gas mass flow rates, it is necessary to calculate the rate of condensation. Applying the mass transfer definition as presented in equation 2.8 and the ideal gas law to the differential volume results in the following expression for the gradient of the vapor mass flow rate,

$$\frac{d(\dot{m}_{v,cond})}{dz} = k_G A_c \frac{M_v}{R}\left[\frac{RH * P^{sat}(T_G)}{T_G} - \frac{P_v^{sat}(T_i)}{T_i}\right] \tag{2.18}$$

Where R is the gas constant in $kg\,kmol^{-1}\,K^{-1}$ and M is the molecular weight in $kg\,kmol^{-3}$. The temperature of the gas, T_G, is, for humid air, equivalent to the DBT. The interface temperature, T_i, is the temperature of the interface between the gas and liquid phase. Now the gas mass transfer coefficient, k_G, is introduced to the balance. Since the mass flow rate of condensation reduced the humidity ratio in the air,

$$\frac{d(\dot{m}_{v,cond})}{dz} = -G_a A_c \frac{d\omega}{dz} \tag{2.19}$$

Where G_a is the dry air mass flux. Combining this definition with the expression for the gradient of the vapor mass flow rate from equation 2.18, the definition of the humidity ratio presented in equation 2.4 and the simplified mass balance in equation 2.17 it can be transformed into the gradient of the humidity ratio in the column.

$$\frac{d\omega}{dz} = \frac{k_G a_e}{G_a}\frac{M_v}{R}\left[\frac{P_v^{sat}(T_i)}{T_i} - \frac{\omega}{0.622+\omega}\frac{P}{T_G}\right] \tag{2.20}$$

With a_e the effective interface area. This expression clearly shows that, as long as there is a negative driving force (in the form of $\frac{P_v^{sat}(T_i)}{T_i} - \frac{RH}{0.622+RH}\frac{P}{T_G}$) there will be a condensation process in the column. Figure 2.6 shows that, for interface temperatures above ~24 °C, an air feed of 28 °C and relative humidity of 80 % will evaporate. Since the interface temperature is close to the liquid phase temperature,

there will be no humidification in the OTWP column with a water feed of 12 °C.

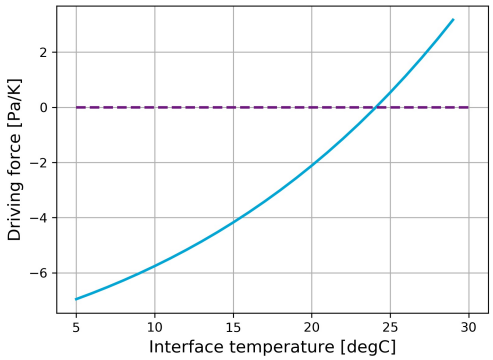

Figure 2.6: Condensation driving force as a function of T_i, for T_G =28 °C and RH = 80 %

ENERGY BALANCE

The main energy transfer mechanisms that take place over the height of the column are:

- heat transfer due to condensation
  $d(\dot{m}_{v,cond})l_v$
- changes in enthalpy of the liquid film and the humid air
  $\frac{d}{dz}(\dot{m}_L h_L)$ and $\frac{d}{dz}(\dot{m}_a h_a + \dot{m}_v h_v)$ respectively
- convective heat transport between the packing and the liquid film
  $\alpha_L(T_p - T_L)a_w A_c$
- convective heat transport between the packing and the humid air
  $\alpha_G(T_G - T_p)(a_p - a_w)A_c$
- convective heat transport between the liquid film and the humid air
  $U(T_G - T_L)a_e A_c$
- conductive heat transport through the packing (this is ignored)

Where h is the specific enthalpy, α is the heat transfer coefficient between a phase and the packing in $W m^{-2} K^{-1}$, U is the overall heat transfer coefficient between the two phases, a_p is the packing surface area per volume, and a_w is the wetted surface area per volume. Figure 2.7 gives a visual representation of the liquid and gas energy transfers in a control volume of height dz.

Applying the conservation of energy to the liquid phase yields,

$$\begin{aligned}(\dot{m}_L h_L)_{z+dz} - (\dot{m}_L h_L)_z + d\dot{m}_{v,cond} l_v \\ + U a_e (T_G - T_L) A_c dz + \alpha_L a_w (T_p - T_L) A_C dz \\ = \frac{d}{dt}(\rho_L v_L h_L A_c dz)\end{aligned} \tag{2.21}$$

$\rho_L v_L h_L A_c dz$ describes heat capacity of the liquid in the control volume. Since only the specific enthalpy changes with time, and steady state is assumed, the liquid enthalpy derivative is found. By expressing $\dot{m}_L$ as LA_c with L the fresh water mass flux, and using equation 2.14, the liquid enthalpy derivative is,

$$\frac{dh_L}{dz} = \frac{G_a}{L}\frac{d\omega}{dz}(l_v - h_L) - \frac{U a_e}{L}(T_G - T_L) - \frac{\alpha_L a_w}{L}(T_p - T_L) \tag{2.22}$$

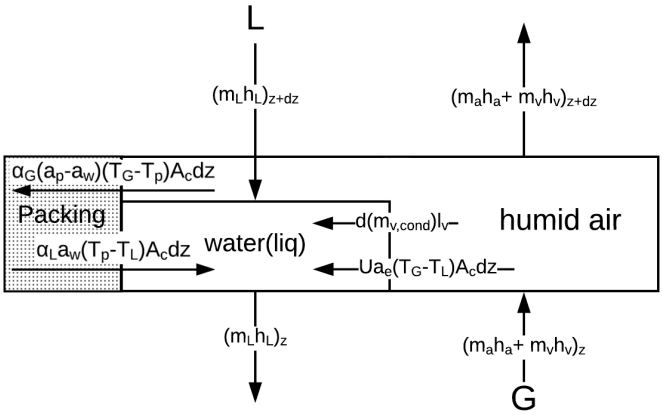

Figure 2.7: Energy transfer control volume of dehumidification model

This enthalpy derivative can be used to calculate the liquid temperature derivative, by dividing it by the thermal capacity c_p. This is done under the assumption of constant pressure.

$$\frac{dT_\mathrm{L}}{dz} = \frac{1}{c_{p,\mathrm{L}}} \frac{dh_\mathrm{L}}{dz} \tag{2.23}$$

In a similar fashion we can apply the conservation of energy to the gas phase in the column,

$$\begin{aligned}(\dot{m}_\mathrm{a} h_\mathrm{a} + \dot{m}_\mathrm{v} h_\mathrm{v})_{z+\mathrm{dz}} - (\dot{m}_\mathrm{a} h_\mathrm{a} + \dot{m}_\mathrm{v} h_\mathrm{v})_\mathrm{z} - d\dot{m}_{\mathrm{v,cond}} l_\mathrm{v} \\ - U a_\mathrm{e} (T_\mathrm{G} - T_\mathrm{L}) A_\mathrm{c} dz - \alpha_\mathrm{G} (a_\mathrm{p} - a_\mathrm{w}) (T_\mathrm{G} - T_\mathrm{p}) A_\mathrm{c} dz \\ = \frac{d}{dt} (m_\mathrm{a} h_\mathrm{a} + m_\mathrm{v} h_\mathrm{v})\end{aligned} \tag{2.24}$$

In this model it is assumed that there is no mass transfer of dry air into the liquid. Taking that, and equation 2.17, into account, $(\dot{m}_\mathrm{a} h_\mathrm{a} + \dot{m}_\mathrm{v} h_\mathrm{v})_{z+\mathrm{dz}} - (\dot{m}_\mathrm{a} h_\mathrm{a} + \dot{m}_\mathrm{v} h_\mathrm{v})_\mathrm{z}$ can be rewritten as $-\dot{m}_\mathrm{a}(1+\omega)\frac{dh_\mathrm{G}}{dz} dz + h_\mathrm{v} \frac{d\dot{m}_{\mathrm{v,cond}}}{dz}$. Similarly, $\frac{d}{dt}(m_\mathrm{a} h_\mathrm{a} + m_\mathrm{v} h_\mathrm{v})$ can be rewritten as $\dot{m}_\mathrm{a}(1+\omega)\frac{dh_\mathrm{G}}{dt}$. Keeping in mind that $l_\mathrm{v}(T_\mathrm{G}) = h_\mathrm{G}(T_\mathrm{G}) - h_\mathrm{L}(T_\mathrm{G})$, and assuming steady state the energy balance can be rearranged as,

$$\frac{dh_\mathrm{G}}{dz} = -\frac{h_\mathrm{L}(T_\mathrm{G})}{(1+\omega)} \frac{d\omega}{dz} - \frac{U a_\mathrm{e} (T_\mathrm{G} - T_\mathrm{L})}{G_\mathrm{a}(1+\omega)} - \frac{\alpha_\mathrm{G} (a_\mathrm{p} - a_\mathrm{w}) (T_\mathrm{G} - T_\mathrm{p})}{G_\mathrm{a}(1+\omega)} \tag{2.25}$$

Since the humidity ratio was calculated in the mass transfer balance (see eq. 2.20), the enthalpy derivative can, according to psychrometrics, be used to calculate the gas temperature derivative (again, assuming constant pressure).

Applying the conservation of energy to the packed bed yields,

$$\alpha_\mathrm{G} (T_\mathrm{G} - T_\mathrm{p}) (a_\mathrm{p} - a_\mathrm{w}) A_\mathrm{c} dz - \alpha_\mathrm{L} (T_\mathrm{p} - T_\mathrm{L}) a_\mathrm{w} A_\mathrm{c} dz = \frac{d}{dt} (\rho_\mathrm{p} v_\mathrm{p} h_\mathrm{p} A_\mathrm{c} dz) \tag{2.26}$$

It will be discussed in section 2.5.1 that, because the heat transfer coefficients of the phases are calculated with an analogy, the heat transfer between the phases and the packing can be neglected.

The liquid and gas temperature derivatives can then be reduced to,

$$\frac{dT_L}{dz} = \frac{G_a}{L}\frac{d\omega}{dz}\frac{(l_v - h_L)}{c_{p,L}} - \frac{Ua_e}{L}\frac{(T_G - T_L)}{c_{p,L}} \tag{2.27}$$

and

$$\frac{dT_G}{dz} = -\frac{h_L(T_G)}{(1+\omega)}\frac{d\omega}{dz}\frac{1}{c_{p,G}} - \frac{Ua_e(T_G - T_L)}{G_a(1+\omega)}\frac{1}{c_{p,G}} \tag{2.28}$$

2.5. THE HEAT AND MASS TRANSFER COEFFICIENTS

The estimation of the behavior of packed bed columns is risky. The formulation above shows that the rate-based simulations for packed bed columns rely on correlations for the mass and heat transfer coefficient and the specific interface area. Available packing correlations are empirical and thus unreliable when they are applied to conditions outside of the system on which they were tested [34]. Wang *et al.* [14] give a comprehensive overview of the correlations used for predicting the mass transfer performance of a packed bed column. Their work concludes that there is a lack of scientific basis for predicting the performance of large diameter columns.

Correlations for liquid and gas-side mass transfers are numerous, and available for both random and structured packed beds. The accuracy of the mathematical model presented above depends on the correctness of the mass and heat transfer coefficients and the wetted packing area. In this section we discuss the methods that were selected to calculate the mass transfer coefficients, the analogy for the heat transfer and how we calculate the two phase pressure drop in the Python and Aspen plus models.

2.5.1. THE HEAT TRANSFER COEFFICIENT

The overall heat transfer coefficient between the phases U, can be calculated as,

$$\frac{1}{U} = \frac{1}{U_L} + \frac{1}{U_G} \tag{2.29}$$

U_L and U_G are the heat transfer coefficients between the two phases, for the liquid and gas phase respectively. The solutions that were obtained for mass transfer in the section before, can be transferred to heat transfer coefficients by means of an analogy. For the heat transfer coefficients in internally forced flows, the most widely used analogy is presented by Chilton and Colburn [56]. This is the analogy that is available in Aspen plus, and the one that was selected for previous versions of the Bluerise B.V. Python model. We adopt the analogy presented by Noordhoek Hegt [3], he researched the exponent of the liquid Prandtl number Pr_L, and concluded that there is reason to use a lower exponent for the gas Prandtl number than for the liquid Prandtl number, leading to the respective gas and liquid phase analogies,

$$\frac{Nu_G}{Pr_G^{1/3}} = \frac{Sh_G}{Sc_G^{1/3}} \tag{2.30}$$

and

$$\frac{Nu_L}{Pr_L^{1/2}} = \frac{Sh_L}{Sc_L^{1/2}} \tag{2.31}$$

Nu is the dimensionless Nusselt number, that describes a ratio between the convective and conductive heat transfer: $\frac{U_j l_0}{\lambda}$, where U_j is either of the phase heat transfer coefficients, λ is the thermal

conductivity and l_0 is the characteristic length. The Prandtl number Pr gives a ratio between the momentum and thermal diffusivity: $\frac{c_p \mu}{\lambda}$, with μ the dynamic viscosity of the phase. The Sherwood number, Sh, gives the ratio between convective and diffusive mass transfer, $\frac{k l_0}{D}$, and the Schmidt number relates the momentum to the mass diffusivity: $\frac{\mu}{\rho D}$. This gives us the following expression for the respective liquid and gas phase heat transfer coefficients:

$$U_{\mathrm{L}} = k_{\mathrm{L}} \left(\rho_{\mathrm{L}} c_{p,\mathrm{L}}\right)^{1/2} \left(\frac{\lambda_{\mathrm{L}}}{D_{\mathrm{L}}}\right)^{1/2} \tag{2.32}$$

and

$$U_{\mathrm{G}} = k_{\mathrm{G}} \left(\rho_{\mathrm{G}} c_{p,\mathrm{G}}\right)^{1/3} \left(\frac{\lambda_{\mathrm{G}}}{D_{\mathrm{G}}}\right)^{2/3} \tag{2.33}$$

The expressions above explain why we ignore the heat transfer between the phases and the packing (see eq. 2.27 and eq. 2.28). Since the mass transfer coefficients are *empirically* decided based on the *interface area*, and the heat transfer coefficients are acquired through an analogy with the mass transfer coefficients, it follows that the heat transfer should be calculated with the interface area. This simplifies the process, since the heat transfer coefficient between the phases and the packing, α_{j}, would not be the same as the heat transfer between the two phases, U_{j}.

It should be mentioned that this conclusion is not in line with the model that was presented by Alnaimat *et al.* [55] (and adopted in previous versions of the Bluerise B.V. Python model), where they use the interface heat transfer coefficients, calculated according to Onda's correlations, to express heat transfer terms between the packing and the phases.

2.5.2. THE PHASE MASS TRANSFER COEFFICIENTS

The phase mass transfer coefficient correlations can be divided into two main groups: correlations for random packing, and correlations for structured packings. The correlations for random packings that were used in the Aspen plus model are shortly described below. Noordhoek Hegt [3] discussed them more extensively. The focus in this section is on the correlations that have been developed to predict mass transfer in structured packings.

RANDOM PACKING

Onda The first and most well-known correlation of conventional mass transfer method for randomly packed beds is the method of Onda *et al.* [18] [14, 34]. Onda's method assumes that the wetted surface on packing pieces is identical with the effective liquid-gas interface. This was later found to be an overestimation, since it does not take into account static and dynamic liquid. The method proposes empirical equations for the mass transfer coefficients.

Billet and Schultes Although Onda *et al.* [18] is still commonly used, more modern approaches are not solely based on empirical calculation, but also designed on the basis of physically proven conditions of fluid dynamics in mass transfer columns, and the kinetic laws of mass transfer in flowing media [13, 14]. An example of this is the model developed by Billet and Schultes [13]. They developed a partly theoretical model that, by using a uniform theory, makes it possible to determine the mass transfer efficiency, the pressure drop, the column hold-up and the load limits. This model can be applied to both random and structured packings and is extensively discussed in the next section.

Maćkowiak The correlation that was adopted by Noordhoek Hegt [3] for the Bluerise B.V. Python model, is the mass transfer correlation developed by Maćkowiak and Maćkowiak [50]. As one of the more recent models, it is not incorporated in Aspen plus V8.8. The more recent correlation deviates from the previously mentioned, as it expands on the mass transfer area that appears as a thin film on the packing surface with a droplet theory. Maćkowiak mentions that his method can be applied to all types of lattice structures, which he defines as highly perforated packing elements, with an open structure. Those lattice packings are a development of the last 30 years, with as main benefit that they do not contain any dead space that can be filled with liquid, and thus have a greater operating range, since the flooding point will not be reached. Maćkoviak mentions three main causes of droplet formation: dripping of the liquid from the sharp edges of the packing elements, runlets (threads) that come in contact with the ledges of packing elements might break and get entrained by the gas flow, and at higher gas velocities the gas kinetic energy can be transferred to runlets and films resulting in droplet formation.

The droplets are said to occur between individual packing elements. Since structured packings do not consist of individual elements it should be clear that the Maćkowiac model does not apply there.

STRUCTURED PACKING

Structured packing correlations are mostly based on empirical fits to physical balances. Although research cannot find consensus on how to relate superficial velocity, viscosity, density, and surface tension of the liquid phase to the effective surface area, there seems the be agreement on the gas-side mass transfer coefficient, that is usually derived from equations proposed by Johnstone and Pigford [52]. There is more variation in the liquid-side mass transfer coefficient: some researchers base it on the penetration theory, and others say the liquid film must be modeled [52].

The two most established models for corrugated structured packings are the ones presented by Rocha *et al.* [5][40] and Billet and Schultes [42][57]. These two models are available in Aspen plus V8.8 and implemented in the Python model. The Billet and Schultes model is an extension on the random packed bed model (discussed extensively by Noordhoek Hegt [3]), and as such, it required packing specific constants for each type of packing. This makes it less appropriate for generalized optimizations. More recently the Delft model was developed [4], a model that is based on packing geometry, and does not need packing specific constants for the calculation of the mass transfer coefficients. Aspen Technology Inc. developed coefficients based on a dimensionless number analysis. The respective correlations are discussed below.

Rocha, Bravo and Fair Bravo et al. initially developed a mass-prediction model for gauze-like packings. In this model they had to assume complete wetting of the surface area, in order to calculate the packing performance. Extending on that, they developed a method (RBF-model) to describe the performance of structured sheet packings of a corrugated nature [5, 40]. They considered the structured packings as a series of wet walls, with the angle and size of the corrugations as geometry variables.

The characteristic length, S, that is considered throughout the presented relationship represents the side of the corrugation and can be expressed by the following equation:

$$S = \sqrt{\frac{W_{cg}^2}{4} + H_{cg}^2} \tag{2.34}$$

where W_{cg} is the base width of the corrugation, and H_{cg} is the height. Figure 2.8 shows the flow channels considered within the package.

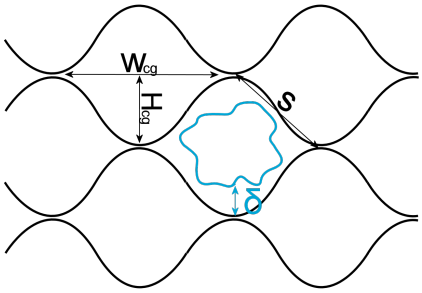

Figure 2.8: Cross section of the structured packing flow channels

As discussed in section 2.3.3, hold-up is very important in pressure drop and mass transfer calculations. This method assumes film flow for the liquid and applies correction factors for both operating and static hold-up, that account for all the surface that is not being wetted. The liquid hold-up, κ_L, for complete wetting of the surface, can be expressed by:

$$\kappa_L = 4\frac{\delta}{S} \tag{2.35}$$

Where δ is the film thickness. This can be easily deducted from figure 2.8: for all four sides the length multiplied by the film thickness results in the amount of liquid that is held-up. Equation 2.36 shows the expression for hold-up when only wetted area is considered.

$$\kappa_L = \left(4\frac{F_t}{S}\right)^{2/3}\left(\frac{3\mu_L u_{L,s}}{\rho_L(\sin\theta)\epsilon g_e}\right)^{1/3} \tag{2.36}$$

Where μ is the viscosity, u_s is the superficial velocity, θ is the corrugation angle and ϵ is the void fraction of the packing. This hold-up model is derived from air/water data for a variety of structured packings. Here, g_e is the effective gravity, and F_t is the correction factor in terms of the effective interface area, based on the Shi and Mersmann [58] correlation.

$$F_t = 29.12(We_{L,s}Fr_{L,s})_L^{0.15}\frac{S^{0.359}}{Re_{L,s}^{0.2}\epsilon^{0.6}(1-0,93\cos\gamma)(\sin\theta)^{0.3}} \tag{2.37}$$

With $We_{L,s}$, $Fr_{L,s}$ and $Re_{L,s}$ the dimensionless liquid Weber, Froude and Reynolds (based on superficial velocity) numbers respectively. Cos γ accounts for surface material wettability and depends on the surface tension σ ($\cos\gamma = 0.9$ for $\sigma < 0.055\,\mathrm{N\,m^{-1}}$ and $\cos\gamma = 5.211 * 10^{-16.835\sigma}$ for $\sigma > 0.055\,\mathrm{N\,m^{-1}}$). The effective gravity in equation 2.36 is the effective force that moves the liquid down the column. It originates from the balance on the liquid film, between gravity, g, and the forces that work against it: buoyancy, vapor pressure drop, and the drag on the liquid film by vapor. It can be expressed as,

$$g_e = g * \left[\frac{(\rho_L - \rho_G)}{\rho_L}\right]\left[1 - \left(\frac{\Delta P/\Delta z}{(\Delta P/\Delta z)_{flood}}\right)\right] \tag{2.38}$$

Rocha *et al.* [5] selected a flooding pressure drop, $(\Delta P/\Delta z)_{flood}$, of $1025\,\mathrm{Pa\,m^{-1}}$ for an air/water

system. The flooding pressure drop depends on the size of the packing, but the chosen value was found to give and adequate fit over a larger selection of packings.

The general equation for the pressure drop is, similar to the one found by Billet and Maćkowiak [59], based on a channel model:

$$\frac{\Delta P}{\Delta z} = \frac{\Delta P_{\mathrm{d}}}{\Delta z}\left[\frac{1}{1-K_1\kappa_{\mathrm{L}}}\right] \tag{2.39}$$

Where the dry pressure drop, $\Delta P_{\mathrm{d}}/\Delta z$, is calculated with a friction factor equation. The friction factor, f, is correlated for the air/water system ($f = 0.177 + 88.774/Re_{\mathrm{G}}$) resulting in the following equation:

$$\frac{\Delta P_{\mathrm{d}}}{\Delta z} = \frac{0.177\rho_{\mathrm{G}}u_{\mathrm{G,s}}^2}{S\epsilon^2(\sin\theta)^2} + \frac{88.774\mu_{\mathrm{G}}u_{\mathrm{G,s}}}{S^2\epsilon\sin\theta} \tag{2.40}$$

With $u_{\mathrm{G,s}}$ the gas superficial velocity. Rocha *et al.* [5] developed a correlation for the air/water system that fits the experimental data in an excellent way. Equation 2.41 shows the linear dependency of the constant K_1 for air/water systems.

$$K_1 = 0.614 + 71.35S \tag{2.41}$$

The set of equations 2.36 to 2.41 holds two unknowns: the liquid hold-up and the pressure drop. The solution approach requires an iteration process. With the calculated liquid hold-up, the effective phase velocities, $u_{\mathrm{G,e}}$ and $u_{\mathrm{L,e}}$, can be defined as:

$$u_{\mathrm{G,e}} = \frac{u_{\mathrm{G,s}}}{\epsilon(1-\kappa_{\mathrm{L}})\sin\theta} \tag{2.42}$$

and

$$u_{\mathrm{L,e}} = \frac{u_{\mathrm{L,s}}}{\epsilon\kappa_{\mathrm{L}}\sin\theta} \tag{2.43}$$

The definitions above use a correction for the space occupied by the liquid.

According to Shi and Mersmann [58] the equation for the ratio between the effective interface area, a_{e}, and the specific packing area, a_{p}, applicable to sheet-metal structured packings is as follows:

$$\frac{a_{\mathrm{e}}}{a_{\mathrm{p}}} = F_{\mathrm{SE}}F_{\mathrm{t}} \tag{2.44}$$

With F_{SE} a factor that accounts for variations in the surface enhancement (= 0.35 for stainless steel). The model above is the hydraulic model for structured packings as presented by [5]. In a second part of that paper they continued their work by developing a mass transfer efficiency correlation. The mass transfer coefficients are calculated according to:

$$k_{\mathrm{G}} = 0.054Re_{\mathrm{G,rv}}^{0.8}Sc_{\mathrm{G}}^{0.33}\frac{D_{\mathrm{G}}}{S} \tag{2.45}$$

and

$$k_{\mathrm{L}} = 2\left(\frac{C_{\mathrm{E}}D_{\mathrm{L}}u_{\mathrm{L,e}}}{\pi S}\right)^{0.5} \tag{2.46}$$

With a gas phase Reynolds number based on relative velocity (= $u_{\mathrm{G,e}} + u_{\mathrm{L,e}}$) as:

$$Re_{\mathrm{G,rv}} = \frac{(u_{\mathrm{G,e}} + u_{\mathrm{L,e}})\rho_{\mathrm{G}}S}{\mu_{\mathrm{G}}} \tag{2.47}$$

and a gas phase Schmidt number as:

$$Sc_G = \frac{\mu_G}{D_G \rho_G} \tag{2.48}$$

Where D is the diffusion coefficient, and C_E a factor to account for parts of the packing where there is no rapid surface renewal, for most well-known structured packings $C_E = 0.9$. As was noted by Olujić *et al.* [4], the factor C_E appears once in the denominator and once in the numerator. Since we reason that the the parts with no rapid surface renewal will have a decreasing effect on the liquid mass transfer coefficient, we placed the factor C_E in the numerator.

RBFadapt-model The factor that accounts for the surface material wettability by defining the contact angle γ, presented by the RBF-model in equation 2.37, has a large influence on the interface area.

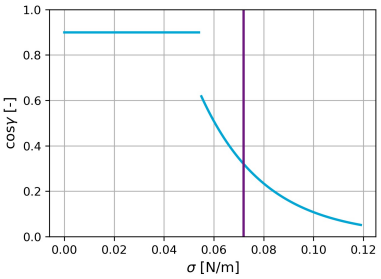

Figure 2.9: Surface material wettability factor $\cos\gamma$ as a function of the liquid surface tension

Figure 2.9 shows the factor as a function of the liquid surface tension, as it was defined in the RBF-model. Water on stainless steel has a contact angle γ of 72° ($\cos\gamma = 0.3$, the purple line in fig. 2.9).

It is likely that the selected packing is treated to have a better wettability, and thus a smaller contact angle. It is assumed that the treatment of the stainless steel surface enhances the wettability enough to get a contact angle lower than 50° ($\cos\gamma = 0.64$): the factor $\cos\gamma$ can be taken as 0.9. This change is made, resulting in the adapted Rocha, Bravo Fair model (RBFadapt-model).

Billet and Schultes Billet and Schultes model (BS-model) [42] [57] is developed to predict mass transfer in counter-current flow columns. Their model for corrugated sheet packings represents an extension of the random packing method by the same authors. The model defines the product of the mass transfer coefficient and the interface area, as this is how the empirical values were determined. It defines correlations for three different flow regions: the pre-loading region, the loading region, and the flooding point.

For the mass transfer correlations, the BS-model model uses the equivalent diameter as the characteristic length:

$$d_{eq} = 4\frac{\epsilon}{a_p} \tag{2.49}$$

Billet and Schultes defined a theoretical liquid hold-up for a perfect channel model, based on a force balance, but argue that the phases do not flow in parallel flow channels, but in all directions. For the hold-up they developed different definitions per hydraulic region: below the loading point,

$$\kappa_L = \kappa_{L,lp} = \left(12\frac{\mu_L a_p^2 u_{L,s}}{\rho_L g}\right)^{1/3}\left(\frac{a_h}{a_p}\right)^{1/3} \tag{2.50}$$

at the flooding point,

$$\kappa_{L,fp} = 2.2\kappa_{L,lp} \tag{2.51}$$

and between loading and flooding points ($u_{G,s} > (u_{G,s})_{lp}$),

$$\kappa_L = \kappa_{L,lp} + (\kappa_{L,fp} - \kappa_{L,lp})\left(\frac{u_{G,s}}{(u_{G,s})_{fp}}\right)^{13} \tag{2.52}$$

With the hydraulic area a_h calculated with a packing specific constant, C_h, as:

$$\left(\frac{a_h}{a_p}\right)_{Re_L<5} = C_h Re_{L,s}^{0.15} Fr_{L,s}^{0.1} \tag{2.53}$$

$$\left(\frac{a_h}{a_p}\right)_{Re_L\geq5} = 0.85 C_h Re_{L,s}^{0.25} Fr_{L,s}^{0.1} \tag{2.54}$$

and the superficial gas velocity at flooding point:

$$(u_{G,s})_{fp} = \left(\frac{2g}{\xi_{fp}} \frac{\kappa_{L,fp}}{a_p} \frac{\rho_L}{\rho_G}\right)^{1/2} \frac{(\epsilon - \kappa_{L,fp})^{2/3}}{\epsilon^{1/2}} \tag{2.55}$$

where ξ_{fp} is the resistance factor for the flooding point, calculated by:

$$\begin{gathered} \xi_{fp} = \frac{g}{C_{fp}^2 \left(\psi(\mu_L/\mu_G)^{0.2}\right)^{2n_{fp}}} \\ \psi \leq 0.4 \rightarrow n_{fp} = -0.194 \\ \psi > 0.4 \rightarrow n_{fp} = -0.708 \end{gathered} \tag{2.56}$$

ψ is the flow parameter defined as: $\psi = L/G(\rho_G/\rho_L)^{1/2}$ and C_{fp} is a packing specific constant.

The liquid phase mass transfer coefficient is presented in two forms: the coefficient below loading point and between loading- and flooding point. The two respective coefficients are:

$$k_L a_e = C_L g^{1/6} \left(\frac{\rho_L}{\mu_L}\right)^{1/6} \left(\frac{D_L}{d_{eq}}\right)^{1/2} a_p^{2/3} u_{L,s}^{1/3} \frac{a_e}{a_p} \tag{2.57}$$

and

$$k_L a_e = 12^{1/2} C_L a_p u_{L,e}^{1/2} \left(\frac{D_L}{d_{eq}}\right)^{1/2} \frac{a_e}{a_p} \tag{2.58}$$

Where the effective phase velocity is calculated with the liquid hold-up ($u_{L,e} = u_{L,s}/\kappa_L$), and C_L is a packing specific constant.

Since the gas phase behaviour does not vary significantly per hydraulic region, it can be expressed with a single equation for the whole operating range:

$$k_G a_e = C_G \frac{a_p^{1.5}}{d_{eq}^{1/2}} \frac{1}{(\epsilon - \kappa_L)^{1/2}} D_G Re_{G,s}^{3/4} Sc_G^{1/3} \frac{a_e}{a_p} \tag{2.59}$$

With the effective phase velocity calculated similarly to the liquid phase velocity, and C_G the packing specific constant. The index s in the dimensionless numbers means that the superficial velocity is used.

The effective interface area is calculated for (below) the loading point, flooding point and between

loading- and flooding point, respectively:

$$\left(\frac{a_e}{a_p}\right)_{lp} = 3\epsilon^{0.5} Re_{L,s}^{-0.2} We_{L,s}^{0.75} Fr_{L,s}^{-0.45} \tag{2.60}$$

$$\left(\frac{a_e}{a_p}\right)_{fp} = 7\left(\frac{\sigma_L}{\sigma_W}\right)^{0.56}\left(\frac{a_e}{a_p}\right)_{lp} \tag{2.61}$$

and

$$\left(\frac{a_e}{a_p}\right)_{u_{G,s}>(u_{G,s})_{lp}} = \left(\frac{a_e}{a_p}\right)_{lp} + \left(\left(\frac{a_e}{a_p}\right)_{fp} - \left(\frac{a_e}{a_p}\right)_{lp}\right)\left(\frac{u_{G,s}}{(u_{G,s})_{fp}}\right)^{13} \tag{2.62}$$

With σ_L the surface tension of the liquid, and σ_W the surface tension of the water, the first term in the correlation for the effective interface area at flooding point for the OTWP system would be 1. Billet and Schultes provide packing constants for both structured and random packings.

The Delft-model Olujić *et al.* [4] developed the Delft-model equations: a more recent performance prediction method that does not require any packing specific constants. Throughout the presentation of this method, it will become clear that it is only applicable in the pre-loading region.

Instead of considering a hydraulic diameter based on the corrugation side or the packing voidage and specific surface area, this method models the gas flow as a continuous zigzag flow through a triangular channel. The total length of the gas flow path is equal to the length of a gas flow channel in an element ($l_{G,el} = H_{el}/\sin\theta$), multiplied by the number of elements. The equivalent diameter of the triangular gas flow channel, specified by the packing geometry presented in figure 2.8 is:

$$d_{eq,G} = \frac{\frac{(W_{cg}H_{cg}-2\delta S)^2}{W_{cg}H_{cg}}}{\left[\left(\frac{W_{cg}H_{cg}-2\delta S}{2H_{cg}}\right)^2 + \left(\frac{W_{cg}H_{cg}-2\delta S}{W_{cg}}\right)^2\right]^{0.5} + \frac{W_{cg}H_{cg}-2\delta S}{2H_{cg}}} \tag{2.63}$$

Throughout the presentation of this model some of the definitions are equal to the ones presented in RBF-model, such as the effective phase velocities (eq. 2.42 and eq. 2.43). In any references to similar equations from previous models, it should be kept in mind that the Delft-model makes use of the equivalent diameter d_{eq} and never of the side corrugation S as characteristic length. In the pre-loading region, it is assumed that there is no entrainment. Nusselt's falling film theory is applied (eq. 2.65), because Olujić *et al.* [4] assume that in this region the liquid hold-up is not affected by the gas flow, and thus counter-current effects are neglected:

$$\kappa_L = \delta a_p \tag{2.64}$$

where

$$\delta = \left(\frac{3\mu_L u_{L,s}}{\rho_L g a_p \sin\theta}\right)^{1/3} \tag{2.65}$$

The gas phase mass transfer coefficient in the Delft-model is represented as an average of a laminar and turbulent coefficient,

$$k_G = \sqrt{k_{G,lam}^2 + k_{G,turb}^2} \tag{2.66}$$

The Delft-model accounts for the sudden change in direction (of both the gas and liquid flow) that

is caused by entrance effect at every packing element. This leads to the use of characteristic dimensionless expressions (Sherwood numbers, Sh). The laminar component shows similarities to the gas phase coefficient presented in equation 2.45,

$$Sh_{G,lam} = k_{G,lam}\frac{d_{eq,G}}{D_G} = 0.664 Sc_G^{1/3}\sqrt{Re_{G,rv}\frac{d_{eq,G}}{l_{G,el}}} \tag{2.67}$$

and

$$Sh_{G,turb} = k_{G,turb}\frac{d_{eq,G}}{D_G} = \frac{Re_{G,rv}Sc_G(\xi_{L,G}\phi/8)}{1+12.7\sqrt{\xi_{G,L}\phi/8}(Sh_G^{2/3}-1)}\left[1+\left(\frac{d_{eq,G}}{l_{G,el}}\right)^{2/3}\right] \tag{2.68}$$

With the dimensionless Reynolds and Schmidt numbers similar to the ones represented in the RBF-model (eq. 2.47 and eq. 2.48). With ϕ the V-shaped fraction of cross section of triangular channel occupied by liquid:

$$\phi = \frac{2S}{W_c + 2S} \tag{2.69}$$

and $\xi_{L,G}$ a very accurate explicit approximation of the liquid-gas friction factor for triangular flow channel:

$$\xi_{L,G} = \left(-2\log\left[\frac{\delta/d_{eq,G}}{3.7} - \frac{5.02}{Re_{G,rv}}\log\left(\frac{\delta/d_{eq,G}}{3.7}+\frac{14.5}{Re_{G,rv}}\right)\right]\right)^{-2} \tag{2.70}$$

The liquid mass transfer coefficient is the same one presented in equation 2.46. Olujić *et al.* [4] made extensive comparison of the currently available correlations and conclude that previous works base their effective interface area too much on behavior related to random packings. The correlation they propose was fitted on experimental data for the absorption of CO_2 in aqueous NaOH solutions:

$$\frac{a_e}{a_p} = \frac{1-\Omega}{1+\frac{A}{u_{L,s}^B}} \tag{2.71}$$

Where Ω is the void fraction of the packing surface (0.1 for structured sheet packings with holes) [60]. The constants A and B, in the correlation are packing specific. They are given for Montzpak B1-250: A=2.143 × 10^{-6}, B=1.5.

This model is mainly designed to predict mass transfer behavior in a pre-loading region and becomes less reliable in the loading region (although still on the safe side) [11]. Equation 2.71 shows this, since a_e is not dependent on hold-up (or gas flow rate).

Del Carlo, Olujić and Pagliant Del Carlo *et al.* [52] propose a new model (Del Carlo-model) for the evaluation of mass transfer in structured packings. They consider the interaction between the falling fluid film and the gas phase. Their research concluded that the fluid mechanics within a packing can be described by simple mechanistic models.

Del Carlo *et al.* [52] use the same equivalent diameter as proposed by Billet and Schultes (eq. 2.49). They mention that there is no satisfactory method to estimate the effective area for structured packing yet, and define an area based on experimental liquid hold-up values from previous absorption process studies. This hold-up, κ_L, is only valid for Mellapak packings, but Del Carlo *et al.* [52] also applied it

for the analysis of other packings,

$$\frac{a_e}{a_p} = \left(\frac{d_{eq}\sin\theta}{4\epsilon}\right)\kappa_L^{1.5}\left(\frac{\rho_L g}{3\mu_L u_{L,s}}\right)^{0.5} \tag{2.72}$$

With

$$\kappa_L = c_1 a_p^{0.83}(3600 u_{L,s})^{c_2}\left(\frac{\mu_L}{\mu_{L,0}}\right)^{0.25}\frac{1}{100} \tag{2.73}$$

Where c_1 and c_2 are constants depending on the liquid load, and $\mu_{L,0}$ is the viscosity of water at 20 °C. The calculations for the vapor-phase mass transfer coefficient, k_G, and the effective velocities $u_{L,e}$ and $u_{G,e}$ are similar to the one proposed by Rocha *et al.* [40] (eq. 2.45), except for the use of the equivalent diameter, d_{eq}, instead of the corrugation side, S, for characteristic length.

The liquid phase mass transfer coefficient that is used in this model is one that was suggested by Brunazzi and Paglianti [7], and is not based on the penetration theory, but on the film thickness δ:

$$k_L = c_3 \frac{G_z^{c_4}}{K_a^{c_5}}\frac{D_L}{4\delta} \tag{2.74}$$

With the dimensionless numbers for the film as,

$$Re_L = \frac{\rho_L(4\delta)\frac{u_{L,s}}{\kappa_L\sin\gamma}}{\mu_L} \tag{2.75}$$

and

$$G_z = Re_L Sc_L \frac{\delta\sin\gamma}{H_{el}} \tag{2.76}$$

and

$$K_a = \frac{\sigma^3\rho_L}{\mu_L^4 g} \tag{2.77}$$

With the effective liquid flow angle, $\sin\gamma$, and the constants c_3, c_4 and c_5 depending on the corrugation angle, as presented in table 2.3. The constants were defined by Brunazzi and Paglianti [7] specifically for MellaPak, and no research has been found to suggest that this can be applied to all types of structured packings. Shear stress can be neglected in Newtonian and laminar systems. This applies to the liquid phase in the OTWP system, and therefore the film thickness can be estimated from [7]:

$$\delta = \left(\frac{3\mu_L}{\rho_L g\sin\gamma}\frac{u_{L,s}}{\kappa_L\sin\gamma}\right)^{0.5} \tag{2.78}$$

Table 2.3: Constants of eq. 2.74 to eq. 2.78 for corrugated sheet packings, as suggested by Brunazzi and Paglianti [7]

Corrugation angle (deg)	45°	60°
c_3	16.43	16.43
c_4	0.915	0.915
c_5	0.09	0.09
γ (deg)	60	69

Hanley and Chen Hanley and Chen [41] developed, with Aspen Technology inc., new mass transfer correlations for Mellapak and FlexiPac. The expressions are derived from dimensionless analysis. They use the equivalent diameter as characteristic length. The correlations for the phase mass transfer coefficients that they deducted for both X (60 deg) and Y (45 deg) configured sheet metal structured

packings are:

$$k_L = 0.33 Re_L^1 Sc_L^{1/3} \left(\frac{D_L}{d_{eq}}\right) \tag{2.79}$$

and

$$k_G = 0.0084 Re_G^1 Sc_G^{1/3} \left(\frac{D_G}{d_{eq}}\right) \left(\frac{\cos\theta}{\cos(\pi/4)}\right)^{-7.15} \tag{2.80}$$

They originally defined a mass transfer coefficient based on mole fraction driving force, in this work their definition is divided by the molar concentrations of the gas and liquid to come to the expression above. Their definition for effective interface area is the following:

$$\frac{a_e}{a_p} = 0.539 Re_G^{0.145} Re_L^{-0.153} We_L^{0.2} Fr_L^{-0.2} \left(\frac{\rho_G}{\rho_L}\right)^{-0.033} \left(\frac{\mu_G}{\mu_L}\right)^{-0.090} \left(\frac{\cos\theta}{\cos(\pi/4)}\right)^{4.078} \tag{2.81}$$

The dimensionless numbers in the correlations by Hanley and Chen are calculated the same as in previous methods, with the characteristic length as specified in equation 2.49.

2.6. THE TWO-PHASE PRESSURE DROP

Most mass transfer models are accompanied by empirical relations to calculate the two-phase pressure drop. In this thesis we present the pressure drop correlations that will be compared in the Python model. The correlation that is most likely to give accurate predictions of the pressure drop in the selected structured packing, will be the empirical correlation that is developed by the packing supplier for that type. Most of those correlations are available in Aspen plus, and will be used in that model, but are not published, and therefore cannot be analyzed.

RBF The pressure drop, as calculated by Rocha *et al.* [5] is necessary to find the liquid hold-up iteratively, and already described in section 2.5.2. It is developed with a force balance on a channel model and fitted with empirical constants (for the air/water system).

Billet and Schultes Billet and Schultes [42] present a model where the two-phase pressure drop in the wetted column depends on the dry pressure drop, the hold-up, and the dry and wet resistance factors. The resistance factors, ξ_d and ξ_w depend on packing specific constants.

They use a Reynolds number that is based on particle diameter $d_{par} = 6(1-\epsilon)/a_p$,

$$Re_{G,par} = \frac{u_{G,s} d_{par} \rho_G}{(1-\epsilon)\mu_G} f_s \tag{2.82}$$

With f_s the wall factor,

$$\frac{1}{f_s} = 1 + \frac{4}{a_p * d_c} \tag{2.83}$$

With that Reynolds number, the resistance factor for the dry bed can be calculated,

$$\xi_d = C_P \frac{64}{Re_{G,par}} + \frac{1.8}{Re_{G,par}^{0.08}} \tag{2.84}$$

Where C_P is the packing specific constant. The dry bed pressure drop is then calculated with,

$$\frac{\Delta P_d}{\Delta z} = \xi_d \frac{a_p}{\epsilon^3} \frac{u_{G,s}^2}{2} \rho_G f_s \tag{2.85}$$

To calculate the two-phase pressure drop, a ratio between the wet and dry resistance factor is required. The wet resistance factor is described as follows,

$$\xi_w = C_P \exp\left[\frac{13300}{a_P^{1.5}}\left(\frac{u_{L,s}^2 a_p}{g}\right)^{1/2}\right]\left(\frac{\kappa_L}{\kappa_{L,lp}}\right)^{0.3}\left(\frac{64}{Re_{G,par}} + \frac{1.8}{Re_{G,par}^{0.08}}\right)\left(\frac{\epsilon}{\epsilon - \kappa_L}\right)^{1.5} \tag{2.86}$$

The liquid hold-up at loading point, $\kappa_{L,lp}$ is calculated with equation 2.50 and the liquid hold-up depends on the operating region. It is calculated with one of the hold-up equations presented in equation 2.50 to 2.52. This leads to the definition of the pressure drop inside the column,

$$\frac{\Delta P}{\Delta z} = \frac{\xi_w}{\xi_d}\left(\frac{\epsilon}{\epsilon - \kappa_L}\right)^3 \frac{\Delta P_d}{\Delta z} \tag{2.87}$$

The Delft-model Olujić [61] describes a pressure drop based on the geometrics of the packing. This means there is no need for packing specific constants. Additionally, the pressure drop takes the scale up factor (the column diameter, d_c) into consideration. This could prove to be a benefit when using the model to design a pilot-plant. He defines a pressure drop over the total packing height, H_p, as,

$$\begin{aligned} \Delta P &= \Delta P_{G,L} + \Delta P_{G,G} + \Delta P_{DC} \\ &= F_{load}(\zeta_{G,L} + \zeta_{G,G} + \zeta_{DC}) \frac{\rho_G u_{G,e}^2}{2} \end{aligned} \tag{2.88}$$

where the subscript $_{G,L}$ refers to pressure drop losses due to gas-liquid film surface interaction, $_{G,G}$ to losses due to gas-gas interaction, and $_{DC}$ to pressure drop losses associated with direction changes at the transitions between packing elements and the column wall.

The pressure loss factor for the gas-liquid interaction is defined as,

$$\zeta_{L,G} = \phi \xi_{L,G} \frac{H_p}{d_{eq,G} \sin\theta} \tag{2.89}$$

The wetted perimeter of the triangular gas flow (eq. 2.69), ϕ, equivalent diameter of the gas flow (eq. 2.63), $d_{eq,G}$, and friction factor between the gas and the liquid phase (eq. 2.70), $\xi_{L,G}$, have been previously defined. The pressure loss factor for the gas-gas interaction is defined as,

$$\zeta_{G,G} = (1 - \phi) \xi_{G,G} \frac{H_p}{d_{eq,G} \sin\theta} \tag{2.90}$$

with $\xi_{G,G}$ the gas-gas friction factor as,

$$\xi_{G,G} = 0.722(\cos\theta)^{3.14} \tag{2.91}$$

The overall pressure loss factor for direction changes, ζ_{DC}, is a function of the bulk zone friction coefficient, ξ_{bulk}, and the wall zone friction coefficient, ξ_{wall}. To relate those two, it is necessary to define

the fraction of flow channels in the structured corrugated packings that end at the column wall, χ, as a function of column diameter,

$$\chi = \frac{2H_{el}}{\pi d_c^2 \tan\theta}\left(d_c^2 - \frac{H_{el}^2}{(\tan\theta)^2}\right)^{0.5} + \frac{2}{\pi}\arcsin\left(\frac{H_{el}}{d_c \tan\theta}\right) \tag{2.92}$$

The pressure loss factor can then be expressed as,

$$\zeta_{DC} = \frac{H_p}{H_{el}}(\xi_{bulk} + \chi\xi_{wall}) \tag{2.93}$$

with,

$$\xi_{bulk} = 1.76(\cos\theta)^{1.63} \tag{2.94}$$

and,

$$\xi_{wall} = \frac{409u_{L,s}^{0.31} + 4715(\cos\theta)^{0.445}}{Re_{G,e}} + 34.19u_{L,s}^{0.44}(\cos\theta)^{0.779} \tag{2.95}$$

In this definition the pressure loss factors are physical balances of empirically fitted friction factors.

Hanley-model Hanley [62] defined a dimensionless two-phase pressure drop per unit packed height:

$$\left(\frac{\Delta P}{\rho_L g z}\right)_{2phase} = k_1 f_L^{(1-k_2\sqrt{f_L})}(k_3 - f_L)^{(-k_4)} \tag{2.96}$$

Here, the dimensionless pressure drop is a function of f_L: the fractional approach to flood at constant liquid loading. k_1 to k_4 are packing specific constants.

$$f_L = \frac{C_s}{\left(c_0(g d_{eq})^{1/4} Bo^{K_1} - m_0 Bo^{K_2}\sqrt{u_{l,s}}\right)^2} \tag{2.97}$$

He based this expression on the Wallis equation, and c_0, K_1, m_0, K_2 are its correlation parameters. C_s is the density corrected superficial vapor velocity, expressed as, $u_{G,s}\sqrt{\rho_G/(\rho_L - \rho_G)}$. Bo is the dimensionless Bond number,

$$Bo = \frac{\rho_L d_{eq}^2 g}{\sigma} \tag{2.98}$$

This expression for two-phase pressure drop in terms of the packing geometry and physical properties of the liquid is highly dependent on the availability and correctness of packing specific constants.

This chapter describes the condensation of atmospheric water in a direct-contact counter-current condenser column fitted with structured packings. Condensation is a combined heat and mass transfer process over an interface area. This area, and the rate of the process is difficult to predict and therefore is determined by correlations. Some of the main mass transfer coefficient correlations and their hydraulic relations were discussed. This work continues with the presentation of the models that are used to examine the suitability of the correlations in predicting the transport rates and the hydraulic behaviour of the experimental OTWP set-up.

3

METHODOLOGY

In this chapter the steps that are used to construct the Aspen plus and Python models of the OTWP column are discussed. The methodology to construct the models involves:

- Construction of an Aspen plus RadFrac model for previously selected random packing
- Validation of the Aspen plus model with previously done experiments
- Adapting the Aspen plus model for structured packing
- Selecting a structured packing
- Construction of a Python model for structured packing

The Aspen plus model and the Python model are described in the following two sections.

3.1. ASPEN PLUS MODEL

The commercial process simulator Aspen plus was used to developed a model that can evaluate the scalability of the Python model. First, it was used to select a structured packing for the experimental set-up by doing a preliminary analysis. Figure 3.1 shows the flow sheet of the final model.

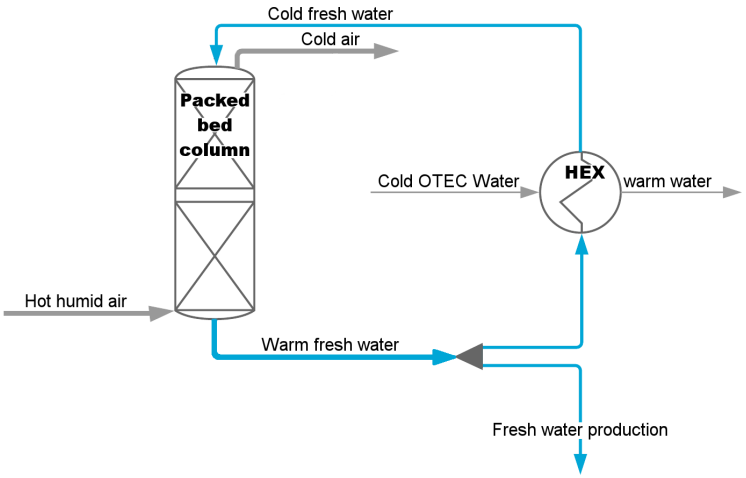

Figure 3.1: Flow sheet of the model used in Aspen plus

An overview of the approach used to develop the Aspen plus model is shown in figure 3.2, and the most important steps are outlined below.

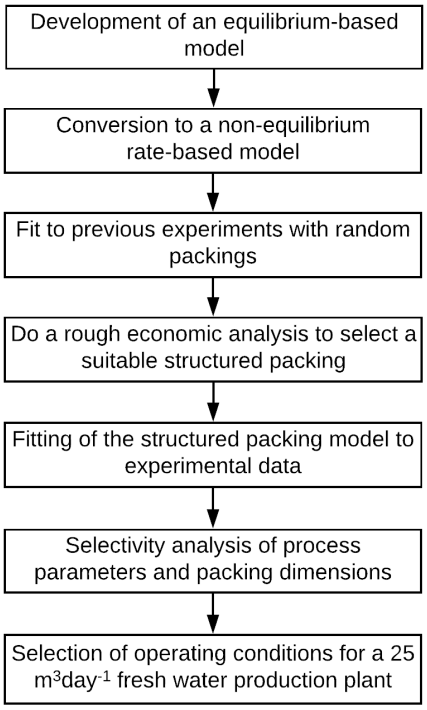

Figure 3.2: Overview of the Aspen plus model methodology

Initially, the column was simulated with a RadFrac module in equilibrium mode. The equilibrium mode requires input of: components, the feed conditions (thermal state, flow rate, and composition), the operating pressure, thermodynamic property model, and the configuration of the column (amount of equilibrium stages). The RadFrac module can be used for distillation or absorption columns. The OTWP simulation is run as a distillation column without reboiler, condenser or reactions. The cold stream containing fresh water is introduced at the top of the condenser, and the hot humid atmospheric air enters the condenser column at the bottom. The water stream that is fed to the top is saturated with air, to minimize the influence of air dissolving in the water.

The equilibrium method is flawed, since streams that leave a real stage are not in equilibrium. The amount of condensation that is achieved depends on the rate of mass transfer between phases, and this rate depends on how much they are not in equilibrium. Thus, the calculation method is changed to rate-based. In the rate-based model the physical dimensions of the column and its internals are provided. The column is initially modeled to the experimental set-up (with random packing). To make sure the rate-based simulation converges, the composition profiles that were generated in the equilibrium model are used as an estimate.

3.1.1. RANDOMLY PACKED COLUMN MODEL

To check if the RadFrac simulation for random packing performs adequately, it is modeled after previously performed experiments. It should be kept in mind that this step only serves the selection of a structured packing. Once a new packing is selected, the experimental set-up is updated, and the model and its performance is appropriately analyzed.

The column has a diameter of 24 cm and is filled with a generic 16 mm metal Pall ring, to a height of 113 cm. Table 3.1 shows the properties of the liquid and gas feed flow that are used for the model check.

Table 3.1: Feed properties for examination

	Pressure	Temperature	Flowrate	Composition
Gas feed	1 atm	28 °C	50 l s^{-1}	Variable
Liquid feed	1 atm	8 °C	0.075 l s^{-1}	$x_a = 1.57 \times 10^{-5}$
				x_w = 1-1.57 $\times 10^{-5}$

Since the behavior of the randomly packed bed column is only roughly analyzed, and pressure

drops in randomly packed beds are difficult to predict and not connected to the prediction of pressure drops in structured packings, the study is restricted to the heat and mass transfer. The mass transfer coefficient correlations for random packings that are available in Aspen plus include: Onda *et al.* [18], Billet and Schultes [42] and Bravo and Fair [38]. To show that the Aspen plus simulation makes a reasonable prediction of the heat and mass transfer behavior, the temperature profile in the column and the fresh water production are compared to previous experimental outcomes. In previous work it was determined that the temperature that is measured in the experimental set-up, is not the vapor or liquid temperature, but a a combination of both, close to the interface temperature [3]. This temperature is modeled in Aspen plus. The conditions of the feed flows and the packing settings are maintained constant, while the type of mass transfer coefficient correlation is varied to study their prediction of the temperature curve and production. Aspen plus uses Chilton and Colburn [56] for the heat transfer coefficient analogy.

Figure 3.3a to 3.3c show the interface temperature profile inside the condenser. The graphs show the experimental data and the simulated temperature profile for the different mass transfer coefficient methods. They depict variations in the predicted temperature profiles. Billet and Schultes [42] (fig. 3.3c) only has packing specific constants for Pall rings with a diameter of 25 mm (C_L = 1.440 and C_G = 0.336), yet it gives the best fitting temperature curve.

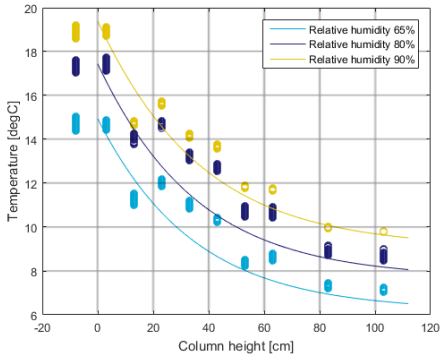

(a) Onda *et al.* [18] for 25 mm Pall rings

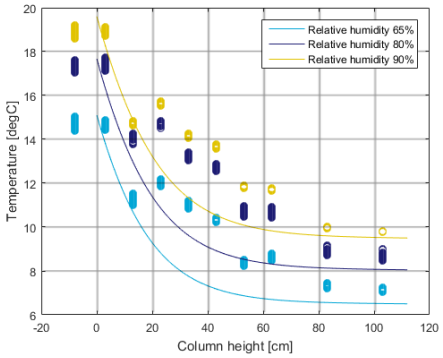

(b) Bravo and Fair for 16 mm Pall rings

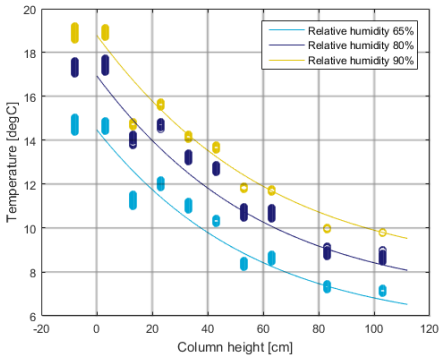

(c) Billet and Schultes for 25 mm Pall rings

Figure 3.3: Condenser temperature profile and humidity variation modeled with different correlations available in Aspen plus (experimental results from Bluerise B.V.)

To evaluate the predicted mass transfer, the production for air feed flows with different relative humidities measured by the experimental set-up and the Aspen plus model are compared. Table 3.2 shows the production that was simulated by Aspen plus and the two different productions that were obtained from the experiment. The first production is the measured increase of the liquid mass in the experiment (scale production), and the second is the production calculated from the mass balance over the experiment (mass balance production). In section 4.1.1 this will be discussed in more detail. For this analysis we will use the mass balance production. With table 3.2 and figure 3.3 we can conclude that the RadFrac column does not show any major errors in the heat and mass balance: it will be used to select a new type of packing for the experimental set-up.

Table 3.2: Simulated and experimented production values for different Relative humidity of air_{in}

RH of air feed	scale production	mass balance production	simulated production
65%	1.77 $\mathrm{kg\,hr^{-1}}$	1.95 $\mathrm{kg\,hr^{-1}}$	2.09 $\mathrm{kg\,hr^{-1}}$
80%	2.11 $\mathrm{kg\,hr^{-1}}$	2.39 $\mathrm{kg\,hr^{-1}}$	2.40 $\mathrm{kg\,hr^{-1}}$
90%	3.00 $\mathrm{kg\,hr^{-1}}$	3.32 $\mathrm{kg\,hr^{-1}}$	3.56 $\mathrm{kg\,hr^{-1}}$

3.1.2. PACKING SELECTION

A structured packing for the experimental set-up was selected with the Aspen plus model. The operational costs of the OTWP are expected to be the main influence on its economic feasibility, so a small pressure drop is desired, and the selection process focused on structured packings. Since the process is not vacuum, and extreme fouling and clotting is not expected, a corrugated sheet metal packing would be appropriate (see section 2.2.2). The selected packing should also be applicable in the pilot-plant and allow for low water production cost. To select a packing that meets these specifications, a sensitivity analysis and design requirement were set in the Aspen model and applied to all available sheet metal structured packings (in Aspen plus V8.8). Since this step is performed prior to the model validation and correlation selection (section 4.4), the Bravo et al. mass transfer coefficient correlation was used. Recall from section 2.5.2 that his method was designed for gauze like packings and assumes complete wetting. This is not realistic for sheet packings, but allows for a general comparison of the packings, without taking into account the highly correlation dependent interface area. Where possible, the packing manufacturers' correlation for pressure drop calculations were used, otherwise a generic pressure drop correlation was applied.

Table 3.3: Model parameters for packing selection

Fixed variable	Air flow	28.9 $\mathrm{kg\,s^{-1}}$
Design requirement	Production	25 $\mathrm{m^3\,day^{-1}}$
Variable	Height of column	0-4 m
Sensitivity analysis	Column diameter	3-6 m
	Water flow	19.4-41.7 $\mathrm{kg\,s^{-1}}$
Analyzed	Pressure drop (air flow energy requirement)	
	Pump head (waterflow energy requirement)	
	Packing investment cost	

Table 3.3 gives an overview of the parameters that were used for the packing selection. The production of the pilot-plant is fixed, and by fixing the temperature of the air exit flow (12.5 °C) the necessary

air feed flow (with a temperature of 28 °C and a RH of 80 %) is calculated to be 28.9 $kg\,s^{-1}$. The production is set as a design requirement, with the column height as variable. The water feed flow rate and the column diameter are set as variables in a sensitivity analysis.

A quotation of some of the better performing packings (per unit of volume) was acquired, and the pump head and necessary fan power calculated. This allowed for a rough economic analysis. A full description of this analysis can be found in appendix B. This resulted in the selection of a packing for the experimental set-up: FlexiPac 350X (also known as FlexiPac 1.4X) by Koch-Glitsch. Table 3.4 gives an overview of the packing characteristics and appendix C contains the datasheet.

Table 3.4: Packing characteristics

Manufacturer	Koch-Glitsch
Model	FlexiPac 350X / 1.4X
Material	Metal
packing specific area a_p	350 $m^2\,m^{-3}$
Corrugation angle θ	60°
Void fraction ϵ	0.985 [63]
Element height H_{el}	285 mm

3.1.3. STRUCTURED PACKED COLUMN

The RadFrac column of the Aspen plus simulation is fitted with two units of the FlexiPac 350X (285 mm each). To validate the prediction of the heat and mass transfer by the Aspen plus model, the available mass transfer coefficient correlations were applied. For sheet structured packing these include the Rocha, Bravo, and Fair model (RBF-model), Billet and Schultes model (BS-model) and the Hanley and Chen model (Hanley-model).

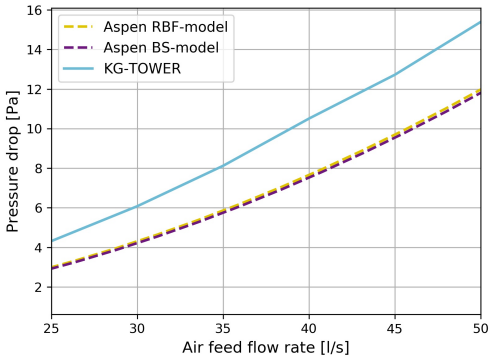

Figure 3.4: Pressure drop predictions by Aspen plus and KG-TOWER

The mass transfer coefficient correlations do not have defined packing specific constants for all packing types. For FlexiPac 350X it was necessary to select the constants of comparable packings. Unfortunately, Aspen plus does not allow manual input of variables in the Hanley-model, so it could not be used for the simulation. This correlations' performance will be evaluated with the Python model. Table 3.5 gives an overview of the packing specific constants that were used in the Python and Aspen plus models. For the BS-model the constants for FlexiPac 350Y [63] were used. The RBF-model uses generic constants for metal corrugated structured sheet packings. The packing geometry (corrugation width and length) was measured from the packing.

Koch-Glitsch communicated that Aspen plus uses the correlations they developed (Brigitte Willems, personal communication, August 30, 2017) but did not disclose the correlation. They do provide a program (KG-TOWER software V5.3) that simulates the pressure drop for different Koch-Glitsch packings. Figure 3.4 shows that the hydraulic calculations of Aspen plus and KG-Tower give a slightly different pressure drop, but follow the same trend. Both simulations will be used in the validation.

Table 3.5: Packing specific constants used to simulate FlexiPac 350X in mass transfer coefficient and pressure drop correlations

BS-model [42] FlexiPac 350Y		RBF(adapt)-model [40] Generic and measured		Hanley-model [41] FlexiPac 1X FlexiPac 1.6X		Delft-model [4] Montzpak B1-250		Del Carlo-model [52] MellaPak Y	
$C_L =$	1.165	$C_E =$	0.9	$k_1 =$	0.0040566	$A =$	2.143×10^{-6}	$\gamma =$	69°
$C_V =$	0.422	$F_{SE} =$	0.35	$k_2 =$	2	$B =$	1.5	$c_3 =$	16.43
$C_p =$	0.172	$W_{cg} =$	17.7 mm	$k_3 =$	1.03326			$c_4 =$	0.915
$C_{lp} =$	0.3157	$H_{cg} =$	7.0 mm	$k_4 =$	0.96498			$c_5 =$	0.09
$C_{fp} =$	2.464			$K_1 =$	−0.0318				
				$K_2 =$	−0.116				
				$c_0 =$	0.7518				
				$m_0 =$	1.305				

3.2. PYTHON MODEL

The Bluerise B.V. Python model of previous works [2][3] was consists of various modules: humidifier, heat exchanger, condenser, and pressure drop in pipes. This work covers the new condenser function, some adaptations in the other functions and the overall structure of the model. Figure 3.5 shows a schematic representation of the OTWP Python model. It consists of three functions: the condenser function, the heat exchanger (HEX) function and the power function that calculates the remaining pressure drops of the system and the energy requirements. The complete model allows for the analysis of the energy requirement per unit of water production. Only the condenser function will be validated with experiments. In the Python model, most temperature dependent properties of humid air and water are obtained from the thermodynamic property library Coolprop. The properties that are calculated from correlations are listed below:

- The water vapor saturation pressure, $P_v^{sat}(T)$ (The Buck equation)
- The self-diffusion coefficient of water, $D_L(T)$[64]
- The diffusion coefficient of water in air, $D_G(T)$[65]
- The surface tension of water, $\sigma_L(T)$[66]
- Latent heat of condensation, $l_v(T)$[67]

3.2.1. CONDENSER FUNCTION

The function that describes the physical phenomena in the condenser calculates, among others, the fresh water production and pressure drop of the column. It follows the theory described in section 2.4. It uses the Chilton and Colburn analogy as described in section 2.5.1, and applies the different correlation methods that are described in section 2.5.2 and section 2.6: BS-model, the RBF-model, the RBFadapt-model, the Delft-model, Del Carlo-model and the Hanley-model. Table 3.5 gives an overview of the packing specific constants that are used in these correlations to simulate FlexiPac 350X.

The condenser function models differential volumes over the height of the column (dz), starting at the bottom ($z = 0$). In each control volume new fluxes and temperatures are calculated as,

$$G_{(z+dz)} = G_{(z)} + G_a \frac{dw}{dz} dz \tag{3.1}$$

$$L_{(z+dz)} = L_{(z)} + G_a \frac{dw}{dz} dz \tag{3.2}$$

and

$$T_{(z+dz)} = T_{(z)} + \frac{dT}{dz}dz \tag{3.3}$$

The calculation of the counter-current flow properties follows an iterative process: Since the outcoming water temperature is unknown ($(T_L)_{z=0}$), an initial estimation is made. The calculations are performed for every differential volume, and the resulting calculated incoming water temperature at the top of the column ($(T_L)_{z=H_p}$) is compared to the actual water feed flow temperature. If this is outside of a pre-defined error margin (0.5 %), the estimate of $(T_L)_{z=0}$ is adapted, and all calculations are performed again. The same is done for the liquid flux, L. The output of the condenser function is the temperature of the fresh water exit flow, the temperature of the air exit flow, the RH of the air exit flow, the pressure drop over the packing and the production rate of the column.

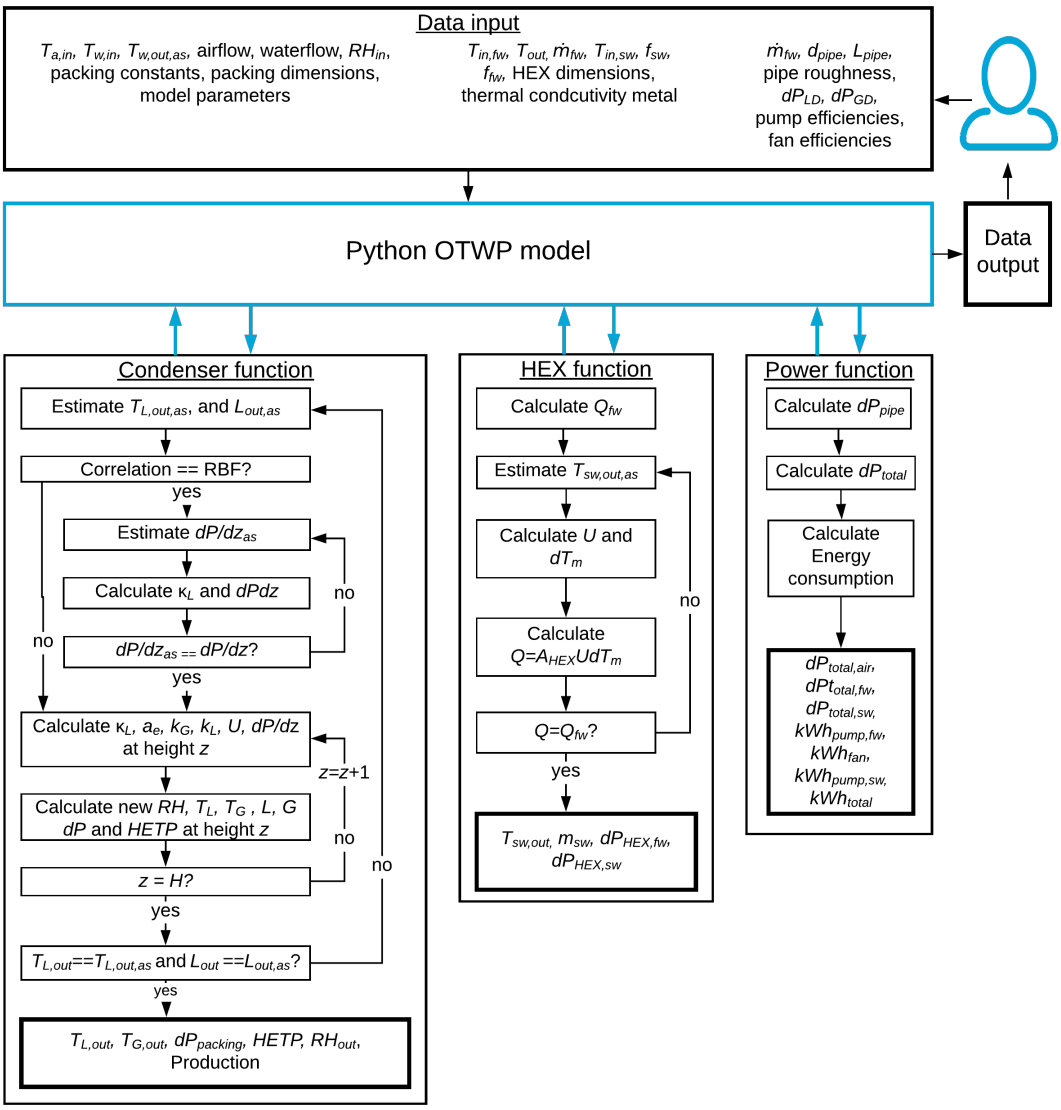

Figure 3.5: Schematic representation of the OTWP Python model

3.2.2. OTHER FUNCTIONS

The humidifier function calculates the amount of steam that has to be added to the experimental set-up to reach a desired humidity in the gas feed flow. Since the goal of this Python model is the design of a pilot-plant, the humidifier function is not useful and is removed from the overall model.

The heat exchanger (HEX) function of the Python model describes a plate HEX model that sets the dimensions of the HEX to then calculate the mass flow that is necessary on the OTEC side to get a cool fresh water loop of 12 °C. The model includes a pressure drop calculation and is adopted so the effect of a larger fresh water loop flow on the overall energy requirements can be included in the economic optimization. The description of the function can be found in appendix D.

The power function includes a calculation of the pressure drop in the pipes (appendix E). Additionally, the function uses the pressure drops (see fig. 3.6) to calculate the energy requirement per unit of fresh water production. Additional information is required on the pressure drop over the gas and liquid distributors (referred to as GD and LD in the figure), and the efficiency of the fan and the pump. These components are selected during the design of the pilot-plant.

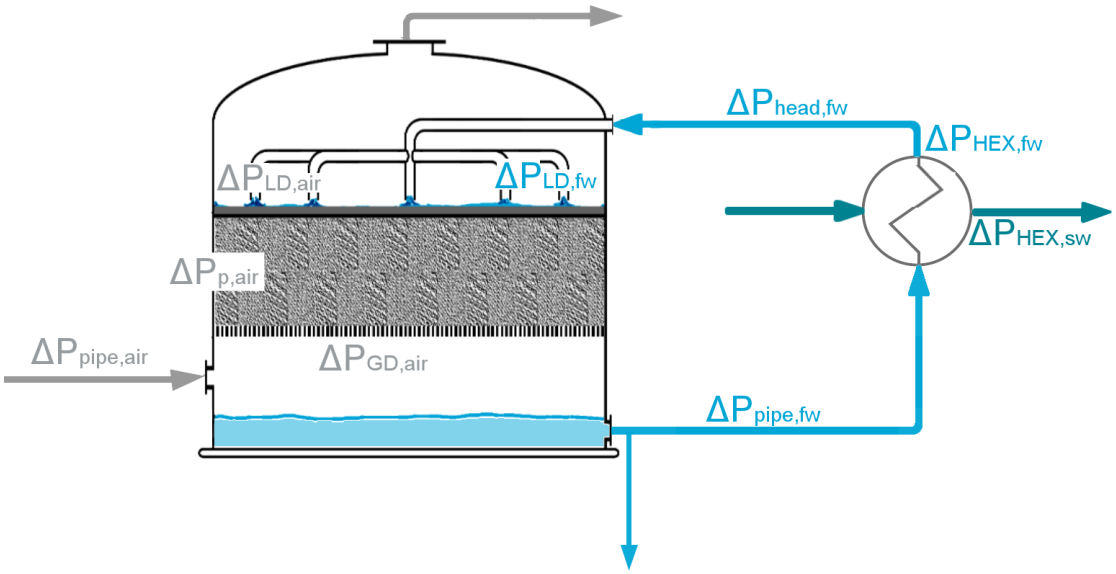

Figure 3.6: Overview of the pressure drops considered in the energy requirement (with GD and LD the gas and liquid distributors, and fw and sw the respective fresh and sea water flows)

This chapter describes the construction of the Aspen plus and Python model. The Aspen plus model was used to select the FlexiPac 350X as a structured packing for the condenser column. Additional to the condenser function the Python model calculates the HEX between the fresh water and the seawater, and calculates the pressure drops and energy consumption of the total system. In the next chapter the correlation that best predicts the behaviour in this packing is selected.

4

ANALYSIS AND VALIDATION OF THE MODELS

In this chapter the analysis and validation of the Aspen plus and Python OTWP models are discussed. The analysis of the models involved the following:

- Adapting the existing experimental set-up and analyzing its performance
- Defining a base-case within the range of the experimental set-up
- Comparing the predictions of the property profiles in the packing by the Aspen plus and Python models for the base-case
- Performing experiments
- Validating the Python and Aspen plus models against the experimental performance data
- The selection of the best fitting correlation for each model

The experimental set-up and its complications are described. A base-case is defined for comparison of model outcomes and experiments. The column profiles of both models are analyzed and compared for this base-case. The predictions by the models are evaluated with experimental results. Finally, a correlation is selected for each model, which will be used for the pilot-plant design in the next chapter.

4.1. EXPERIMENTAL SET-UP

The OTWP experimental set-up in the Process & Energy lab of the Delft University of Technology is shown in figure 4.1. The OTWP set-up is connected to the OTEC test facility. It is used to measure the condensation of water vapor from hot humid air and is comprised of three main units: the condenser column, the heat exchanger (HEX), and the tropical air generator (TAG). These three units contain seven main components: a water pump for the waterflow on the OTEC

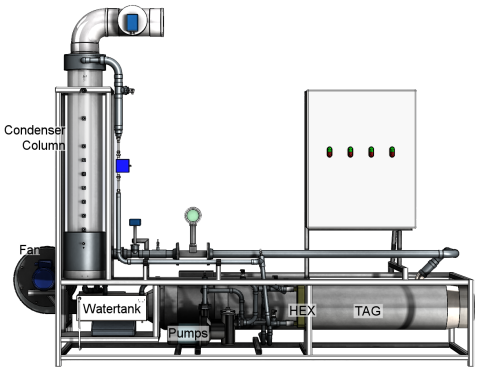

Figure 4.1: A render of the Bluerise B.V. experimental set-up

side of the HEX, a water pump for the fresh water loop, a plate HEX, the water tank, a condenser column filled with structured packings, and the TAG (consisting of a heater and a steam valve).

The condenser column has an inner diameter of 24 mm, and was initially packed with 113 cm of stainless steel Pall Rings of 16 mm as selected by Lopez [2]. For this thesis it was replaced by two units of FlexiPac 350X. There is no gas distributor, as the column diameter is small enough for proper gas distribution. The liquid distributor is a cross shaped showerhead. Different spray nozzles were tested, but all resulted in a large liquid flow on the sides of the column.

The atmospheric air conditions of Curaçao are recreated in the TAG, where steam is added to dry, cold atmospheric air, and the air is heated to a desired temperature, creating hot humid air. This hot humid air is fed to the bottom of the condenser column. The temperature, humidity and mass flow of this feed stream are measured, as are the pressure, mass flow and temperature of the fresh water feed flow. The fresh water flow is fed to the top of the column. Inside the column, the gas and liquid flows are in direct contact.

Figure 4.2 shows that the temperature gradient in the column is measured by the thermal sensors TT-02 to TT-11. The pressure drop over the column is measured with a differential pressure drop sensor, PT-11. The humidity and temperature of the outgoing vapor flow are measured, TT-17 and HT-02, as is the temperature of the outgoing liquid flow, TT-14. The tank that is used for the fresh water loop is weighted, MT-01, and the increase over the duration of the experiment should provide a production in unit of weight over time. A full schematic overview of the OTWP and OTEC experimental facility can be found in appendix F.

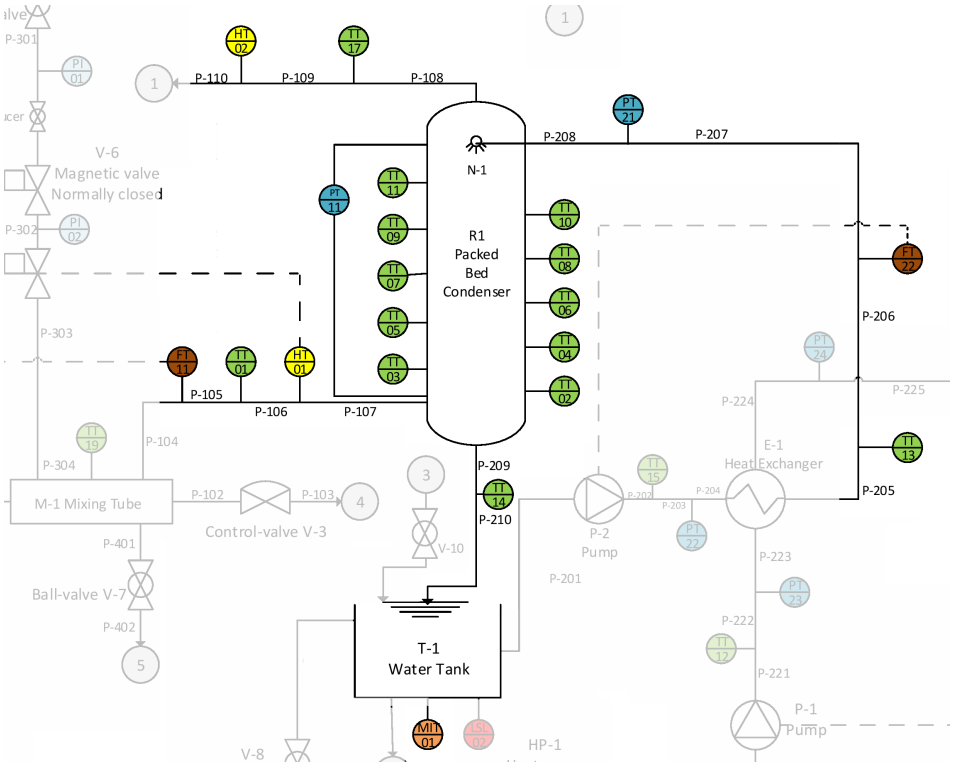

Figure 4.2: Schematic diagram. With TT, PT, HT, FT and MT the temperature, pressure, humidity and mass flow transmitters, and the scale respectively

Table 4.1 gives an overview of the sensors in the experimental set-up that are used for the model performance evaluation. Not all sensors give stable measurements, and some complications were encountered that could not be solved over the duration of this thesis.

Table 4.1: Available data for the column and conditions of the feed and exit flows

	Temperature	Humidity	Pressure	Mass flow	Mass
Air feed flow	TT-01[1]	HT-01[1]		FT-11[1]	
Water feed flow	TT-13[1]		PT-21	FT-22[1]	
Air exit flow	TT-17[2]	HT-02[2]			
Water exit flow	TT-14[2]				
Inside column	TT-02 to TT-11 [3]		(ΔP) PT-11[2,3]		
Production					MT-01[2,3]

[1] Used for control [2] Used for validation [3] Unstable measurements

4.1.1. COMPLICATIONS

The temperature sensors in the column do not give a gradual temperature profile, the measurements of the pressure differential transmitter (PT-11) are unstable, and the weight measured by the scale (MT-01) does not correspond with the mass balance over the column. This section discusses the causes and potential solutions.

COLUMN PRESSURE DIFFERENTIAL TRANSMITTER PT-11

The pressure drop over the column is essential for optimization, thus important to validate. Unfortunately, the pressure drop measurements are not repeatable and thus unreliable.

The pressure drop measurements fluctuate over time and per experiment. It seems unlikely that the actual pressure drop in the column is subject to such large variations. Initially, it was thought that the range of the pressure drop sensor that was used (Jumo 404304, range 0-1000 Pa) was too large to predict the pressure drop in the structured packing (expected pressure drop is around 20 Pa for two packing elements, see fig. 3.4). A new pressure differential transmitter with a much smaller range (Jumo 404304, range 0-160 Pa) was installed, but resulted in similar behaviour.

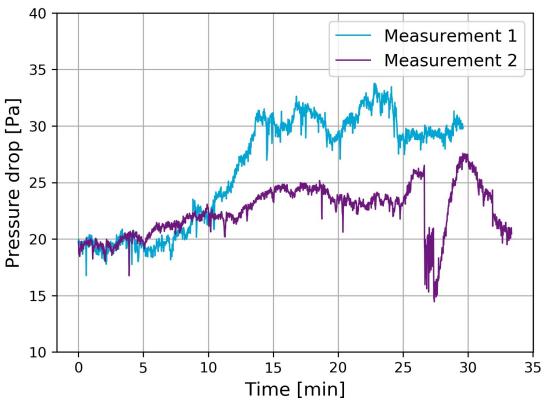

Figure 4.3: Pressure drop of two similar measurements

Figure 4.3 shows two examples of the new pressure drop sensor output over time, with the same experiment conditions. The relative fluctuation of these pressure drops is very high. Since the sensor is connected at the top and bottom of the column with small diameter tubes, one possible explanation is that (one of) the tubes gets covered with a water droplet. This might be solved by connecting the pressure drop sensor with larger diameter tubes to the condenser column, to prevent water droplets from completely covering them. The duration of this thesis did not allow for another re-installation and evaluation of the pressure sensor; For this thesis the mean value of the pressure differential measurement over the time of the experiment is taken.

WATERTANK SCALE MT-01

Since the fresh water pump circulates a constant mass flow, the weight of the watertank is a measure for the fresh water production. This is shown by a simple mass balance over the column,

$$\dot{m}_{L,in} + \dot{m}_a \omega_{in} = \dot{m}_{L,in} + \text{Production} + \dot{m}_a \omega_{out} \tag{4.1}$$

All parameters of humid air can be determined if any two are known under constant pressure (see section 2.1). The pressure variation in the column is so small, it has little to no effect on the thermodynamic properties of air and can be ignored. Since the temperature and RH of the air in the feed flow and exit flow are known, the humidity ratio at those locations can be determined (eq. 2.4). Rearranging the mass balance (eq. 4.1) shows that the fresh water production should be,

$$\dot{m}_a(\omega_{in} - \omega_{out}) = \text{Production} \tag{4.2}$$

By applying this balance to the experimental data, summing the calculated production at every measurement point and dividing it by the duration of the experiment, the production rate (mass balance production) can be calculated.

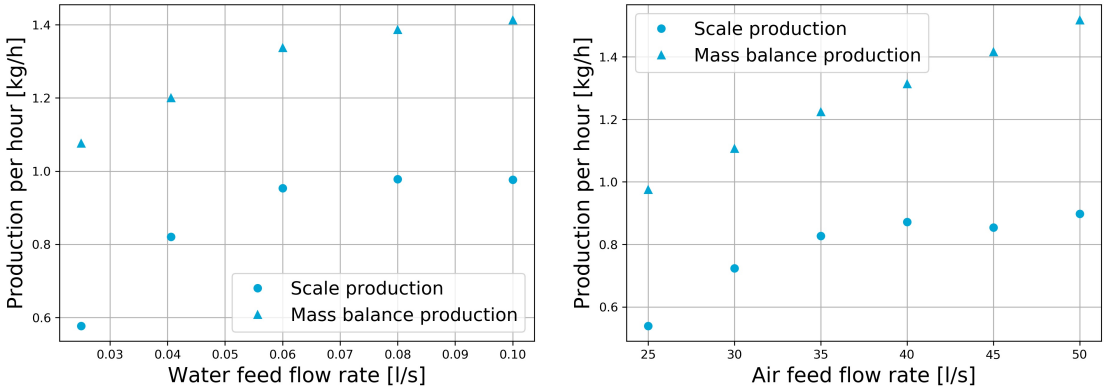

(a) Calculated and measured production over water feed flow rate

(b) Calculated and measured production over air feed flow rate

Figure 4.4: Unbalance between properties of air feed and exit flow, and the scale measurement

Figure 4.4 shows how this mass balance production deviates from the output of MT-01 (scale production), for various air and water feed flows. Potential causes are outlined below and ruled out where possible. As the cause of the deviation could not be determined, the mass balance production will be considered correct for the validation of this work.

Scale output A liter of water was added to the scale, and the output of MT-01 increased by one kilogram. Additionally, volume checks were performed while experiments were running to eliminate the influence of time or vibrations on the scales' output. In these tests the increase in water mass that was detected was equal to the increase in water volume.

Leakage in the system Since the difference between the mass balance production and the scale production is significant (in some cases more than $0.5\,\mathrm{l\,h^{-1}}$), it should be possible to visually determine an external leakage. An internal leakage could only take place in the HEX, since this is the only location where the fresh water flow is connected to the OTEC system. An internal leakage was ruled out by making sure the pressure on the OTEC side of the HEX was higher than the pressure on the OTWP side of the HEX. This did not eliminate or reduce the unbalance in the column.

Finally, the experiment was run without an air flow. If there is a leakage, the content of the water tank should still reduce. Figure 4.5a shows little to no variation in scale output, hence, there is no leakage in the fresh water loop.

Entrainment Water could also leave the system at the gas discharge through over-saturation of the air, or when the gas flow is large enough to entrain the liquid. Both those options seem unlikely, since the humidity sensor that measures the air exit flow does not reach 100 %, and the air flow rate is relatively low (not close to loading point). But, to rule out entrainment, a 'coffee filter test' was performed: a coffee filter was placed in the air vent and removed after experiments. The coffee filter appeared dry, meaning no water leaves the system through the air vent.

Temperature sensors Since no leakage was detected, and the scale output was validated, it follows that one of the sensors gives an incorrect output. To make sure the temperature sensors work correctly they were calibrated with new reference sensors. Since the condenser column is a two-phase system (in direct contact), it is difficult to determine if the temperature sensors register the gas or liquid temperature. The sensors that are used in the feed and exit flows are only in contact with a single phase. It is possible that condensation forms on the temperature sensors, in which case the measured temperature would not be the dry bulb temperature, but something closer to the wet bulb temperature. Since the air is close to saturation in the air exit flow, those two temperatures would be almost the same. In the air feed flow, a temperature closer to the WBT would always be lower (eq. 2.6). If the actual humid air temperature would be higher than the measured humid air temperature, the difference between the scale production and mass balance production would be larger, not smaller. Hence, error in production measurements caused by the condensation on the temperature sensors is unlikely.

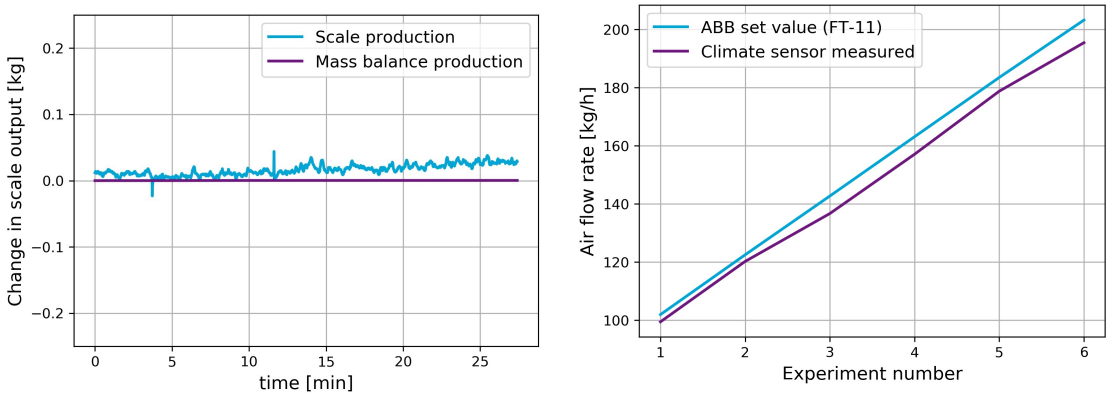

(a) Production without airflow

(b) The set airflow and the measured airflow

Figure 4.5: Validation of the scale measurement and the ABB air flow sensor

Humidity sensors The humidity sensors have been checked by Noordhoek Hegt [3], right before the start of this research, and are assumed validated.

ABB vortex flow meter FT-11 The air flow sensor FT-11 is a vortex flow meter, and its output was validated by measuring the velocity of the exiting air. A climate sensor was placed in the center of the air discharge pipe, to measure the maximum air velocity. With a maximum air velocity in a pipe, the average velocity can be calculated according to,

$$u_G = u_{G,max} \frac{2n^2}{(n+1)(2n+1)} \tag{4.3}$$

with,

$$n = -1.7 + 1.8 \log Re_{G,umax} \tag{4.4}$$

From the average velocity, and the temperature measured with TT-17, the density and thus mass flow can be calculated. This allows for a rough validation of the flow sensor FT-11. Figure 4.5b shows the relation between the set flow (FT-11) and the flow that is measured in the air discharge pipe, for different experiments. The air exit mass flow is expected to be a bit lower, since this validation does not account for the mass flow reduction due to water production.

Evaporation from the watertank Although the tank water is colder than the surrounding temperature, the humidity is also low, and there is a driving force for evaporation (see fig. 2.1). Additionally, this would explain the increase in mass balance production with air flow rate (higher air flow rates result in higher tank water temperatures, fig. 4.4b), and the lower difference in mass balance production and scale production that was registered in the validation of the random packing (these experiments had lower temperature water feed, table 3.2). A rough prediction of tank water evaporation was made with the following assumptions,

- The surrounding air temperature in the building is 18 °C with an RH of 50 %
- The temperature of the water in the tank varies between 16 and 21 °C
- The air in the building is still
- The movement of the water has no effect on the surface area of the water tank
- The water surface in the tank is square shaped with a width and length of 0.4 m

The evaporation from the water tank can be approached as a natural-convection problem. Approximated expressions for the mass transfer conductance G in kg m^{-2} s^{-1} from a cooled and heated (squared) surface respectively, with characteristic length l_0 =0.4 m, facing up are [65],

$$G_{cond} = \frac{\mu_G}{Sc\, l_0} 0.82 (GrPr)^{1/5} \tag{4.5}$$

$$G_{cond} = \frac{\mu_G}{Sc\, l_0} 0.14 (GrPr)^{1/3} \tag{4.6}$$

with Gr the Grashoff number for general characteristic length l_0,

$$Gr = \frac{g l_0^3 \Big((\rho_G(T_G) - \rho_G(T_L) \Big) / \rho_G}{(\mu_G / \rho_G)} \tag{4.7}$$

The properties of air are taken at an average between the external gas temperature T_G and the gas temperature at the water surface T_L. For a Schmidt number of 0.61 (water/air) and a Prandtl number of 0.69 (pure air) figure 4.6 shows that the roughly estimated evaporation is large enough to explain the difference in scale production and mass balance production. This could be solved by closing off the water tank in the experimental set-up.

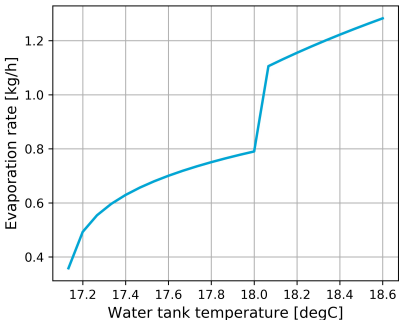

Figure 4.6: A rough estimate of the evaporation from the water tank over tank water temperature

4.2. BASE-CASE

Prior to the model performance validation, a base-case was defined and evaluated. For the validation, it is important that the base-case falls within the range of the experimental set-up and that it complies with the feed conditions of the pilot-plant. Table 4.2 gives an overview of the base-case feed conditions. The air feed flow temperature and humidity are determined by the atmospheric conditions of the Caribbean, and set to a relative humidity of 80 % and a temperature of 28 °C. Since Bluerise B.V. expects that the waste sea water flow that leaves the OTEC plant will have a temperature between 10 and 12 °C [3], the temperature of the liquid feed (fresh water) is set to 12 °C. The limiting variable of the experimental set-up is the gas feed flow rate. The fan of the set-up has a range of 22 to 50 $l\,s^{-1}$. This is a relatively low flow rate for a column with a 24 cm diameter (maximum gas velocity of 1.1 $m\,s^{-1}$). The gas feed flow rate is taken in the middle of this range, as 35 $l\,s^{-1}$. Since the ratio between gas feed flow rate and liquid feed flow rate has a large influence on the performance of the column, this is taken as 1 for the base-case, giving a volumetric fresh water feed flow of 0.0406 $l\,s^{-1}$.

Table 4.2: Feed flow conditions for the base-case

	Pressure	Temperature	Flow rate	Relative humidity
Gas feed	1 atm	28 °C	35 $l\,s^{-1}$	80 %
Liquid feed	1 atm	12 °C	0.0406 $l\,s^{-1}$	-

In the previous section it was discussed that the experimental set-up allows for the reliable measurement of the feed and exit flow conditions but does not provide constant measurements of the profile conditions. Although the model profile predictions of the column variables cannot be validated with experiments, it is interesting to study the differences between the Python and Aspen plus models.

To allow for a closer comparison of the mass transfer coefficient and pressure drop correlations, and to get an insight in how the Aspen plus and Python simulations perform relative to each-other, the profiles of the main properties of the base-case over the height of the packing are analyzed. The bottom of the packing is taken as $H = 0$ m, and the top of the packing as $H = H_p$. The results of the profile comparison are outlined below and include: temperature profiles, mass flow profiles, pressure drop, and efficiency profiles.

Heat transfer Figure 4.7 shows the change of the liquid and gas temperature over the height of the packing. Figure 4.7a shows that most of the correlations predict a comparable liquid and gas temper-

ature profile. The Python RBF-model and BS-model have similar predictions to the respective Aspen RBF-model and BS-model. Both RBF-models deviate significantly from the predictions of the other correlations. For the gas phase (see fig. 4.7b), the heat transfer of the Hanley-model is much faster. The BS-models, Delft-model and RBFadapt-model show very similar predictions.

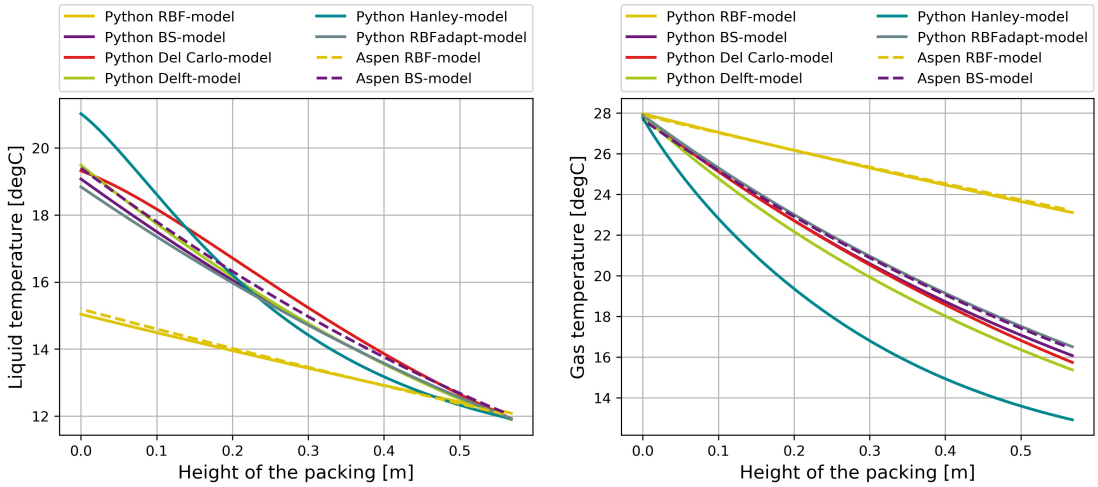

(a) Liquid temperature over packing height

(b) Gas temperature over packing height

Figure 4.7: Temperature profiles in the packing for all correlation models

Mass transfer The mass transfer in the packing is represented by the increase in liquid mass flow rate (at $H = 0$ this equals the predicted production). The Hanley-model in figure 4.8a also shows a faster mass transfer rate. The RBF-models show, like the heat transfer, a much smaller mass transfer rate. The mass transfer profile of the Python BS-model and the Aspen BS-model shows some difference, but a similar production. The relative humidity profiles are shown in figure 4.8b. A variation in RH does not allow for assessment of production without the corresponding air temperature (see fig. 2.1). Most correlations predict saturation of the air at the column exit, but since they predict different temperatures (fig. 4.7b) the simulated production varies.

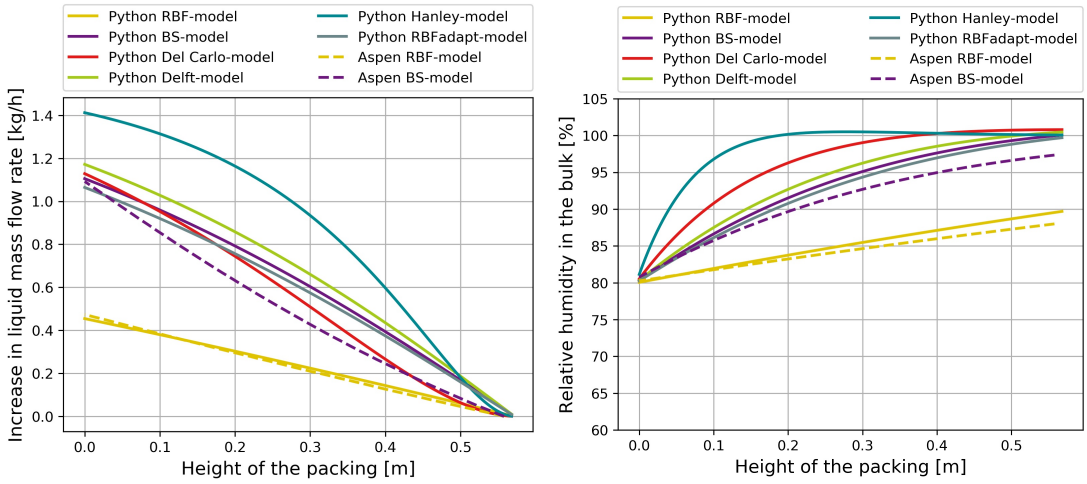

(a) Increase in liquid mass flow rate

(b) Relative humidity over packing height

Figure 4.8: Humidity and liquid mass flow rate profiles over the packed bed height

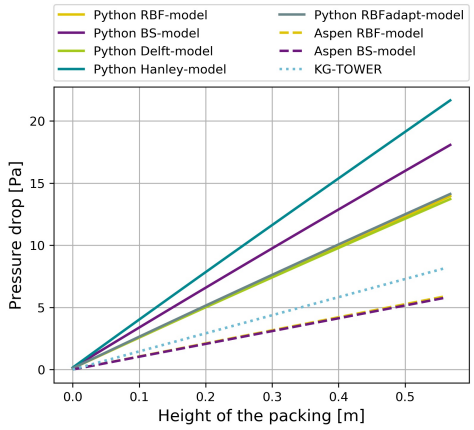

Pressure drop The Aspen model predicts the same pressure drop for both mass transfer coefficient correlations, since it applies the same pressure drop correlation in both models: the correlation provided by Koch-Glitsch, the packing developer. The pressure drop simulations of the other correlations diverge significantly from this prediction. The Del-Carlo correlation does not include a pressure drop prediction, and the KG-TOWER software uses an equilibrium method, and thus does not provide profile information.

Figure 4.9: Pressure drop over packing height

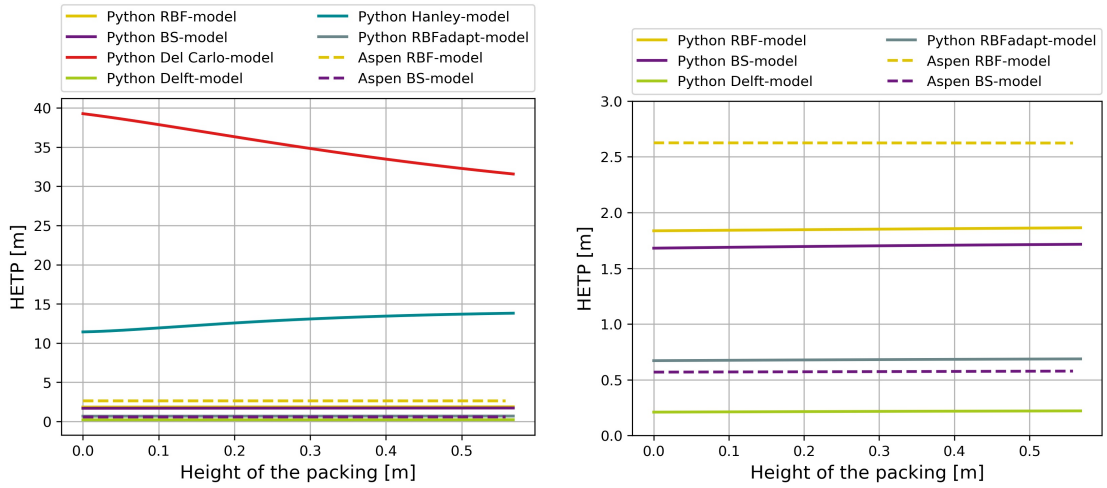

(a) HETP over column height

(b) zoom-in HETP over column height

Figure 4.10: Height equivalent to plate over column

Efficiency The efficiency in the packing represented by the HETP. A higher HETP means a higher packing efficiency. The predicted packing efficiencies vary significantly for the different correlations, and between the Aspen plus and Python models.

The difference between the predictions by the RBF-models and the other correlations can be explained by a significantly smaller predicted interface area, resulting in a smaller heat and mass transfer. This explains why the profiles predicted by the RBFadapt-model are much more in agreement with the other correlations (these have larger interface areas due to the assumed smaller contact angle, see section 2.5.2). Similar predictions by the Aspen plus and Python models with the same correlations suggest a comparable heat and mass balance. The minor differences could be explained by the use of different temperature dependent variables and the diffusion of air in the water (considered by Aspen plus, not by Python). Although the relative variations in pressure drop predictions are large, in absolute numbers the variation, 15 Pa, is small. The predicted packing efficiencies of the Aspen plus and Python model do not correspond to each-other. Since the HETP cannot be evaluated with the current experimental set-up, a proper packing efficiency analysis could be considered as part of future work.

4.3. MODEL VALIDATION

To validate the models, their performance is compared to experimental values. The influence of variables on the exit flow properties, the production, and the pressure drop have been measured with the experimental set-up. Table 4.3 gives an overview of the experimental variables and how they are used in the validation. The influence of three different variables is examined:

1. The volumetric air feed flow rate of the experiment is varied from 25 l s^{-1} to 50 l s^{-1}. The other input variables are kept constant. Since the liquid feed flow rate remains the same, the change in air flow rate leads to a varying liquid to gas feed ratio (L/G) of 1.4 to 0.7.
2. The volumetric water feed flow rate is varied from 0.02 l s^{-1} to 0.08 l s^{-1} with the air feed flow rate constant at 35 l s^{-1}.
3. Since atmospheric relative humidity has a large influence on the production, it is interesting to examine if the models predict production accurately for feeds with varying RHs. The RH is varied from 60 to 90 %.

Table 4.3: Validation variables

Independent variables		Dependent variables	Controlled variables
Air feed flow rate	25 to 50 l s^{-1}	T_G of air exit flow	T_G of air feed flow
Water feed flow rate	0.02 to 0.08 l s^{-1}	T_L of water exit flow	T_L of water feed flow
RH of the air feed flow	60 to 90 %	RH of the air exit flow	
		Production	
		Pressure drop	

The results of the Aspen plus and Python model validations are presented in three sections: Heat transfer, Mass transfer and Pressure drop.

Heat transfer Figure 4.11 shows the influence of the three independent variables on the exit flow temperatures. Figure 4.11a and figure 4.11b show that for smaller gas feed flows the temperature of the water exit flow is lower, as is the temperature of the exit air flow (there is less hot air, so less heat in the column). Figure 4.11c and figure 4.11d show an opposite trend for the water feed flow rate. Figure 4.11e and figure 4.11f show that an increase in relative humidity causes an increase in the exit water flow temperature, but has no effect on the exit air flow temperature. This is expected, as the condensation of more hot water vapor from the air will cause a temperature rise in the liquid flow.

All graphs in figure 4.11 show that the experiments have a slightly lower heat transfer than predicted by most correlations. This is to be expected, as the models assume a perfect liquid distribution, which is not achieved in the experiment. The Hanley-model predicts the largest heat transfer, and the RBF-models the smallest. Equation 2.80 shows that the Hanley-model has a larger Reynolds exponent than the other correlations (1 instead of ~0.8). Since the heat transfer coefficient is related through an analogy to the mass transfer coefficient, this explains the higher transfer rates. The RBF-models' slow transfer rate can be explained by a smaller interface area. It can be seen that the adaptation of the model, with the decreased water contact angle (section 2.5.2), performs better. According to the graphs the BS-models, the Delft-model, the Del Carlo-model and the RBFadapt-model all have a decent prediction of the exit flow temperatures and follow the trend over the variables well.

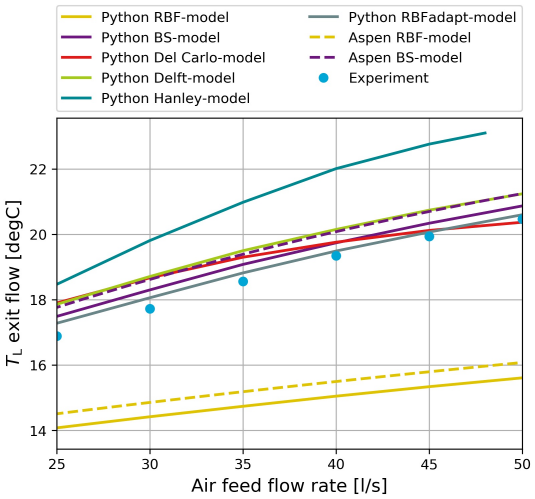

(a) $(T_L)_{H=0}$ over volumetric water feed flow rate

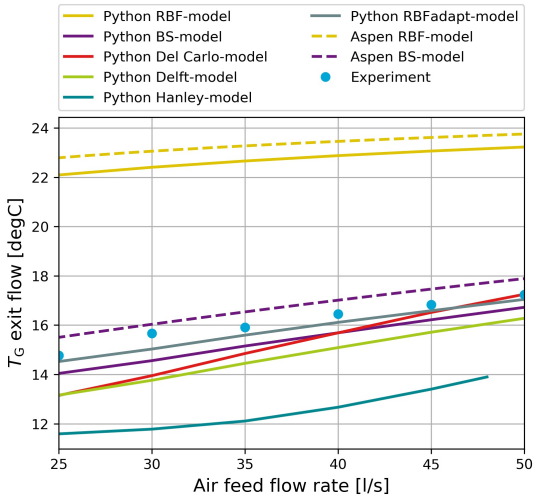

(b) $(T_G)_{H=H_p}$ over volumetric liquid feed flow rate

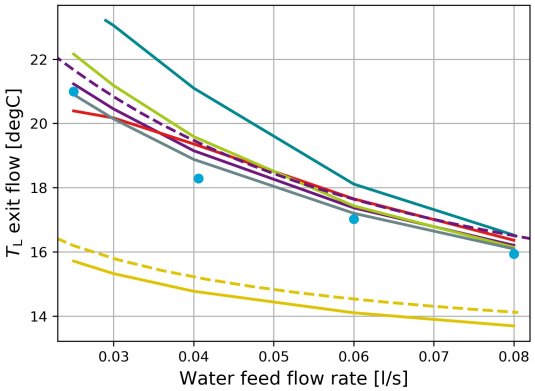

(c) $(T_L)_{H=0}$ over volumetric air feed flow rate

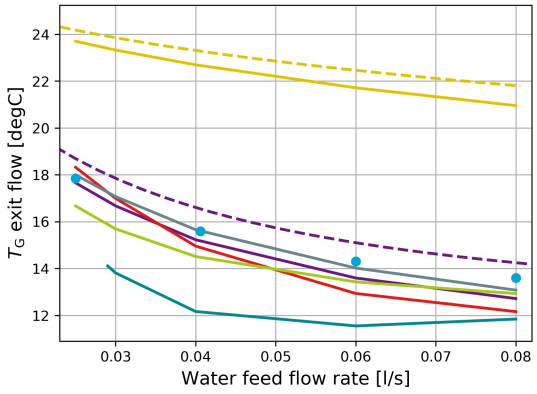

(d) $(T_G)_{H=H_p}$ over volumetric air feed flow rate

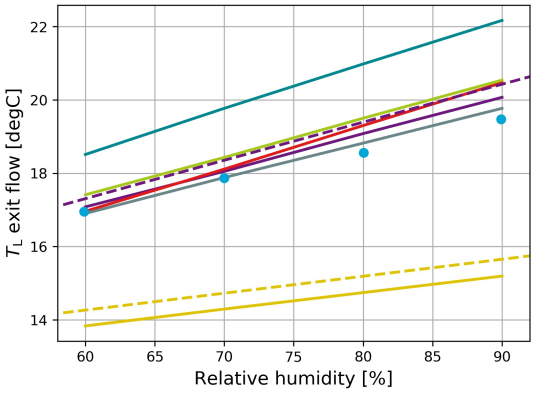

(e) $(T_L)_{H=0}$ over the RH of the air feed flow

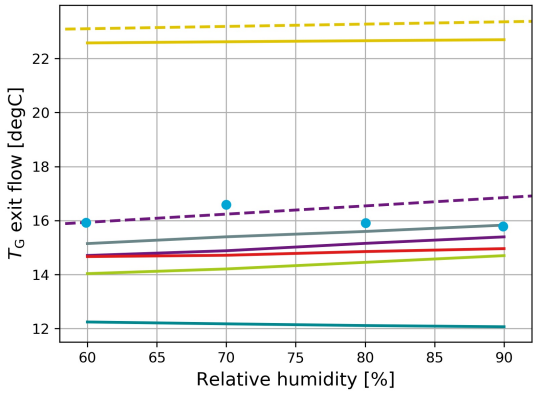

(f) $(T_G)_{H=H_p}$ over the RH of the air feed flow

Figure 4.11: The predicted and measured temperatures of the exit flows over the independent variables RH, air feed flow rate and water feed flow rate

Mass transfer To evaluate the mass transfer, the predictions of the relative humidity of the exit flow and the production are studied. The production of the experimental set-up is calculated from the mass balance, as presented in equation 4.1. This means that a correct prediction of the air exit flow temperature and humidity results in an accurate prediction of the fresh water production. Figure 4.12 shows the predicted and measured relative humidity and production over the independent variables.

Figure 4.12a, 4.12c and 4.12e show that, except for the RBF-models, the measured relative humidity is mostly lower than the predicted relative humidities. This could be explained by the position of the humidity sensor: the humidity sensor is located at the top of the condenser column, above the packing. Figure 4.11b, 4.11d, and 4.11f show that the exit air temperature is lower than the previously assumed surrounding air temperature in the lab (around 18 °C). This means it is possible that the air heated up between the packing and exit air flow temperature sensor (TT-17), which would result in slightly lower relative humidity.

The water feed flow rate has a large influence on the production. Figure 4.12b, 4.12d, and 4.12f suggest that a higher L/G ratio will be beneficial for production. The relative humidity of the feed flow has a linear relation to the production. The individual model predictions for the mass transfer show similar behaviour as they did for the heat transfer. The RBF-models underpredict the mass transfer (due to the small interface area prediction), the Hanley-model overpredicts the mass transfer, and the other models all show a similar prediction, close to experimental outcomes.

Pressure drop Although, as mentioned before, the pressure measurements of the experimental set-up were subject to complications, they are assumed reasonable in this section. Figure 4.13 shows the pressure drop predictions and experimental results over the independent variables. The pressure drops measured in the experimental set-up are higher than predicted by any of the models. One possible explanation is that there are additional pressure drops in the column, for example caused by the liquid distributor and the friction of the column walls between the pressure sensor measure point and the top of the packing. Figure 4.13b shows that if these additional pressure losses together are assumed 10 Pa, the experimental values and the model predictions are in better agreement for varying air feed flow rates.

The relative humidity of the air feed flow and the water feed flow rate were not expected to have a noticeable influence on the pressure drop under these operating conditions (pre-loading region). Figure 4.13c and figure 4.13d show that experiments with a higher RHs in the air feed, or with higher water feed flow rates, display larger pressure drops. For this work, these outcomes are assigned to measurement fluctuations. A larger experiment database and/or an improved experimental set-up should establish if these trends are repeatedly observed.

The software of the packing manufacturer, KG-TOWER, makes a more optimistic pressure drop estimation than the other models. The larger range of the air feed flow rate in figure 4.13b shows that it predicts the same pressure drop progression as the RBF-models, RBFadapt-model and the Delft-model. The BS-model makes a significantly different prediction. In the experiments' operating range it seemed to have a better prediction of the pressure drop over air feed flow rate (fig. 4.13a), but figure 4.13b shows that over larger air flow rates it increases more rapidly than the other models. The Hanley-model predictions are close to the experimental value (highest) but show an unexpected linear relation to the independent variables.

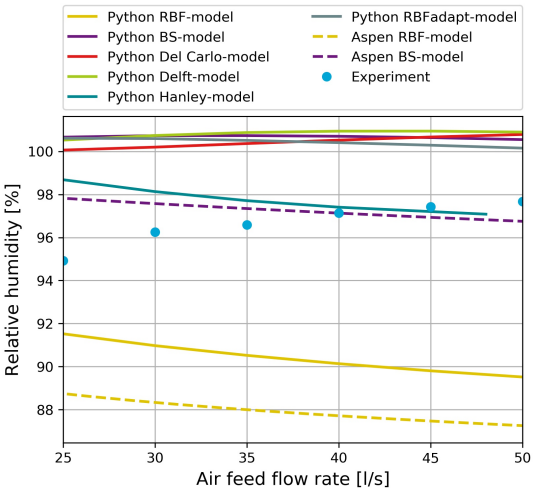

(a) RH of the exit air flow

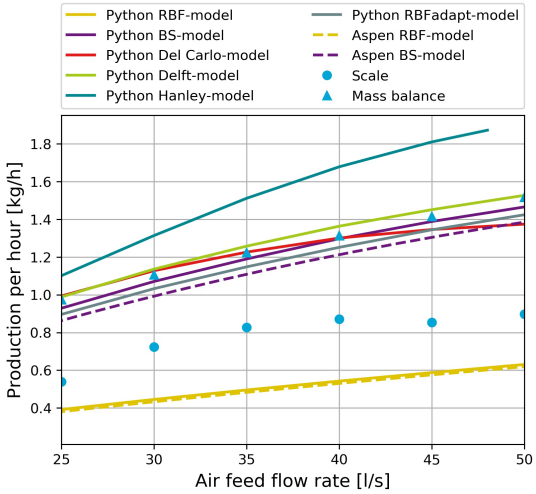

(b) Increase in liquid mass flow rate

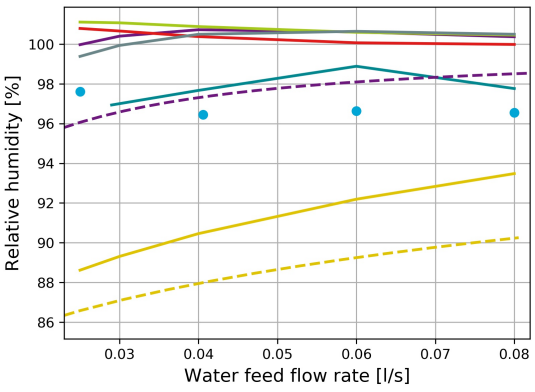

(c) RH of the exit air flow

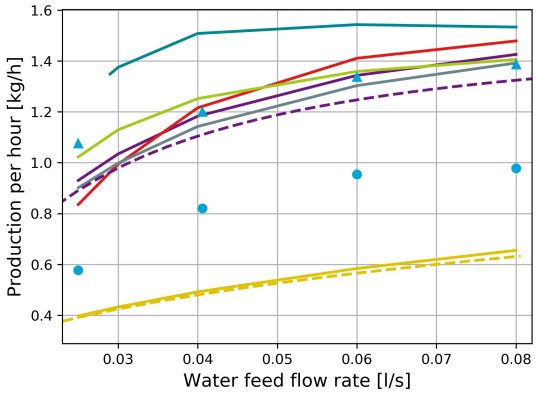

(d) Increase in liquid mass flow rate

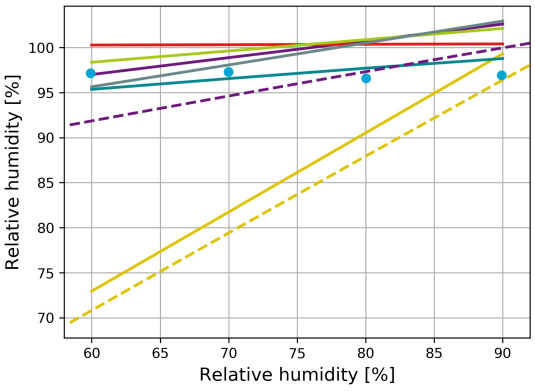

(e) RH of the exit air flow

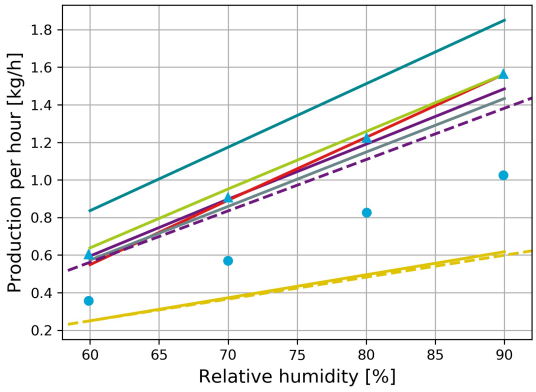

(f) Increase in liquid mass flow rate

Figure 4.12: The predicted and measured production(s) and the RH of the exit air flow over the independent variables

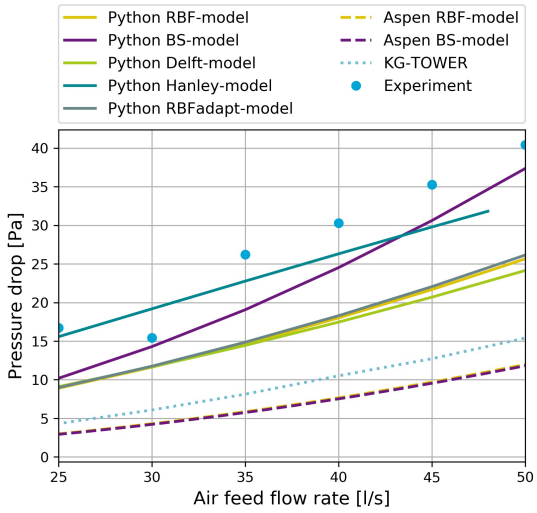

(a) Pressure drop over air feed flow rate

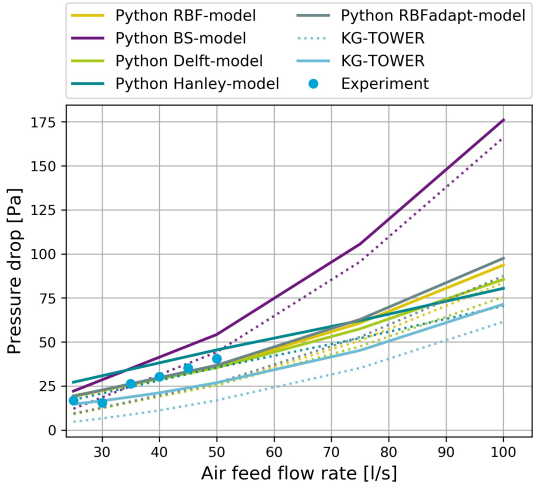

(b) Pressure drop over air flow rate, simulations shifted-up 10 Pa

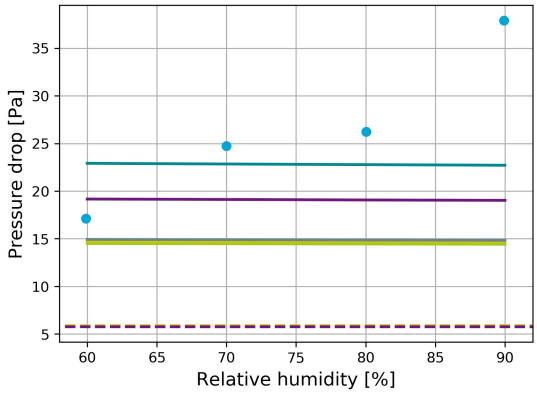

(c) Pressure drop RH of air feed flow

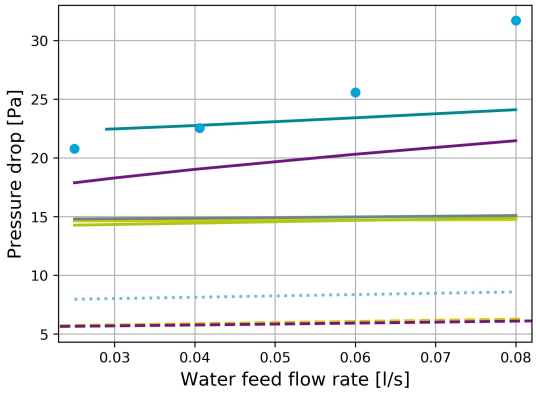

(d) Pressure drop over water feed flow rates

Figure 4.13: The predicted and measured pressure drops over the independent variables

4.4. CORRELATION SELECTION

To select the best fitting correlation the 'mean absolute percentage error (MAPE) function' is applied. The MAPE function is a measure for the quality of the prediction of the correlations. It expresses the accuracy of the simulation as a percentage, and is defined as,

$$MAPE = \frac{100}{n} \sum_{t=1}^{n} \left| \frac{Y_{\text{exp}} - Y_{\text{m}}}{Y_{\text{m}}} \right| \tag{4.8}$$

With Y_{exp} the experimental values, and Y_{m} the values that were predicted by the models. The MAPE function is applied to all experiments and simulations and returns a value for the quality of the prediction in percentage. The predicted variables were: the temperatures of the exit flows, the RH of the exit air flow, the production (Y_{exp} = mass balance production) and the pressure drop. Table 4.4 gives an overview of the MAPEs for the simulations for all experiments. The increased pressure drops predictions (ΔP+10 Pa) from figure 4.13b will be used for the pilot-plant design, and therefore that MAPE value is included in the table.

Table 4.4: MAPEs [%] between the simulations and all experiments

	Python model						Aspen plus model	
	RBF	BS	Del Carlo	Delft	Hanley	RBFadapt	RBF	BS
Production	59.0	3.8	5.4	2.5	21.9	6.6	59.9	9.5
T_{G} exit	42.9	4.9	6.6	8.2	20.7	2.8	46.8	4.4
T_{L} exit	19.9	2.6	3.4	4.6	14.2	1.4	17.4	4.3
RH exit	8.3	3.6	3.7	3.9	1.3	3.5	10.5	1.9
ΔP	39.6	22.6	-	40.5	16.9	38.7	75.6	76.0
ΔP+10 Pa	16.5	24.4	-	16.9	25.2	16.3	34.6	35.0

A correct prediction of the production is considered most important, since it directly affects the economic feasibility of the pilot-plant. The selected models are: with a MAPE for the production of 2.5 % over all experiments, the Python Delft-model and, with a MAPE for the production of 9.5 %, the Aspen plus BS-model.

Although some complications were encountered with the results from the experimental set-up of the OTWP system, by process of elimination the possible causes were pin-pointed, and the experimental results were used to analyze the models. The Delft correlations in the Python model show the most accurate mass transport predictions, with an overall mean absolute percentage error of 2.5 % in all experiments. For Aspen plus the BS-model shows the more accurate predictions. Both of those results are well within engineering practice. The analysis of the pressure drop predictions proved more difficult, showing greater deviations to less reliable experimental results. With deviations of 16.9 %, but only a slight deviation in trend, the Delft-model makes the best hydraulic predictions. However, it is advised to redo the experiments once the differential pressure drop sensor gives consistent results to confirm this. In the next chapter one of the models with their respective selected correlations will be used to make a pilot-plant design.

5

PILOT-PLANT DESIGN

This chapter describes the preliminary design and analysis of an OTWP pilot-plant. The design of the pilot-plant involved:

- Selection of the properties for the large-scale OTWP column models
- Comparing the scaled-up Aspen plus and Python model predictions
- Collecting component data
- Executing a technical performance analysis of the packed bed column with the Python model
- Performing a preliminary economic analysis with the Python model

The performances of the models, with their selected correlation methods, are compared over a set of larger variables. The systems' components are discussed, and the energy requirement for a water production of 25 $m^3\,day^{-1}$ for different feed flow properties and column dimensions is analyzed. Additionally, an economic analysis of the full system is performed: The operational expenditure (OPEX) and capital expenditure (CAPEX) are considered, resulting in an estimated levelized cost per unit of water production.

5.1. LARGE-SCALE MODELS

The Python and Aspen plus models are compared in a range of properties selected for the pilot-plant. The air feed flow temperature and humidity are taken at 28 °C and 80 % respectively. The fresh water feed temperature is 12 °C, and exit air temperature is set to 13 °C. For this air temperature, and if the exit air is assumed to be saturated, the required air feed mass flow rate can be calculated according to equation 4.2. The required air feed mass flow rate for a production of 25 $m^3\,day^{-1}$ is approximately 30 $kg\,s^{-1}$. The available water feed flow is much larger, since it originates from the OTEC plant, and is considered a non-limiting variable. The effect of a changing water feed flow rate on the OTWP column is examined: it is set as a sensitivity analysis variable (SA-variable). The second SA-variable is the column diameter.

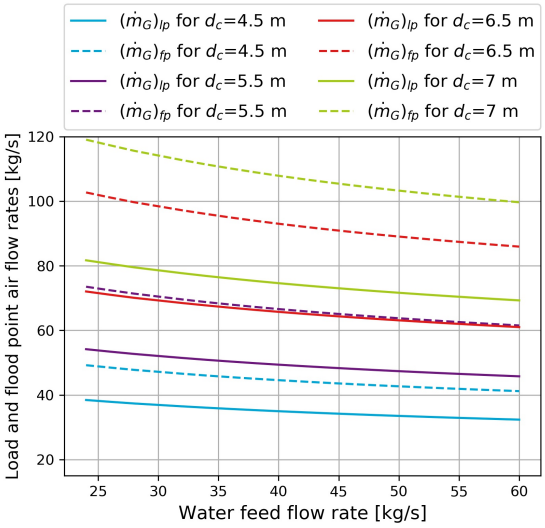

Figure 5.1: Air flow rates at loading (—) and flooding points (- -) for different packing diameters

The column diameter has an effect on the superficial flow velocities, and therefore on the transfer rates and hydraulic characteristics of the column. Figure 5.1 shows the air mass flow rates at flooding and loading point for different diameters and water feed flow rates according to the Python BS-model. For an air feed flow rate of 30 kg s^{-1} the minimum column diameter is estimated at 4.5 m (smaller diameters result in flooding).

Table 5.1 gives an overview of the column parameters and feed conditions used for the large-scale OTWP column analysis. The column height is set as the design requirement variable (DR-variable); meaning the necessary column height to reach the desired production is calculated for all SA-variables.

Table 5.1: Packing parameters and feed conditions for the large-scale analysis

Packing parameters		Feed conditions			
		Air feed flow		Water feed flow	
Diameter	SA-variable (>4.5 m)	Temperature	28 °C	Temperature	12 °C
Height	DR-variable	Flow rate	30 kg s^{-1}	Flow rate	SA-variable
Type	FlexiPac 350X	Pressure	1 atm	Pressure	1 atm
		Composition	$y_w = 0.0299$	Composition	$x_w = 1-1.57\times10^{-5}$
			$y_a = 0.9701$	Aspen plus	$x_a = 1.57\times10^{-5}$
				Composition	$x_w = 1$
				Python	$x_a = 0$

The selected correlation models for Aspen plus and Python were the BS-model and the Delft-model respectively. Before studying the performance of the two correlation models, the Python BS-model is compared to the Aspen plus BS-model, to assess the performance of the heat and mass balances.

5.1.1. ASPEN PLUS AND PYTHON BS-MODELS

Figure 5.2 shows the predictions of the two BS-models for a production of 25 m^3 day^{-1}. The calculated packing height is shown in figure 5.2a. The similarity between the BS-models for this property suggests an equal mass transfer rate. An increase in column diameter means a lower gas and liquid velocity, thus a lower mass transfer coefficient, (see eq. 2.59) but also an increase in packing area (and interface area). Since the necessary height increases slightly with an increase in column diameter, it can be deducted that the packing area increase has less influence than the mass transfer coefficient reduction in the BS-model. Figure 5.2c shows the water exit flow temperature

over water feed flow rate for different column diameters. The temperature decreases over the water feed flow rate and is the same for all column diameters. This is explained with an energy balance $(\dot{m}_{\mathrm{L}} c_{p\mathrm{L}}((T_{\mathrm{L}})_{H=H_{\mathrm{p}}} - (T_{\mathrm{L}})_{H=0}) = \dot{m}_{\mathrm{G}} c_{p\mathrm{G}}((T_{\mathrm{G}})_{H=H_{\mathrm{p}}} - (T_{\mathrm{G}})_{H=0}))$, since the mass flow rate does not change with an increase in diameter, this does not have an effect on the exit liquid temperature. The pressure drop in the column is related to the required height of the column. Figure 5.2d shows the pressure drop prediction according to the Koch-Glitsch correlation used by Aspen, and the BS-model used by Python. The different predictions, but with similar trend, was already evident in the small-scale experimental validation (see fig. 4.13d). Overall, the Aspen plus and Python model make the same predictions for the BS-correlation.

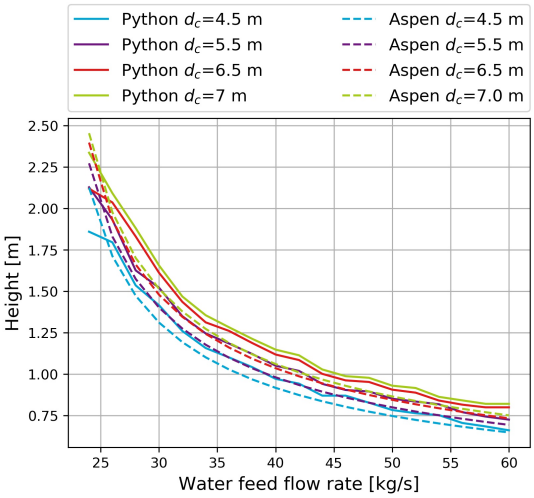

(a) H_{p} over water feed flow rate for different packing diameters

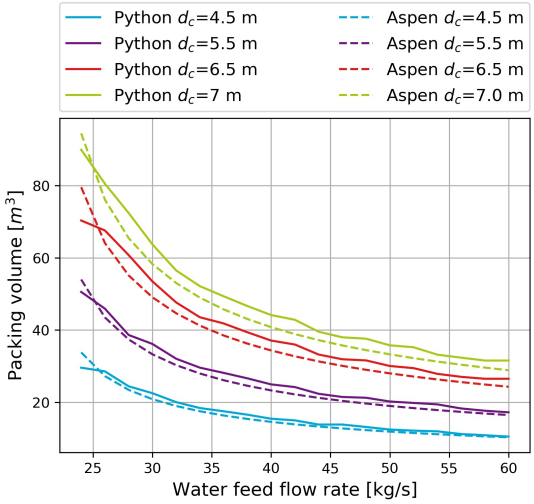

(b) Packing volume over water feed flow rate for different packing diameters

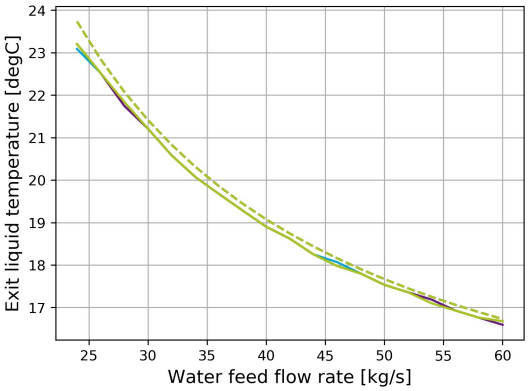

(c) $(T_{\mathrm{L}})_{H=0}$ over water feed flow rate for different packing dimensions

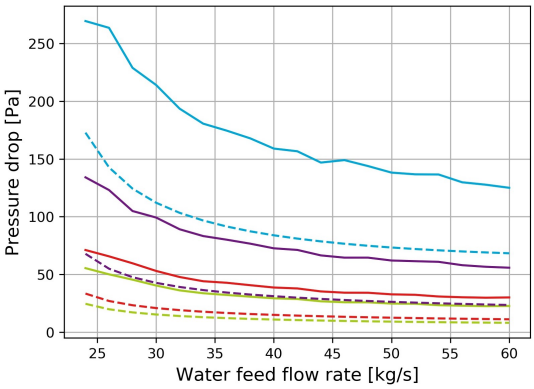

(d) Pressure drop over water feed flow rate for different packing dimensions for the supplier pressure drop correlation (Aspen) and the BS-model (Python)

Figure 5.2: The large-scale Aspen plus and Python BS-model predictions for a 25 $\mathrm{m}^3\,\mathrm{day}^{-1}$ fresh water production

5.1.2. ASPEN BS-MODEL AND PYTHON DELFT-MODEL

Figure 5.3a shows the calculated height of the column for the required production by the Aspen BS-model and Python Delft-model. It illustrates the difficulty of large-scale column predictions. Although both models were validated, and performed in accordance with the experimental values, they predict different DR-variables for the large-scale design. For the Delft-model, as opposed to the BS-model, the height decreases for larger diameters. Figure 5.3b shows that the Delft-model computes a smaller packing volume for lower water feed flow rates and the opposite for higher values compared to the BS-model.

The pressure drop predictions of the Delft-model are, opposite to the predictions for the experimental set-up pressure drops (fig. 4.13d), lower than the predictions by Aspen. As mentioned before (section 2.6), the Delft-model takes a scale-up factor for column diameters into account, which results in lower pressure drops (for larger diameters, a smaller fraction of the flow channels ends at the column wall, see eq. 2.92).

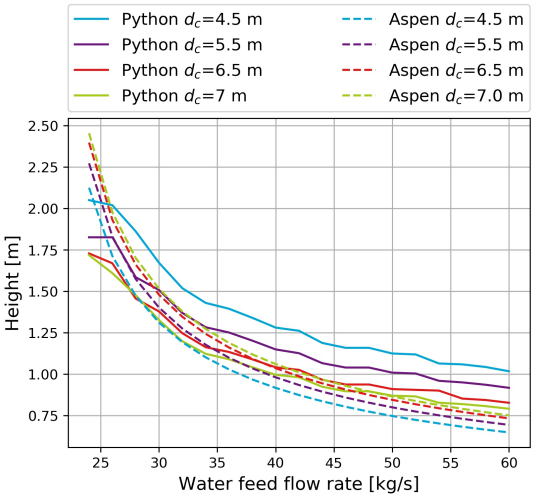

(a) H_p over water feed flow rate for different packing diameters

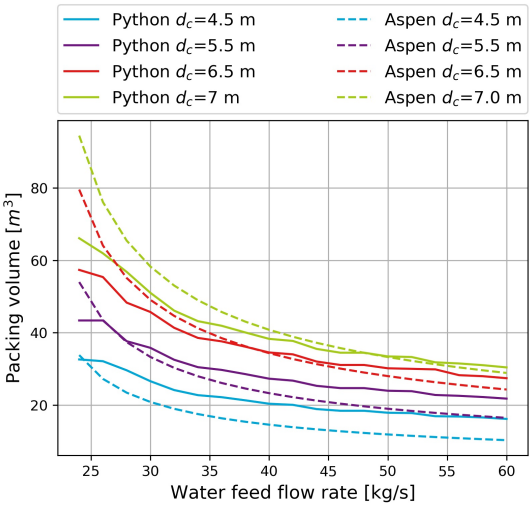

(b) Packing volume over water feed flow rate for different packing dimensions

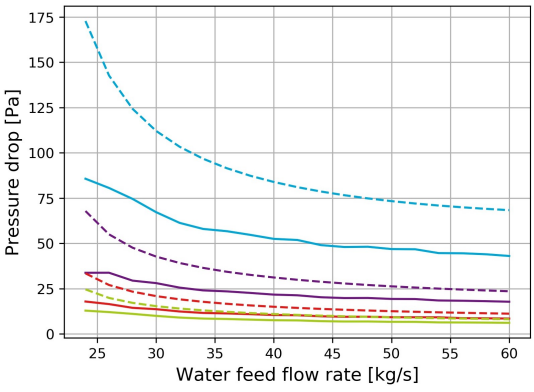

(c) Pressure drop over water feed flow rate for different packing dimensions for the supplier pressure drop correlation (Aspen) and the BS-model (Python)

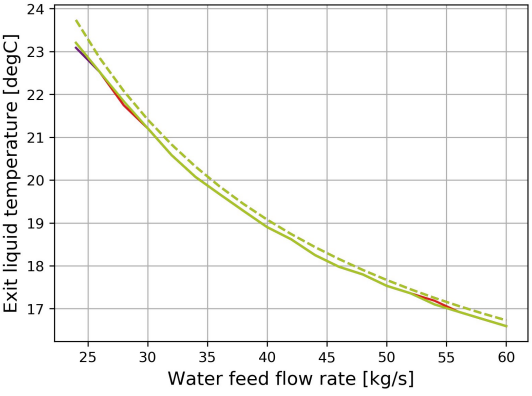

(d) $(T_L)_{H=0}$ over water feed flow rate for different packing dimensions

Figure 5.3: The large-scale Aspen plus Delft-model and Python BS-model predictions for a 25 $m^3\,day^{-1}$ fresh water production

Overall, the Python model seems to perform adequately and in agreement with the Aspen plus model. The Python Delft-model will be used for the technical and economic performance analysis. This model performed best in the experimental set-up validations and its large-scale predictions are considered appropriate. It should be kept in mind that the pressure drop predictions by the Delft-model are lower than the predictions by the Koch-Glitsch model since it considers the additional influence of the column diameter on the pressure drop

5.2. TECHNICAL PERFORMANCE ANALYSIS

To analyze the influence of the column diameter and the fresh water feed flow rate on the OTWP systems' technical performance, the heat exchanger and power drop function are introduced. As a measure for technical performance, the energy consumption per unit of water production is examined. This requires the calculation of total pressure drop on the air-side of the system, the total pressure drop on the water-side of the system and equipment efficiencies.

5.2.1. COMPONENT SELECTION

HEX The objective of the HEX function in the Python model is not to design a heat exchanger, but to calculate the sea water mass flow, the sea water exit flow temperature, and the pressure drops of the sea and the fresh water flows. The HEX should cool the fresh water flow from the exit flow temperature to the feed flow temperature. The maximum allowed pressure drop that is set for this HEX is 35 kPa [10]. The selected dimensions should give a combined pressure drop of ~35 kPa for the higher range fresh water flow (in this case 60 $kg\,s^{-1}$). The assumed available OTEC sea water flow temperature is 11 °C [3]. Table 5.2 gives an overview of the HEX dimensions that were selected for the pilot-plant. Not varying the size of the HEX means that the varying water feed flow rate of the condenser column will have an influence on the energy requirements of the system but will not affect the CAPEX of the HEX. It also means that the HEX is over-designed for lower fresh water flow-rates.

Table 5.2: Dimensions of the HEX selected for the pilot-plant design

Plate length	1.8 m
Plate width	0.9 m
Plate thickness	0.4 mm
Correction for waves	1.22
Chevron angle	30°
Distance between plates	3 mm
Number of plates	168
Material of plate	stainless steel
Thermal conductivity of plate	16 $W\,m^{-1}\,K^{-1}$

Liquid distributor The selected liquid distributor for the OTWP column is a single stream gravity flow liquid distributor, since these have no additional pressure drops on the fresh water flow and are appropriate for large diameter columns. The liquid velocity in the column is $\ll 2\,m\,s^{-1}$, and the gas capacity factor ($= u_{G,s} * \sqrt{\rho_G}$) is around 2.2 $kg^{1/2}\,m^{-1/2}\,s^{-1}$. A system distributor would be an option for a large diameter column with those flow characteristics (see appendix A). Kolev [8] discusses how to determine the layout of the distributors.

Koch-Glitsch recommends a minimum of 85 liquid distribution points per square meter for the Flexipac 350 packings. For OTWP pilot-plant flow rates and this drip-point density the necessary orifice diameter is ~6 to ~8 mm [68]. Sulzer B.V. mentioned that the pressure drop over their liquid distributors is extremely small. They tested on packings with pressure drops as low as 0.2 $mbar\,m^{-1}$, and the pressure drop generated by the liquid distributor was negligible in that system (personal com-

munication, July, 2017). For the pilot-plant design the contribution of the liquid distributor to the pressure drop in the column is ignored.

Gas distributor Since the range of the pilot-plant analysis covers a relatively large column diameter, and the structured packing was selected for its low pressure drop, the gas is expected to show poor initial distribution; A gas distributor in the column will be necessary. For the pilot-plant design the orifice baffle is selected. A pressure drop limit of 10 Pa is set for the gas distributor. The distance between the gas distributor and the bottom of the packing is taken as $0.15d_c$. The pressure drop of the airflow associated with this extra column length, and extra head are considered in the pressure drop function (see appendix E).

Pipes The height to which the fresh water is raised is a sum of the following: the required height between the air feed flow and the packing, the height of the packing, and the height between the water feed flow and the packing. This height is used to calculate the additional pipe length, its related pressure drop, and the required fresh water pump power. The height between the water feed flow and the packing is taken as 40 cm. This space is for the liquid distributor and the branching of the water feed. The pressure drop due to pipe branching before the liquid distributor is ignored. To select the pipe performance, and thus diameter, a maximum allowable pressure drop was set to 10 % of the total pressure drop on the fresh water side. The fresh water pipe diameter varies between 18 cm and 30 cm.

Water pumps The required fresh water pump power depends on the dimensions of the column. The pressure drop due to head, friction in the pipes and the HEX add up to the required pump power. The sea water pump power requirement is only dependent on the pressure drop in the HEX (pressure drops in those pipes are not considered). To calculate the energy requirements of the system an estimation of pump efficiency is required. The loads of the water pumps will be stable, so they can be selected to operate close to their rated loading. For generic centrifugal pumps an efficiency (including mechanical and electrical efficiency) of 80 % should be achievable.

Fan Since the volumetric air flow rate through the column is large, the total fan load is expected to be an important factor in the systems energy requirement. The two main kinds of fans are axial and centrifugal. Axial fans are better suitable for high volume low differential pressure flows. The air flow rate of of the pilot-plant (93 000 $m^3 h^{-1}$) is close to the maximum that axial fans can deliver. The selected fans should have their optimum operating point in a low static air pressure drop (around 50 Pa, see fig. 5.3c). For this system two air feed points would allow for more flexibility when selecting a fan model (since they would not operate at the maximum). Additionally, it has the advantage that they can be distributed over the circumference of the column to provide a better initial gas distribution.

The fan unit efficiency can be calculated as a factor of the total fan efficiency, the belt efficiency and the motor efficiency. To achieve a reduction in CO_2 emissions of at least 20 % by 2020, the European union has commission regulations (No 327/2011) for total industrial fan efficiencies. For example, the minimum fan efficiency (at the peak efficiency point) for axial fans of 1 kW is 52 %. Since the fan efficiency in the OTWP system is an important aspect, and the operating point is fixed, a high efficiency fan with a peak point close to operating point will be selected. A fan efficiency of 62 % is

achievable. An example of an axial fan with such an efficiency can be found in appendix G. The drive efficiency depends on the type of drive that is selected. A direct drive will have an efficiency of 100 % [69]. With a motor efficiency of 80 %, the total fan efficiency will be approximately 50 %. This efficiency is only achievable if the gas feed design is changed to fit the available technology.

5.2.2. ENERGY CONSUMPTION

With the selected components an energy consumption evaluation can be performed. Figure 5.4 shows the energy consumption for varying diameters and fresh water flow rates. Figure 5.4a shows that for columns with a diameter bigger than 6.5 m the energy requirement for the fresh water production stays below 3.5 $kWh\,m^{-3}$. It can be seen in figure 5.4b that the air fan is a main contributor to the energy consumption of the system. With higher flow rates the energy requirement of the fresh water pump increases and becomes of greater influence. It should be noted that these values rely heavily on the estimated fan unit efficiencies. For slightly lower efficiencies the energy requirement increases significantly.

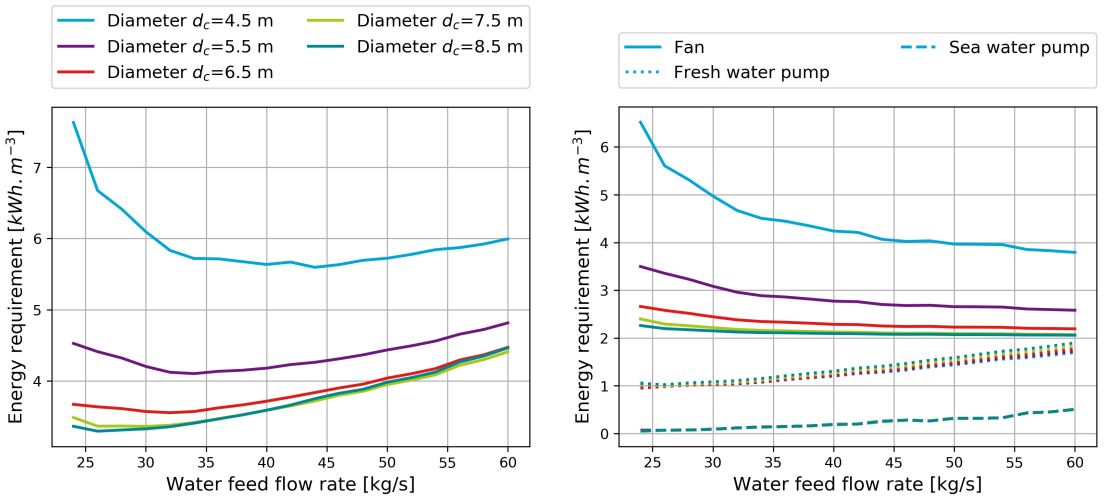

(a) The total energy consumption of the system for different diameters

(b) The energy consumption per component for different diameters

Figure 5.4: The energy consumption of the OTWP pilot-plant over water feed flow rate. Different column diameters are presented with different colors

Appendix H gives an overview of the pressure drops, power requirements and energy consumption of the individual components.

5.3. ECONOMIC ANALYSIS

The levelized production costs of the fresh water (LCOWP) from the OTWP system consist of the equipment and installation costs, and the operational costs. This estimate neglects the maintenance and carbon emission costs.

5.3.1. CAPITAL COST

The equipment costs are calculated from cost correlations [10, 70] and retrieved from a price booklet [71]. Appendix I describes the full capital cost analysis. Figure 5.5 shows the total estimated equipment cost of the OTWP system. The individual equipment costs can be found in appendix I.1.

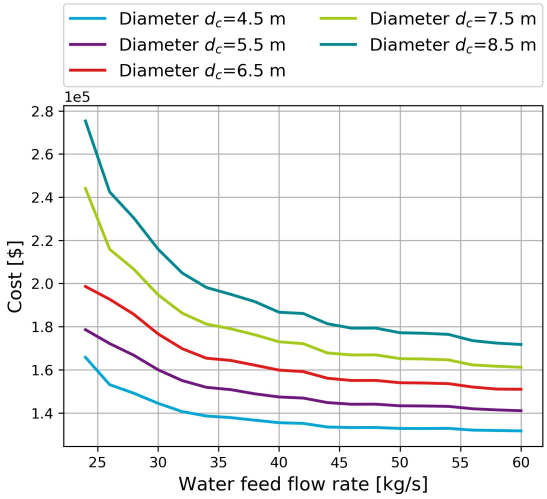

Figure 5.5: Combined equipment cost

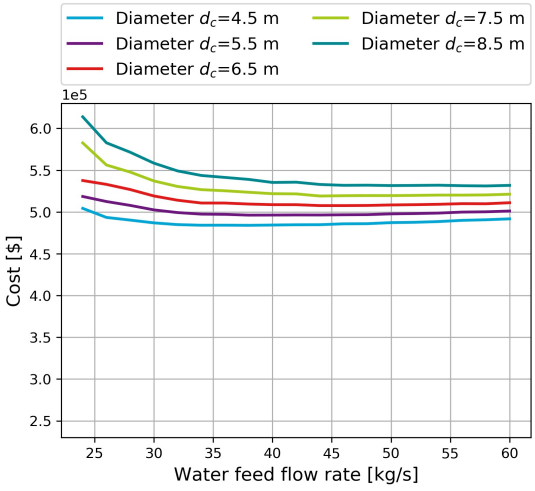

(a) CAPEX according to the installation factors suggested by Towler and Sinnott [10]

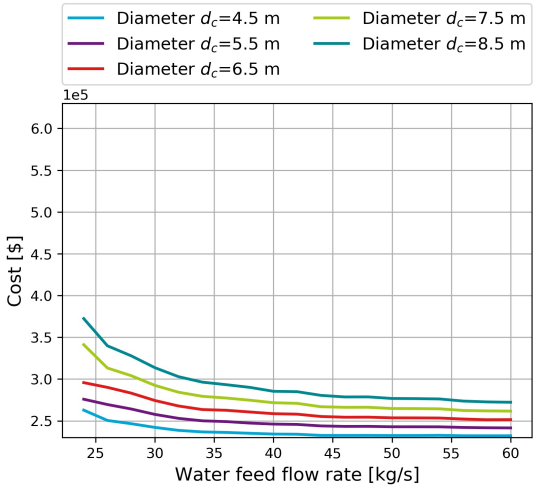

(b) CAPEX according to the installation factors suggested by Couper *et al.* [70]

Figure 5.6: The investment cost for a 25 $m^3\,day^{-1}$ OTWP system with a lifetime of 10 years

The capital expenditures of the system include the installation cost of the equipment. These express the labor costs, transportation costs and any other additional costs that come with the OTWP installation. To obtain this, the purchase costs are multiplied with an installation factor F_i (for this rough economic analysis: CAPEX = $F_i * \sum C_{Eq}$). The installation factors that are proposed by Towler and Sinnott [10] and Couper *et al.* [70] differ considerably. The CAPEX of the OTWP system is calculated with each installation factors and compared. The total CAPEX of the system for the different

installation factors over a varying fresh water flow feed rate and column diameter is shown in figure 5.6. There is a relatively small increase in cost with column diameter, but the costs mainly increase with a lower water feed flow rate. This is caused by the higher column height for those flow rates. The lowest achievable CAPEX of the OTWP system is around 230 k$.

5.3.2. OPERATIONAL COST

The operational costs is subject to the energy requirement of the system and the electricity price. The electricity price on Curaçao (based on Aqualectra industrial standard prices of July 2017) is 0.27 $\$\,kWh^{-1}$. Multiplying this with the energy requirements (fig. 5.4a) will result in the operational cost. The operational cost depends on the electricity price and therefore has to be updated each year. In LCOWP calculation, this is done with a discount rate. Additionally, there is an opportunity of production cost reduction by using the electricity from the OTEC plant. In this work the cost of electricity from the grid is considered.

5.3.3. LEVELIZED COST OF WATER PRODUCTION

The estimated OTWP system lifetime is based on lifetimes taken in research on the comparable HDH systems [24, 26], and set to 10 years. It is assumed that the plant will be running 95 % of the time. The levelized cost of water production (LCOWP) is calculated according to,

$$LCOWP = \frac{\sum_{y=1}^{n} \frac{I_y + M_y + E_y}{(1+r)^y}}{\sum_{y=1}^{n} \frac{WP_t}{(1+r)^y}} \tag{5.1}$$

With I_y the investment cost in year y, M_y the operation and maintenance cost in year y and E_y the electricity cost in year y. WP is the water production and r the discount rate. The discount rate is assumed to be 6 %. Since maintenance cost for simple processes are estimated around 3 % of the CAPEX [10] they are low enough to be ignored in this preliminary calculation. The calculated LCOWP for the different installation factors are used to select the operating conditions and column dimensions of the OTWP pilot-plant.

5.4. THE OTWP PILOT-PLANT DESIGN

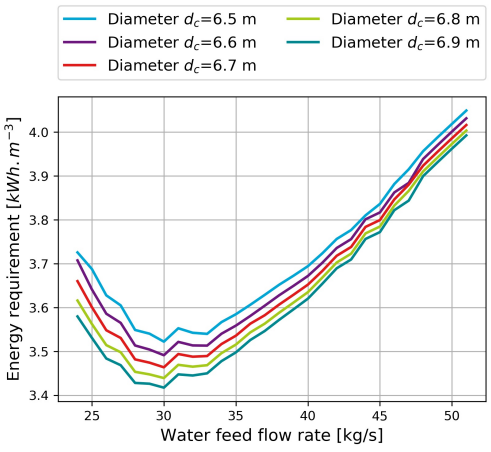

Figure 5.7: The energy consumption of a 25 $m^3\,day^{-1}$ OTWP system

The energy requirement of the OTWP system shows a clear dip around an L/G ratio of 1 (fig. 5.7). To be competitive with other desalination systems the aim of the pilot-plant design is to stay below an energy consumption of 3.5 $kWh\,day^{-1}$. To reach this, the water feed flow rate should be set to 30 $kg\,s^{-1}$ with a minimum column diameter of 6.6 m.

For the preliminary pilot-plant design the LCOWP are presented in figure 5.8. Figure 5.8a shows the production cost according to higher installation factors suggested by Towler and Sinnott [10], and figure 5.8b shows the LCOWP according to the Couper *et al.* [70]

installation factors. The difference in installation factors leads to a different minimum LCOWP at different water feed flow rates. The influence of the column diameter on the LCOWP is small. Deviation from the optimum point shows a relatively small increase in production cost.

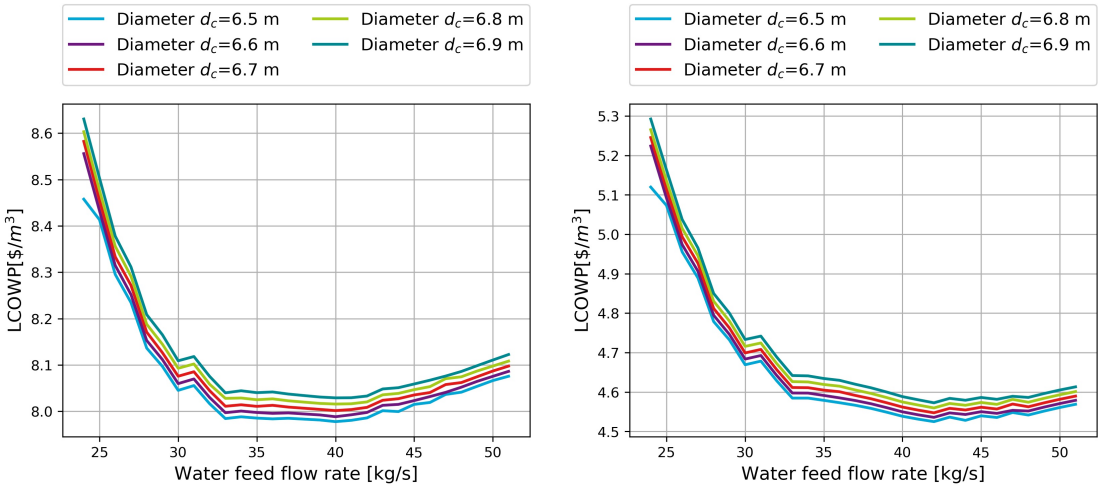

(a) LCOWP according to the installation factors suggested by Towler and Sinnott [10]

(b) LCOWP according to the installation factors suggested by Couper *et al.* [70]

Figure 5.8: The levelized cost of water production for a 25 $m^3\,day^{-1}$ OTWP system with a lifetime of 10 years

Because the production costs at a water feed flow rate of 30 $kg\,s^{-1}$ are similar to the minimum production cost, this is chosen as an operating point, leading to a required packing height of 1.24 m. The resulting LCOWPs are 8.08 $\$\,m^{-3}$ for the Towler and Sinnott [10] installation factors and 4.68 $\$\,m^{-3}$ for the Couper *et al.* [70] installation factors.

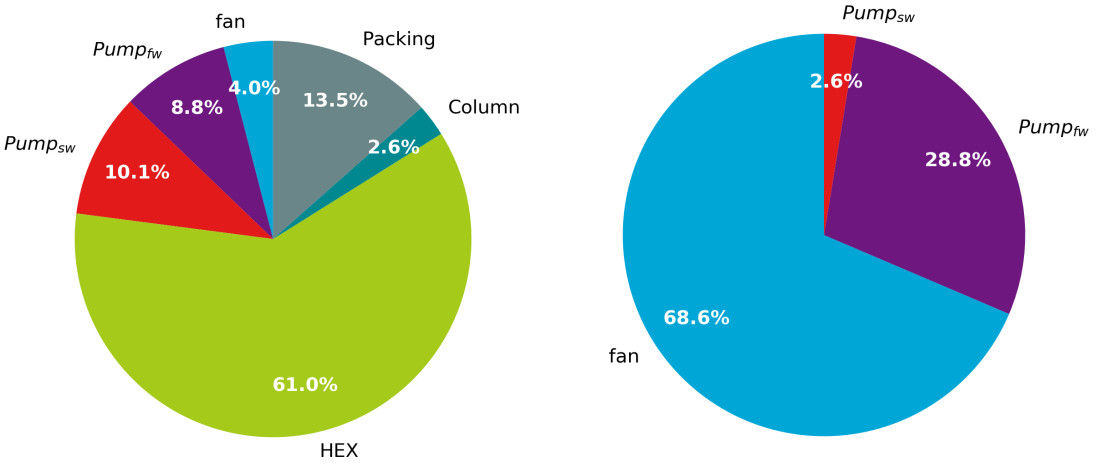

(a) The CAPEX division according to installation factors by Towler and Sinnott [10]

(b) The OPEX cost divisions

Figure 5.9: Cost division of the CAPEX and OPEX

Bourouni *et al.* [22] found that desalination is only competitive if the OPEX is lower than the

CAPEX. The OPEX for the OTWP column with the selected properties would be 0.95 $\$\,m^{-3}$; For both installation factors the CAPEX make up more than 80 % of the LCOWP. The transportation of materials to the islands, and the travel and housing expenses of experts will significantly increase the installation costs. This makes the installation factors proposed by Towler and Sinnott [10] more likely. Figure 5.9 shows the origin of the CAPEX and OPEX for the higher installation factors. More information on the costs distribution on the selected operating point for the pilot-plant can be found in appendix J.

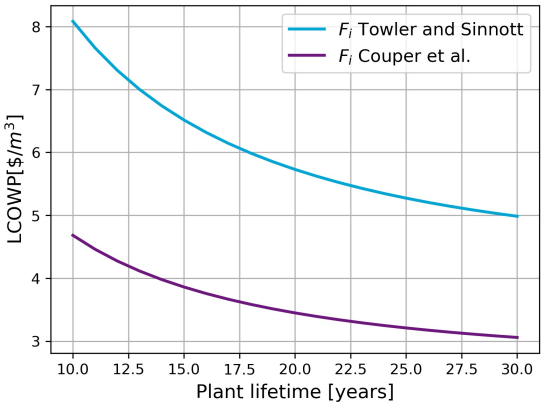

Figure 5.10: The LCOWP of a 25 $m^3\,day^{-1}$ OTWP system for different lifetimes

The heat exchanger is responsible for more than 60 % of the OTWP pilot-plants' CAPEX. Allowing a higher pressure drop and optimizing it for the selected water flow rate will result in a significant cost reduction. Since the CAPEX has a large influence on the LCOWP, an extended lifetime reduces the production cost considerably. If a lifetime of 25 years is assumed, figure 5.10 shows that the LCOWP (for the higher installation factors) would be 5.28 $\$\,m^{-3}$.

The pilot-plant design meets the energy requirement goal for the selected production of 25 $m^3\,day^{-1}$. The LCOWP for a system with a lifetime of 10 years is 8.08 $\$\,m^{-3}$. One explanation for the high costs are the high installation factors. Most of the CAPEX is caused by the investment cost of the HEX. Optimizing the HEX for the selected fresh water feed flow rate, and allowing a higher pressure drop is an important step in decreasing the LCOWP.

6

CONCLUSION

The objective of this thesis was to select (and validate) the most suitable packing and properties for an Ocean Thermal Water Production (OTWP) pilot-plant in the Caribbean with a fresh water production of 25 $m^3\,day^{-1}$. After a comprehensive study on the formulation of mass and heat transfer in structured packed beds, two models were developed: one in the established chemical process software Aspen plus, and one in Python. The numerical Python model was based on previous work by Noordhoek Hegt [3]. The performance of the two models and their mass transfer coefficient and hydraulic formulations were examined with experimental studies. They were fitted with the best performing correlations and used to perform a techno-economic analysis. Additionally, their heat and mass transport and hydraulic predictions for large-scale columns were compared. The aim of developing these models was to determine the design and operating conditions of an OTWP pilot-plant with an energy consumption below 3.5 $kWh\,m^{-3}$. The Python model was extended with a heat exchanger and additional pressure drop functions to examine the pilot-plant performance for different column diameters and water feed flow rates.

Small-scale model performances The main physical phenomena that occur in the packed bed column are the mass transfer through the gas phase and the heat transfer through convection and condensation of the atmospheric water vapor. To define the rate at which these transports happen, it is necessary to apply correlations for the calculation of the mass transfer coefficients. A rough initial analysis with the Aspen plus model showed that the corrugated sheet packing FlexiPac 350X is a good choice of packing for the OTWP system. It provides a low pressure drop, necessary because of the high volumetric air flow rates in the OTWP system, without being too expensive.

The presented numerical Python model, with the mass transfer coefficient correlation by Olujić *et al.* [4], outperforms the Aspen plus prediction with the Rocha *et al.* [5] correlation. Closer examination shows that this is due to the better performance of the selected mass transfer correlations; for the same correlations the models show identical predictions. The Python model predictions of the mass transfer rate are in better agreement with the experimental results (MAPE of 2.5 %) than the predictions of the heat transfer (within a MAPE of 10 %). However, there is an issue with the production measurements in the experiment: even when the mass balance over the experiments shows good cor-

respondence with the models, the scale output does not match these results. It is unlikely that the balance is incorrect, and therefore somewhere in the experimental set-up water must be lost. Many attempts to find a reason for this deviation in experimental outcomes are described in this work, but unfortunately a definitive cause was not determined. The differential pressure sensor outputs suggested a reasonable prediction by both models (MAPE of 16.9 % and 35.0 %), but the experimental database and reliability was not good enough for a validation. A good sign was that different hydraulic calculation methods showed that, on the experimental scale, the predicted trend is similar to the trend predicted by the KG-TOWER software. Assuming that the packing manufacturers developed the pressure drop in KG-TOWER experimentally to fit the FlexiPac 350X, it should make a good prediction on small-scale. This suggests that the actual pressure drops in the packing are lower than found in the experimental study; a lower pressure drop would result in lower OPEX and possibly allow the selection of a cheaper and less efficient packing in an optimized pilot-plant. For now, the hydraulic Delft-model is accepted as the most reliable for large-scale simulations, since it is the only method that takes the column diameter into account.

All in all, both the Python and Aspen plus model make a good prediction of the phase properties in the column, but their hydraulic calculations should be validated with more consistent experiments. It should be kept in mind that pressure drop is influenced by column size, so validation for a small-scale column diameter does not give assurance for large-scale predictions.

Pilot-plant design The energy requirement of fresh water production in the OTWP pilot-plant is decreased with both larger column diameter and mass feed flow rate of the condenser column. For an 25 $m^3\,day^{-1}$ OTWP plant, a column diameter of 6.6 m and a water feed flow rate of 30 $kg\,s^{-1}$ attained an energy requirement of 3.5 $kWh\,m^{-3}$ with a levelized production cost (LCOWP) of 8.08 $\$\,m^3$. The large column diameter with low column height (1.24 m) is not an obvious choice for column dimensions, but for the OTWP system minimum energy requirement is attained outside of the loading-region: the common operating area of columns. The large diameter does increase the difficulty of phase distribution. Including the phase distributors in the economic analysis might lead to the conclusion that multiple smaller condenser columns reduce the LCOWP.

Future recommendations The validations of the hydraulic calculations require that the experimental set-up is improved. One possibility would be a different connection of the pressure differential sensor to the condenser column, to eliminate the influence of water droplets on the measurements. If this does not result in more consistent experimental results it might be necessary to select a different type of pressure sensor. Although the models could be validated with the mass balance production of the experiments, the deviation from the weight increase of the water tank is still unsolved. By the time of finalizing this research the assumption of evaporation from the water tank was tested and dismissed.

Although this work proves the similarity between the large-scale predictions of the two models, a useful next step would be to validate on large-scale columns. This requires performance data of a similar system such as the dehumidification columns of Humidifaction-DeHumidifaction pilot-plants.

An optimization over the complete OTWP system should be performed and will reduce LCOWP. This requires the integration of a heat exchanger design in the analytical model. Additionally, the

current economic analysis of the pilot-plant only provides a rough estimate of the cost. The assumed plant lifetime and equipment installation factors are dominant elements that make up the LCOWP. It is necessary to establish installation costs and a lifetime specific for this type of plant and location to provide a more reliable cost estimate.

It would be interesting to investigate the efficiency of a multi-column system. Smaller diameter columns would increase the liquid and gas distribution and allow operation closer to loading point. Over the past couple of years CFD studies have shown good results in predicting the pressure drop, mass transfer efficiencies and initial phase distributions in structured packing [49, 72–74]. Since the initial phase distributions have a large influence on the feasibility of the column, and current model does not consider them, a CFD study on the gas and liquid distributor would contribute to finding the optimum column dimensions.

Overall, the analysis in this work has shown that there is great potential for the use of OTEC plant waste streams in the production of fresh water in the Caribbean. The energy demand is significantly lower than conventional desalination techniques, and the production cost of the presented pilot-plant design are comparable to reverse osmosis. The optimization of the OTWP system would reduce the cost even further. Additionally, since the system solely needs electrical energy, which it can get from the OTEC plant, it provides a sustainable alternative to current water production methods.

BIBLIOGRAPHY

[1] S. Van der Drift, *Atmospheric water extraction with deep ocean water: a techno-economic assessment*, Master's thesis, Delft University of Technology (2014).

[2] M. C. M. Lopez, *Ocean Thermal Water Production*, Master's thesis, Delft University of Technology (2016).

[3] F. Noordhoek Hegt, *Atmospheric Water Extraction*, Master's thesis, Delft University of Technology (2017).

[4] Ž. Olujić, A. Kamerbeek, and J. De Graauw, *A corrugation geometry based model for efficiency of structured distillation packing,* Chemical Engineering and Processing: Process Intensification **38**, 683 (1999).

[5] J. A. Rocha, J. L. Bravo, and J. R. Fair, *Distillation columns containing structured packings: a comprehensive model for their performance. 1. hydraulic models,* Industrial & engineering chemistry research **32**, 641 (1993).

[6] R. Sander, *Compilation of henry's law constants for inorganic and organic species of potential importance in environmental chemistry,* (1999).

[7] E. Brunazzi and A. Paglianti, *Liquid-film mass-transfer coefficient in a column equipped with structured packings,* Industrial & engineering chemistry research **36**, 3792 (1997).

[8] N. Kolev, *Packed bed columns: for absorption, desorption, rectification and direct heat transfer* (Elsevier, 2006).

[9] VDI, *VDI heat atlas* (Spinger-Verlag, Heidelberg, Berlin, 2010).

[10] G. Towler and R. Sinnott, *Chemical Engineering Design - Principles, Practice and Economics of Plant and Process Design (2nd Edition)* (Elsevier, 2013).

[11] P. Nawrocki, Z. Xu, and K. Chuang, *Mass transfer in structured corrugated packing,* The Canadian Journal of Chemical Engineering **69**, 1336 (1991).

[12] J. Kucera, *Desalination: water from water* (John Wiley & Sons, 2014).

[13] R. Billet and M. Schultes, *Prediction of mass transfer columns with dumped and arranged packings: updated summary of the calculation method of billet and schultes,* Chemical Engineering Research and Design **77**, 498 (1999).

[14] G. Wang, X. Yuan, and K. Yu, *Review of mass-transfer correlations for packed columns,* Industrial & engineering chemistry research **44**, 8715 (2005).

[15] N. R. C. Committee on Advancing Desalination Technology, *Environmental Issues,* in *Desalination: A National Perspective* (National Academies Press, 2008) pp. 108 – 146.

[16] K. W. L. Lie, M. C. V. Etten, Q. C. Bauer, and C. P. Molhoek, *Verdampingskoelen: Drinkwater productie met direct contact condensatie.* (2014).

[17] Y. Li, J. F. Klausner, R. Mei, and J. Knight, *Direct contact condensation in packed beds,* International journal of heat and mass transfer **49**, 4751 (2006).

[18] K. Onda, H. Takeuchi, and Y. Okumoto, *Mass transfer coefficients between gas and liquid phases in packed columns,* Journal of Chemical Engineering of Japan **1**, 56 (1968).

[19] J. Mackowiak, *Fluid dynamics of packed columns,* Principles of the Fluid Dynamic Design of Columns for Gas/Liquid and Liquid/Liquid Systems, London, New York (2010).

[20] M. Isaka, *Water Desalination Using Renewable Energy*, Technology brief 112 (International Renewable Energy Agency and Energy Technology Systems Analysis Programme, 2012).

[21] A. Eslamimanesh and M. Hatamipour, *Economical study of a small-scale direct contact humidification–dehumidification desalination plant,* Desalination **250**, 203 (2010).

[22] K. Bourouni, R. Martin, and L. Tadrist, *Analysis of heat transfer and evaporation in geothermal desalination units,* Desalination **122**, 301 (1999).

[23] M. Mehrgoo and M. Amidpour, *Constructal design and optimization of a direct contact humidification–dehumidification desalination unit,* Desalination **293**, 69 (2012).

[24] K. Bourouni, M. Chaibi, and L. Tadrist, *Water desalination by humidification and dehumidification of air: state of the art,* Desalination **137**, 167 (2001).

[25] H. Müller-Holst, M. Engelhardt, and W. Schölkopf, *Small-scale thermal seawater desalination simulation and optimization of system design,* Desalination **122**, 255 (1999).

[26] H. A. Ahmed, I. Ismail, W. F. Saleh, and M. Ahmed, *Experimental investigation of humidification-dehumidification desalination system with corrugated packing in the humidifier,* Desalination **410**, 19 (2017).

[27] B. M. Hamieh and J. R. Beckman, *Seawater desalination using dewvaporation technique: experimental and enhancement work with economic analysis,* Desalination **195**, 14 (2006).

[28] J. R. Beckman, *Dewvaporation Desalination 5,000-Gallon-Per-Day Pilot Plant*, Desalination and Water Purification Research and Development Program Report 120 (U.S. Department of the Interior Bureau of Reclamation, 2008).

[29] R. Xiong, S. Wang, L. Xie, Z. Wang, and P. Li, *Experimental investigation of a baffled shell and tube desalination column using the humidification-dehumidification process,* Desalination **180**, 253 (2005).

[30] X. Qi, Z. Liu, and D. Li, *Performance characteristics of a shower cooling tower,* Energy conversion and management **48**, 193 (2007).

[31] R. Ramkumar and A. Ragupathy, *Optimization of cooling tower performance with different types of packings using taguchi approach,* Journal of the Brazilian Society of Mechanical Sciences and Engineering **37**, 929 (2015).

[32] *Aspen plus V8.8,* Aspen Technology Inc. (2015).

[33] J. A. Queiroz, V. M. Rodrigues, H. A. Matos, and F. Martins, *Modeling of existing cooling towers in aspen plus using an equilibrium stage method,* Energy conversion and management **64**, 473 (2012).

[34] H. Sadeghifar and A. Sadeghifar, *A new method to calculate efficiency of randomly-packed distillation columns and its comparison with the methods utilized in aspen plus,* Fuel processing technology **96**, 65 (2012).

[35] N. Ramzan, M. Faheem, R. Gani, and W. Witt, *Multiple steady states detection in a packed-bed reactive distillation column using bifurcation analysis,* Computers & chemical engineering **34**, 460 (2010).

[36] M. Thiels, D. S. Wong, C.-H. Yu, J.-L. Kang, S. S. Jang, and C.-S. Tan, *Modelling and design of carbon dioxide absorption in rotating packed bed and packed column,* IFAC-PapersOnLine **49**, 895 (2016).

[37] L. Spiegel and M. Duss, *Structured packings,* in *Distillation: Equipment and Processes* (Elsevier, 2014) pp. 145–181.

[38] J. L. Bravo and J. R. Fair, *Generalized correlation for mass transfer in packed distillation columns,* Industrial & Engineering Chemistry Process Design and Development **21**, 162 (1982).

[39] J. Stichlmair, J. Bravo, and J. Fair, *General model for prediction of pressure drop and capacity of countercurrent gas/liquid packed columns,* Gas Separation & Purification **3**, 19 (1989).

[40] J. A. Rocha, J. L. Bravo, and J. R. Fair, *Distillation columns containing structured packings: a comprehensive model for their performance. 2. mass-transfer model,* Industrial & engineering chemistry research **35**, 1660 (1996).

[41] B. Hanley and C.-C. Chen, *New mass-transfer correlations for packed towers,* AIChE journal **58**, 132 (2012).

[42] R. Billet and M. Schultes, *Predicting mass transfer in packed columns,* Chemical engineering & technology **16**, 1 (1993).

[43] A. A. Tsonis, *An introduction to atmospheric thermodynamics* (Cambridge University Press, 2002).

[44] A. De Angelis, O. Saro, G. Lorenzini, S. D'Elia, and M. Medici, *Simplified models for assessing heat and mass transfer in evaporative towers,* Synthesis Lectures on Engineering **8**, 1 (2013).

[45] M. Schultes, *The impact of tower internals on packing performance,* Chemie Ingenieur Technik **86**, 658 (2014).

[46] S. Adler, E. Beaver, P. Bryan, S. Robinson, and J. Watson, *Vision 2020: 2000 separations roadmap*, Tech. Rep. (EERE Publication and Product Library, 2000).

[47] R. Darakchiev, *Inlet and internal devices for packed columns,* Chemical and biochemical engineering quarterly **18**, 145 (2004).

[48] M. Wehrli, S. Hirschberg, and R. Schweizer, *Influence of vapour feed design on the flow distribution below packings,* Chemical Engineering Research and Design **81**, 116 (2003).

[49] M. Haghshenasfard, M. Zivdar, R. Rahimi, and M. Nasr Esfahany, *Cfd simulation of gas distribution performance of gas inlet systems in packed columns,* Chemical Engineering & Technology **30**, 1176 (2007).

[50] J. Maćkowiak and J. F. Maćkowiak, *Random packings,* in *Distillation: Equipment and Processes* (Elsevier, 2014) pp. 85–144.

[51] A. Orlando Jr, L. Medina, M. Mendes, and E. Nicolaiewsky, *Hetp evaluation of structured packing distillation column,* Brazilian Journal of Chemical Engineering **26**, 619 (2009).

[52] L. Del Carlo, Ž. Olujić, and A. Paglianti, *Comprehensive mass transfer model for distillation columns equipped with structured packings,* Industrial & engineering chemistry research **45**, 7967 (2006).

[53] J. Maćkowiak, *Model for the prediction of liquid phase mass transfer of random packed columns for gas–liquid systems,* Chemical Engineering Research and Design **89**, 1308 (2011).

[54] I. J. Maćkowiak, *Two-phase flow and operating range,* in *Fluid Dynamics of Packed Columns* (Springer, 2010) pp. 25–121.

[55] F. Alnaimat, J. F. Klausner, and R. Mei, *Transient analysis of direct contact evaporation and condensation within packed beds,* International Journal of Heat and Mass Transfer **54**, 3381 (2011).

[56] T. H. Chilton and A. P. Colburn, *Distillation and absorption in packed columns a convenient design and correlation method,* Industrial & Engineering Chemistry **27**, 255 (1935).

[57] R. Billet and M. Schultes, *Prediction of mass transfer columns with dumped and arranged packings: updated summary of the calculation method of billet and schultes,* Chemical Engineering Research and Design **77**, 498 (1999).

[58] M. G. Shi and A. Mersmann, *Effektive austauschfläche in füllkörperkolonnen,* Chemie Ingenieur Technik **56**, 404 (1984).

[59] R. Billet and J. Maćkowiak, *How to use the absorption data for design and scale-up of packed columns,* European Journal of Lipid Science and Technology **86**, 349 (1984).

[60] A. B. Erasmus, *Mass transfer in structured packing*, Ph.D. thesis, Stellenbosch: University of Stellenbosch (2004).

[61] Ž. Olujić, *Effect of column diameter on pressure drop of a corrugated sheet structured packing,* Chemical Engineering Research and Design **77**, 505 (1999).

[62] B. Hanley, *On packed column hydraulics,* AIChE Journal **58**, 1671 (2012).

[63] H. Cherif, *Comparison of models for the prediction of hydrodynamic parameters in structured packing columns for biogas purification,* International Journal of Renewable Energy Research (IJRER) **7**, 866 (2017).

[64] M. Holz, S. R. Heil, and A. Sacco, *Temperature-dependent self-diffusion coefficients of water and six selected molecular liquids for calibration in accurate 1h nmr pfg measurements,* Physical Chemistry Chemical Physics **2**, 4740 (2000).

[65] A. F. Mills, *Basic heat and mass transfer*, 2nd ed. (Pearson Education Limited, 2014).

[66] R. Cini, G. Loglio, and A. Ficalbi, *Temperature dependence of the surface tension of water by the equilibrium ring method,* Journal of Colloid and Interface Science **41**, 287 (1972).

[67] G. P. Brasseur and D. J. Jacob, *Modeling of Atmospheric Chemistry* (Cambridge University Press, 2017).

[68] *Intalox packed tower sytems, Packed Tower Internals*, Koch-Glitsch (2010).

[69] T. Mathson and M. Ivanovich, *AMCA's Fan Efficiency Grades: Answers to Frequently Asked Questions*, AMCA International (2011).

[70] J. R. Couper, W. R. Penney, and J. R. Fair, *Chemical Process Equipment-Selection and Design (Revised 3rd Edition)* (Elsevier, 2012).

[71] N. D. Prijzenboekje, *Dace (dutch association of cost engineers),* The Netherlands (2005).

[72] C. F. Petre, F. Larachi, I. Iliuta, and B. Grandjean, *Pressure drop through structured packings: Breakdown into the contributing mechanisms by cfd modeling,* Chemical Engineering Science **58**, 163 (2003).

[73] Y.-L. Zhang, H.-M. Zhu, and Q.-X. Yin, *Cfd study on the local mass transfer efficiency in the gas phase of structured packing,* Chemical Engineering & Technology **36**, 1138 (2013).

[74] F. Yin, A. Afacan, K. Nandakumar, and K. T. Chuang, *Liquid holdup distribution in packed columns: gamma ray tomography and cfd simulation,* Chemical Engineering and Processing: Process Intensification **41**, 473 (2002).

[75] S. Piché, F. Larachi, and B. P. Grandjean, *Flooding capacity in packed towers: database, correlations, and analysis,* Industrial & engineering chemistry research **40**, 476 (2001).

A

LIQUID DISTRIBUTOR

This section gives an overview of the application areas of various liquid distributor, as described by Kolev [8].

Table A.1: Overview of the application areas of the described liquid distributors[8]

Type	d_c	Turndown ratio	Liquid superficial velocity			Gas capacity factor			
	cm		$m^3\,m^{-2}\,s^{-1}$			$F_v = u_v * \sqrt{\rho_g}$ $kg^{1/2}\,m^{-1/2}s^{-1}$			
			$u_{l,s} < 2$	$2 < u_{l,s} < 80$	$u_{l,s} > 80$	$F_v < 1$	$1 < F_v < 2$	$F_v > 2$	$F_v > 3.5$
DT1	> 500	2.5:1		x		x	x		
DT2	> 1200	10:1		x	x	x	x		
DR2	< 1200	2.5:1		x	x	x	x		
DR3	< 1200	10:1		x	x	x			
DP1	> 500	5:1		x	x	x	x	x	
DT-MF	> 300	2.5:1-5:1	x	x	x	x	x	x	
DT-S	> 300	2.5:1		x		x	x		
DP-S	> 800	3:1	x	x	x	x	x		
PLD	> 500	5:1		x	x	x	x	x	x
TLD	> 500	2.5:1		x	x	x	x	x	x
RCD	> 300	2.5:1		x	x	x	x	x	x
STD	< 300	5:1		x	x	x	x	x	

In table A.1 the following liquid distributors are listed: the trough distributor type DT 1, the trough distributor with weirs type DT 2, distributor with gas risers type DR 2, distributor with gas risers type DR 3, pipe liquid distributor type DP 1, distributor type Multi-Flow DT-MF, system distributor DT-S, pipe lamella type distributors PLD, through lamella type distributors TLD, round column distributor RCD and the shower type distributor STD.

B

STRUCTURED PACKING SELECTION

This appendix describes the selection of a structured packing for the Bluerise B.V. experimental set-up, by making a preliminary financial analysis for a 25 $m^3\,day^{-1}$ fresh water production pilot plant.

B.1. INTRODUCTION

This document gives an overview of an initial financial comparison between various structured (metal) packings for the Bluerise B.V. pilot plant.The pilot plant will have a production of 25 $m^3\,day^{-1}$. The goal of the analysis is to select a packing for the experimental set-up in the Process and Energy lab of the Delft University of Technology. It is desirable to select a packing that is similar to the final design of the pilot plant. Therefore the financial comparison is mainly based on the properties of the pilot plant.

B.2. COLUMN AND FLOW PROPERTIES

B.2.1. TECHNICAL OPTIMIZATION

Preceding the economical analysis a technical selection of the most suitable packings for the experimental set-up was made. The selection was based on the ratio between the production and pressure drop for different heights of the packing. The selection was made for an air feed of 50 $l\,s^{-1}$, 28 °C, 80 % relative humidity and a water feed of 0.074 $kg\,s^{-1}$ and 12 °C.

Table B.1 gives and overview of the selected top 5 for the Sulzer and Koch-Glitsch structured packings that are available in Aspen plus V8.8. Section B.6 gives an overview of the top 5 performances for various heights. Aspen Plus only has a limited amount of available packings, mainly the plastic packings are lacking and are therefore not considered in this preliminary analysis .

B.2.2. INITIAL PROPERTIES FOR THE PILOT PLANT

A preliminary design for the pilot plant was made and used as a base for this economic analysis. Figure B.1 shows the flowsheet of the Aspen plus model. It was assumed that, since the pilot plant is essentially an upscaled version of the experimental set-up, the top 5 packing selections are also applicable to the pilot plant.

Table B.1: Top 5 packings from the technical selection for the experimental set-up

Sulzer	Koch
BXPLUS	Flexipac 500X
MellaPak 170X	Flexipac 350X
MellaPak 250X	Flexipac 1.6X
MellaPak 350X	Flexipac 1X
MellaPak 500X	Flexipac 250X

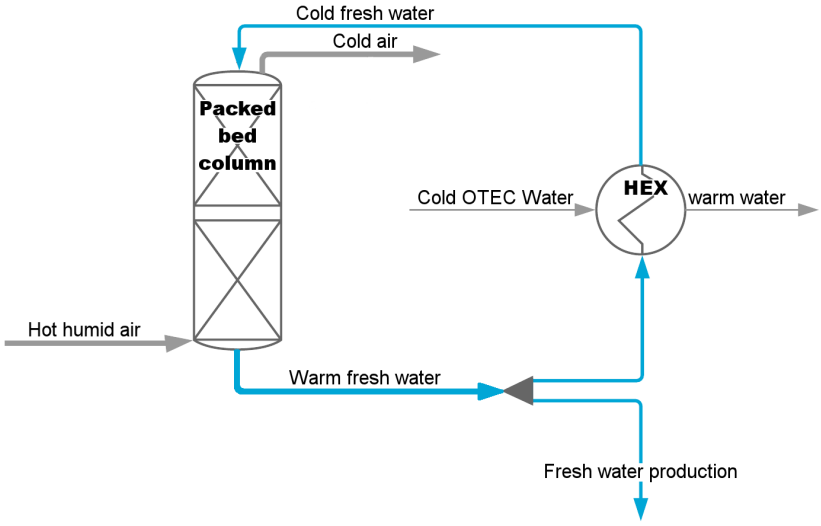

Figure B.1: Flowsheet of the Aspen plus model used for a preliminary pilot plant design

AIR FEED FLOW

Molliers diagram shows that for air of 80 % relative humidity (RH) that cools from 28 °C to 12.5 °C approximately 10.2 g of water per 1 kg of dry air can be produced. This means that for a production of 25 $m^3\,day^{-1}$ (= 1042 $kg\,hr^{-1}$) of water, a dry air inflow of 102 156 kg hr−1 is required. This equals an incoming airflow of 104 100 $kg\,hr^{-1}$.

WATER FEED FLOW

To define the water feed flow it is necessary to set an initial column diameter. The diameter is chosen at 3 m, based on previous research done by Lopez[2]. A sensitivity analysis for the flow and height was performed on the FlexiPac 250X structured packing. Figure B.2 shows the fresh water production for different water feed flows and varying column height. Based on this, the water feed flow is set to 120 000 kg h−1. Because this analysis compares the performance of the packings, the water feed flow is kept constant for the different packings.

COLUMN DIAMETER

In literature much has been written about the consequence of various operating parameter on the efficiency of the column. According to Piche et al. [75] these studies can be divided into those related to mass transfer efficiencies, and those related tot the hydrodynamic phenomena. For the second category, they stress the importance of the flooding capacity, since it influences liquid hold-up, flow behaviour and pressure drops across the bed. Larger liquid flows will obstruct the gas flow and result

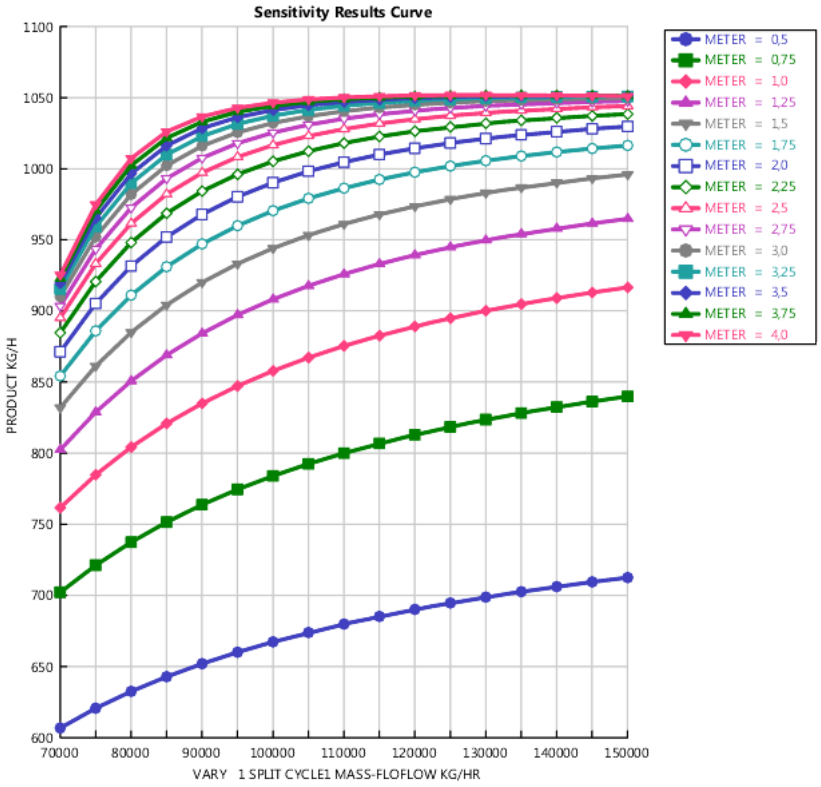

Figure B.2: Fresh water production as a function of water feed flow and packing height for the FlexiPac 250X packing

in greater liquid hold-ups. Because a capacity close to flooding often means a higher HETP (Height Equivalent to Plate, a measure of packing efficiency), but too close to flooding causes a high pressure drop, the capacity is set at 70 %. It should be noted that this capacity is not optimized, but taken as a constant for all the packings.

Because the feed flows have already been set, the main influencer of the flooding capacity is the column diameter. Table B.2 lists the column diameters per packing that result in the desired flooding capacity.

PACKING HEIGHT AND PRESSURE DROPS

For the initial cost the packing height is an important parameter. It is analysed in Aspen Plus what the necessary packing height is, for the set feed properties and column diameter, to reach a water production of 1042 $\mathrm{kg\,h^{-1}}$. The packing height significantly influences the pressure drop over the packing. Table B.2 lists the required packing heights and the pressure drops.

Table B.2: Packing dimensions and pressure drop over packing

Packing	Diameter	Height	Total volume	Pressure drop
BXPLUS	3.62 m	1.16 m	11.95 m^3	183.66 Pa
MellaPak 170X	2.9 m	3.63 m	23.98 m^3	343.96 Pa
MellaPak 250X	3.18 m	2.43 m	19.30 m^3	454.32 Pa
MellaPak 350X	3.50 m	1.56 m	15.01 m^3	290.61 Pa
MellaPak 500X	3.82 m	1.01 m	11.58 m^3	212.34 Pa
Flexipac 500X	4.25 m	0.93 m	13.19 m^3	112.04 Pa
Flexipac 350X	3.69 m	1.50 m	16.04 m^3	194.34 Pa
Flexipac 1.6X	3.47 m	1.90 m	17.97 m^3	277.66 Pa
Flexipac 1X	3.9 m	1.15 m	13.74 m^3	177.31 Pa
Flexipac 250X	3.35 m	2.37 m	19.66 m^3	284.34 Pa

B.3. ENERGY DEMAND

The energy demand per kg of produced water is calculated not as an absolute accuracy, but as a comparative study. This means that the constant demands have been left out. This includes fan power for kinetic pressure drops over the pipes and pump power for the pressure drops over the pipes and the heat exchanger.

On top of the packing height an extra 40 cm is taken for the sprinkler, this is added to the head of the waterpump. The waterpump is estimated to have an efficiency of 65 %. For the fan only the power required for the pressure drop over the packing is considered. The fan efficiency is estimated around 70 %.

For larger diameters the energy requirements go down. The energy requirement is a balance between two factors. Firstly, for higher packing density, a larger pressure drop per quantity of height can be observed, thus needing more fan power. But higher density packings require less packing height for the air to reach 12.5 °C, this decreases the water pump head.

A similar process happens with te water flow variable. The energy requirement seems stable, because for higher water flow-rates, less column height is required.

Table B.3 gives an overview of the energy demand per kilogram of fresh water production for the different packings. To produce 1 kg_{water} between 4.48 Wh and 16.93 Wh of electrical energy is required. Section B.7 gives an overview of the energy and power consumption for the water pump and fan per packing.

Table B.3: Energy demand per kg of water for a water production rate of 0.29 $kg\,s^{-1}$ for different packings

	electricity demand [kW_{el}]	Energy demand per kg of water [$Wh\,kg^{-1}_{water}$]
BXPLUS	7.34	7.04
MellaPak 170X	14.30	13.73
MellaPak 250X	17.64	16.93
MellaPak 350X	11.36	10.90
MellaPak 500X	8.29	7.95
Flexipac 500X	4.67	4.48
Flexipac 350X	7.89	7.57
Flexipac 1.6X	11.07	10.62
Flexipac 1X	7.11	6.82
Flexipac 250X	11.54	11.08

B.4. COSTS

To determine the feasibility of the process a preliminary estimate of the costs are made. The total production costs consist of the fixed production costs, the variable production costs and the overhead costs. For the fixed production cost only the price of the packing is considered. The size of the column also varies with packing height, but this cost variable is considered negligible. The price per volume of the packings is deducted from the cost estimations that were provided by the distribution companies of Sulzer and Koch-Glitsch. It is common to assume a depreciation time between 3 and 5 years for process plants. For these packings we assume a depreciation time of 3 years.

The variable production costs are taken as the costs of electricity. The current electricity price in Curaçao is 0.24 € kWh^{-1} for industrial use (according to Aqualectra on July 1st 2017). It is assumed that the fresh water production runs for 95 % of the time.

Table B.4: Energy and material cost expressed per day for various packings

Packing	Energy cost € day^{-1}	Packing cost € day^{-1}	Total cost € day^{-1}
BXPLUS	4.01	65.57	69.58
MellaPak 170X	7.82	96.94	104.77
MellaPak 250X	9.65	83.61	93.25
MellaPak 350X	6.21	73.69	79.90
MellaPak 500X	4.53	61.85	66.38
Flexipac 500X	2.55	15.83*	18.39
Flexipac 350X	4.32	15.83	20.15
Flexipac 1.6X	6.05	20.61	26.66
Flexipac 1X	3.89	23.35	27.24
Flexipac 250X	6.31	18.66	24.97

*is based on the price for Flexipac 350x

B.5. CONCLUSION

Because Sulzer did not provide a price per 10 m^3 for the packings, the material cost estimation is based on the quotation provided for the experimental set-up. This results in very high prices, therefore the production price becomes mostly dependent on the packing cost. It must be concluded that

the economic analysis for the Sulzer Packing is not reliable. For the Koch-Glitsch packing, assuming that the pricing of Flexipac 500X will be significantly higher, the Flexipac 350X gives the best results ($20.15 €\,day^{-1}$).

B.6. DATA FOR TECHNICAL SELECTION OF STRUCTURED PACKINGS

The data for the pressure drop and production was generated with Aspen plus, for a condenser column diameter of 24 mm, a water inflow of 0.074 kgs−1 and 12 °C, an air inflow of 50 ls^{-1}, 28 °C and a relative humidity of 80 %.

B.6.1. SULZER

Table B.5: Top 5 Sulzer packings of the technical selection for the demo plant

Packing Height m	Production kgh^{-1}	Pressure drop pa	Production over Pressure drop $kgh^{-1}\,pa^{-1}$
BXPLUS			
0.1	1.50483563	4.79560222	0.313794923
0.2	1.99761981	9.47999296	0.210719546
0.3	2.24871062	14.1099858	0.159370155
0.4	2.40028713	18.705277	0.128321389
0.5	2.49816835	23.2758865	0.107328602
0.6	2.56361212	27.8277478	0.092124312
0.7	2.60823809	32.3648234	0.080588671
0.8	2.63905844	36.8901061	0.07153838
0.9	2.66049949	41.4059352	0.064254061
1	2.67548207	45.9142268	0.058271308
MellaPak - 170 X			
0.1	0.754613478	2.53453666	0.297732319
0.2	1.21325113	5.04092534	0.240680242
0.3	1.51324125	7.52947294	0.200975721
0.4	1.7242692	10.004983	0.172341042
0.5	1.88195979	12.4700783	0.150918041
0.6	2.00523031	14.9263956	0.134341228
0.7	2.10464502	17.3750757	0.121130121
0.8	2.18663467	19.8170974	0.110340815
0.9	2.2552966	22.2532378	0.101346897
1	2.31344723	24.6841281	0.093722056
MellaPak -250X			
0.1	1.03302903	3.33319184	0.309921865
0.2	1.53608915	6.61763118	0.232120695
0.3	1.82891678	9.87398341	0.185225831
0.4	2.02393486	13.1102332	0.15437825
0.5	2.16471389	16.3306933	0.132554929
0.6	2.27110728	19.5383694	0.116238322
0.7	2.35369127	22.7353941	0.103525422
0.8	2.41898534	25.9233495	0.093312993
0.9	2.47124999	29.1034318	0.084912666
1	2.51347271	32.2765889	0.077872935
MellaPak -350X			
0.1	1.30504053	4.52691222	0.288284921
0.2	1.81288086	8.97242973	0.20205016
0.3	2.08546557	13.3744906	0.155928598
0.4	2.25864049	17.7466169	0.127271609
0.5	2.37730704	22.0964333	0.107587818
0.6	2.46185414	26.4287126	0.09315074
0.7	2.52347251	30.7466627	0.082073054
0.8	2.5690941	35.0526545	0.073292426
0.9	2.60321244	39.3485255	0.066157814
1	2.62890692	43.6357936	0.060246571
MellaPak -500X			
0.1	1.62352366	6.66835283	0.24346697
0.2	2.10238999	13.1911103	0.159379305
0.3	2.33743323	19.6438831	0.118990386
0.4	2.47334213	26.0518652	0.094939157
0.5	2.55705469	32.4278119	0.078853754
0.6	2.61028874	38.7795122	0.067311026
0.7	2.64472366	45.1124451	0.058625146
0.8	2.66722289	51.4308867	0.051860333
0.9	2.6819972	57.7382192	0.046450986
1	2.69172095	64.0371616	0.042033733

B.6.2. KOCH-GLITSCH

Table B.6: Top 5 Koch-Glitsch packings of the technical selection for the demo plant

Height [m]	Production [kg/h]	Pressure drop [Pa]	[Pa/kg/h]
Flexipac 500X			
0.1	1.64306678	3.76684995	low production
0.2	2.12137085	7.45813989	low production
0.3	2.35336936	11.1108894	4.721268828
0.4	2.48619084	14.7376836	5.927816708
0.5	2.56720124	18.3452595	7.146015363
0.6	2.61819269	21.93798	8.37905479
0.7	2.6508292	25.5190841	9.626830767
0.8	2.67192276	29.0911766	10.88773113
0.9	2.68562392	32.6563624	12.15969301
1	2.69454559	36.2163419	13.44061204
Flexipac 350X			
0.1	1.30737357	2.2218894	low production
0.2	1.81628533	4.4055685	low production
0.3	2.08892174	6.56847356	low production
0.4	2.26183332	8.71679294	low production
0.5	2.38016928	10.8540201	4.560188299
0.6	2.46439122	12.9823881	5.267989918
0.7	2.52571148	15.1034292	5.979871145
0.8	2.5710683	17.2182953	6.696942007
0.9	2.60495645	19.3278968	7.41966216
1	2.63045437	21.4329972	8.148020906
Flexipac 1.6X			
0.1	1.15990866	2.0052336	low production
0.2	1.67100662	3.97843659	low production
0.3	1.95630611	5.93374912	low production
0.4	2.14213705	7.87631776	low production
0.5	2.27335721	9.80904389	low production
0.6	2.37008821	11.73384	4.950803076
0.7	2.44318536	13.6520345	5.587801369
0.8	2.49938731	15.5646103	6.227370299
0.9	2.54309696	17.4723212	6.870489594
1	2.57737748	19.3757803	7.517633894
Flexipac 1X			
0.1	1.4870263	3.54949734	low production
0.2	1.98412461	7.03242269	low production
0.3	2.23751951	10.4805353	low production
0.4	2.39093363	13.9048338	5.815650265
0.5	2.49047645	17.3113197	6.951007186
0.6	2.55739362	20.7037581	8.095647826
0.7	2.60328921	24.0848047	9.251682298
0.8	2.63518113	27.4565448	10.41922488
0.9	2.6575108	30.8206817	11.59757533
1	2.67321989	34.1786526	12.7855747
Flexipac 250X			
0.1	1.01825199	1.45387895	low production
0.2	1.52289655	2.88589913	low production
0.3	1.8180344	4.30538543	low production
0.4	2.01451177	5.71592822	low production
0.5	2.15626657	7.11949336	low production
0.6	2.26344666	8.51738846	low production
0.7	2.34674506	9.91054364	4.22310195
0.8	2.41271503	11.2996529	4.683376511
0.9	2.46562212	12.6852436	5.144844985
1	2.50845188	14.0677342	5.60813397

B.7. LISTS OF ENERGY CONSUMPTION SPECIFICATION

The energy demand and power consumption are only taken for the column. This means it only includes pump head due to packing height and pressure drops over the packing.

Table B.7: Power demand and energy consumption for the fan and waterpump for different packings

	Pump Power kW	Pump energy $Wh\,kg^{-1}$	Fan power kW	Fan energy $Wh\,kg^{-1}$	Total Power kW	Total energy $Wh\,kg^{-1}$
BXPLUS	0.785303077	0.753649786	6.554164224	6.28998486	7.339467301	7.043634646
MellaPak 170X	2.0274	1.945681382	12.27469414	11.7799368	14.30209414	13.72561818
MellaPak 250X	1.423707692	1.366322162	16.21304525	15.55954438	17.63675294	16.92586655
MellaPak 350X	0.986030769	0.946286727	10.3708247	9.952806818	11.35685547	10.89909354
MellaPak 500X	0.709338462	0.680747084	7.577650176	7.27221706	8.286988638	7.952964144
Flexipac 500X	0.669092308	0.642123136	3.998304256	3.8371442	4.667396564	4.479267336
Flexipac 350X	0.955846154	0.917318766	6.935294976	6.655753336	7.89114113	7.573072102
Flexipac 1.6X	1.157076923	1.110438506	9.908685824	9.509295417	11.06576275	10.61973392
Flexipac 1X	0.779769231	0.748338993	6.327555584	6.072510157	7.107324815	6.82084915
Flexipac 250X	1.393523077	1.337354201	10.14707098	9.738071954	11.54059405	11.07542615

C

FLEXIPAC 350X DATASHEET

FLEXIPAC® Structured Packing

KOCH-GLITSCH

As the industry standard, FLEXIPAC structured packing has been used in thousands of columns worldwide. FLEXIPAC packing provides a lower pressure drop per theoretical stage and increased capacity compared to trays and conventional random packings. Columns packed with FLEXIPAC packing have resulted in:

- Improved product yields
- Improved product purities
- Reduced reflux ratios
- Increased throughput
- Lower pressure drop
- Reduced liquid holdup
- Increased heat transfer

FLEXIPAC structured packing is available in a variety of corrugation crimp sizes, each at two inclination angles. The "Y" designated packings have a nominal inclination angle of 45° from the horizontal, and are the most widely used. The "X" packings have a nominal inclination angle of 60° from horizontal and are used where high capacity and low pressure drop are the overwhelming requirements for a specific application. The benefit of the "X" packings is that they provide a lower pressure drop per theoretical stage for the same surface area.

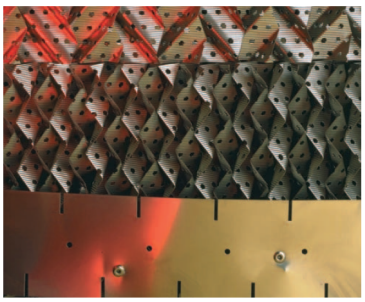

FLEXIPAC® Structured Packing with perforated and textured surface shown with attached wall wiper band

The plot below provides approximate efficiency information for FLEXIPAC structured packing as typically seen in distillation service of hydrocarbons operating under atmospheric to moderate vacuum conditions. From years of applications experience, Koch-Glitsch has an extensive collection of efficiency information for a wide variety of processes and operating conditions. Consult Koch-Glitsch for further information.

FLEXIPAC® Structured Packing
Approximate Efficiency in Atmospheric Distillation.

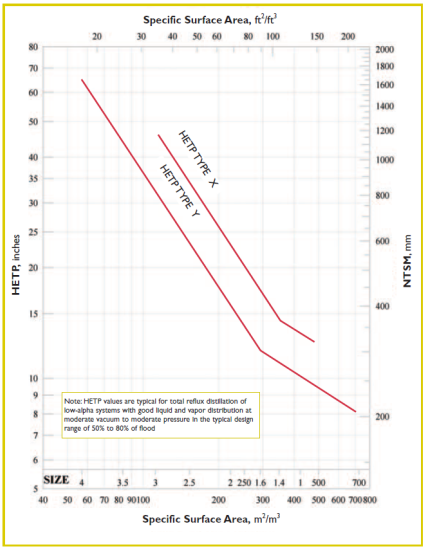

Increasing Capacity ←

→ Increasing Efficiency

FLEXIPAC® Structured Packing Surface Area												
	ft²/ft³	17	25	34	47	68	77	90	106	129	152	220
	m²/m³	55	80	110	155	225	250	295	350	420	500	725
Inclination Angle												
	45°	4Y	3.5Y	3Y	2.5Y	2Y	250Y	1.6Y	1.4Y/350Y	1Y	500Y	700Y
	60°	4X	3.5X	3X	2.5X	2X	250X	1.6X	1.4X/350X	1X	500X	700X

D

HEX FUNCTION OF THE PYTHON MODEL

The heat exchanger function of the Python model is described below. Some changes have been made in comparison to previous model presented by Noordhoek Hegt [3]. He correlated a Nusselt number based on experimental outcomes. Since the experiment does not work with sea water, and the behavior of single phase water along plates is well studied, this work makes use of the dimensionless Nusselt number for plate heat exchangers as presented ny Towler and Sinnott [10].

Table D.1: Energy balance over the HEX

Index $_{\text{fw}}$ is fresh water (OTWP) and index $_{\text{sw}}$ is seawater (OTEC)

Energy Balance:	
Overall heat transferred Q	$Q = UA_{\text{HEX}}\Delta T_{\text{m}}$
	$Q = \dot{m}_{\text{fw}} c_{p\text{fw}} (T_{\text{in,fw}} - T_{\text{out,fw}}) = \dot{m}_{\text{sw}} c_{pc} (T_{\text{out,sw}} - T_{\text{in,sw}})$
Average temperature difference between two fluids T_{m}:	
Temperature difference T_{m}	$T_{\text{m}} = F_{\text{t}} \Delta T_{\text{lm}}$
Mean temperature difference ΔT_{lm}	$\Delta T_{\text{lm}} = \frac{\left(T_{\text{in,a}} - T_{\text{out,w}}\right) - \left(T_{\text{out,a}} - T_{\text{in,w}}\right)}{\ln \frac{T_{\text{in,a}} - T_{\text{out,w}}}{T_{\text{out,a}} - T_{\text{in,w}}}} = 2.82\,^{\circ}\text{C}$
Number of Transfer units NTU	$NTU = \frac{T_{\text{in,fw}} - T_{\text{in,sw}}}{\Delta T_{\text{lm}}}$
Correction factor F_{t}	Read from figure 19.58 in Towler and Sinnott [10]
total HEX surface area A_{HEX}:	
Total HEX surface area	$A_{\text{HEX}} = \frac{Q}{U \Delta T_{\text{m}}}$
With N_{pl} the number of plates	$A_{\text{HEX}} = N_{\text{pl}} A_{\text{plate,eff}}$
Effective plate surface area $A_{\text{plate,eff}}$	$A_{\text{plate,eff}} = W_{\text{pl}} L_{\text{pl}} \Phi$
Plate pattern correction factor Φ	$\Phi = 1.22$ [9]
Overall heat transfer coefficient U:	
Assumed overall heat transfer coefficient U_{as}	
Calculated overall heat transfer coefficient U_{calc}	$\frac{1}{U_{\text{calc}}} = \frac{1}{\alpha_{\text{sw}}} + \frac{1}{f_{\text{sw}}} + \frac{d_{\text{pl}}}{\lambda_{\text{pl}}} + \frac{1}{f_{\text{fw}}} + \frac{1}{\alpha_{\text{fw}}}$
Fouling factors f_{fw} and f_{sw}	f_{fw}=3000 $\text{W m}^{-2}\,\text{K}^{-1}$ [10]
Thermal conductivity stainless steel	16 W/m K[9]
Wall thickness d_{pl}	$d_{\text{pl}} = 0.4$ mm[2]
Component film heat transfer coefficient α_{j}	$\alpha_{\text{j}} = \frac{Nu_{\text{j}} \lambda_{\text{j}}}{d_{\text{h}}}$
Plate Hydraulic diameter d_{h}	twice the gap between the plates
Component dimensionless Nusselt number Nu_{j}	$Nu_{\text{j}} = 0.26 Re_{\text{j}}^{0.65} Pr_{\text{j}}^{0.4}$ [10]

Table D.2: Pressure drop in the HEX for laminar flows [9]

Pressure drop per component	$\Delta P_j = \xi_j \frac{L_{pl}}{d_h} \frac{\rho_j u_j^2}{2}$	
With friction factor ξ_j	$\frac{1}{\sqrt{\xi}} = \frac{\cos\varphi}{\sqrt{b\tan\varphi + c\sin\varphi + \xi_0/\cos\varphi}} + \frac{1-\cos\varphi}{\sqrt{\xi_1}}$	b= 0.18
		c=0.36
Friction factor ξ_0	$\xi_{0,j} = B_0/Re_j$	$B_0 = 64$
and friction factor $\xi_{1,j}$	$\xi_{1,j} = a(B_1/Re_j + C_1)$	$B_1 = 597$
		a =3.8
Port pressure drop per component $\Delta P_{port,j}$	$\Delta P_{port} = 1.3\rho_j \frac{2\dot{m}_j}{\rho_j \pi d_{port}^2}$	

Table D.3: Dimensions of the selected HEX for the Pilot-Plant design

plate length	L_{plate}	1.8 m
plate width	W_{plate}	0.9 m
correction for plate pattern	Φ	1.22
chevron angle	φ	30°
Distance between plates	$0.5d_h$	3 mm
number of plates	N_{plate}	168
material of plate	stainless steel	
thermal conductivity of plate	k_{plate}	16 $W m^{-1} K^{-1}$
Port diameter	d_p	0.6 m

E

PRESSURE DROP FUNCTION OF PYTHON MODEL

The pressure drop function of the Python model calculates the pressure drops in the pipes on the air and fresh water side, and the pressure drop associated with the fresh water pump head. It then adds the pressure drops that are calculated in the HEX function and Condenser function, resulting in a total pressure drop for the fresh water flow, air flow, and seawater flow. With this information pumps and fans can be selected, and the energy consumption of the OTWP system is calculated.

Table E.1: Calculation for the fresh water pressure drops in the pipes

Darcy-Weisbach equation	
	$\Delta P = \frac{\rho u^2}{2}\left(\xi_D \frac{L_{pipe}}{d_{pipe}} + \sum K\right)$
Darcy friction factor ξ_D	
Laminar	$\xi_D = \frac{64}{Re}$
Turbulent (smooth-pipe)	$\xi_D = \frac{0.316}{Re^{0.25}}$
K-factors	
90 deg elbow curved (R/d=1.5)	K =0.45
Pipe exit (water feed flow)	K =1
Flush entrance (water exit flow)	K =0.5
pipe length	
Length of the pipes L_{pipe}	$L_{pipe} = H_{GD} + H_p + H_{LD} + R_p$
With H_{GD} the distance between the GD and packing	$H_{GD} = 0.15 d_c$
With H_{LD} the distance between the LD and packing	$H_{GD} = 0.4$ m
With R_c the distance to the column center g	$R_c = 0.5 d_c$

Table E.2: Calculation for the air pressure drops in the pipes and the column before packing

Darcy-Weisbach equation	
	$\Delta P = \frac{\rho u^2}{2} \sum K$
K-factors	
Exit (air exit point)	K =1
Flush entrance (air feed point)	K =0.5

Table E.3: Calculation for the fresh water pressure drop associated with pump head

Pressure drop of fresh water due to head	$\Delta P_{\text{head,L}} = \rho_{\text{L}} g H$
The height, H	$H = H_{\text{p}} + H_{\text{LD}} + H_{\text{GD}}$
Height of packing. H_{p}	$H_{\text{p}} = n H_{\text{el}}$
Distance between gas feed and packing, H_{GD}	$H_{\text{GD}} = 0.15 d_{\text{c}}$
Distance between liquid feed and packing, H_{LD}	$H_{\text{LD}} = 40 cm$

Table E.4: Energy requirements

Fresh water pump	
Total pressure drop $\Delta P_{\text{tot,fw}}$	$\Delta P_{\text{tot,fw}} = \Delta P_{\text{head,fw}} + \Delta P_{\text{pipes,fw}} + \Delta P_{\text{HEX,fw}}$
Efficiency	= 0.8
Power requirement	Power = $Q * \Delta P$/efficiency
Sea water pump	
Total pressure drop $\Delta P_{\text{tot,sw}}$	$\Delta P_{\text{HEX,sw}}$
Efficiency	= 0.8
Power requirement	Power = $Q * \Delta P$/efficiency
Fan	
Total pressure drop $\Delta P_{\text{tot,a}}$	$\Delta P_{\text{pipe,a}} + \Delta P_{\text{GD,a}} + \Delta P_{\text{p,a}} + \Delta P_{\text{LD,a}}$
Fan efficiency	= 0.62*0.8
Power requirement	Power = $Q * \Delta P$/efficiency

F

EXPERIMENTAL SET-UP

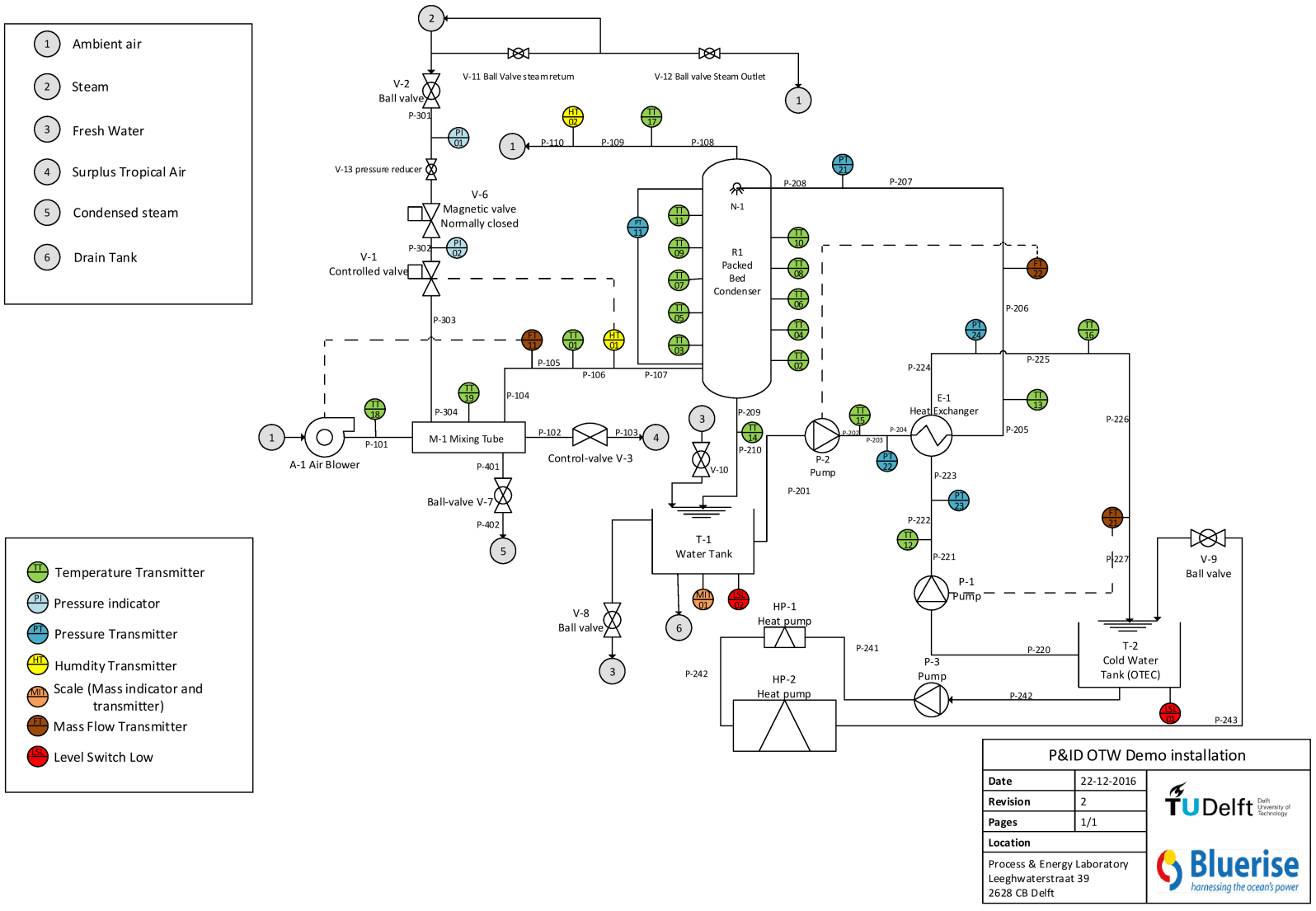

Figure F.1: The OTWP experimental set-up technical sheet

G

FAN PERFORMANCE EXAMPLE

This appendix gives an example of an axial fan that will perform at a 62 % efficiency for half of the required air feed flow rate of the pilot-plant (assuming two air feed points).

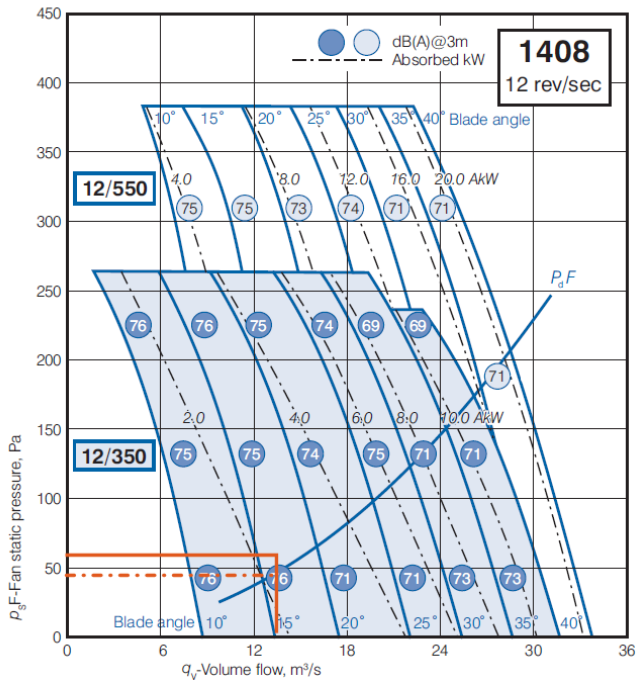

Figure G.1: Axial flow fan performance data of the 1408 mm 12 rev/sec axial fan by FANTECH 2016

Figure G.1 gives an example ofa large diameter axial fan performance data. The orange lines point out the approximate operating point of the pilot-plant. The volumetric feed flow rate of one fan would be around 13 $m^3 s^{-1}$ with a total column pressure drop around 60 Pa. The efficiency of this fan at that operating point can be calculated according to,

$$\text{efficiency} = \frac{Q\Delta P_{\text{t,fan}}}{10 P_{\text{R}}} \tag{G.1}$$

Where Q is the volumetric air feed flow rate in $m^3 s^{-1}$, $\Delta P_{\text{t,fan}}$ is the total fan pressure drop (sum of the static fan and dynamic fan pressure drop, $P_s F + P_d F$) and P_{R} is the fan impeller power in kW. For this fan model and the pilot-plant operating point that would give a fan efficiency of,

$$\text{efficiency} = \frac{13(60+50)}{102.3} = 62\% \tag{G.2}$$

H

PILOT-PLANT ENERGY REQUIREMENTS

This appendices includes the results of the pressure drop and power requirement calculations for the OTWP pilot-plant. The pressure drop in the fresh water flow, sea water flow and air flow are presented over fresh water flow rate and column diameter, with their respective power requirements.

H.1. PRESSURE DROPS

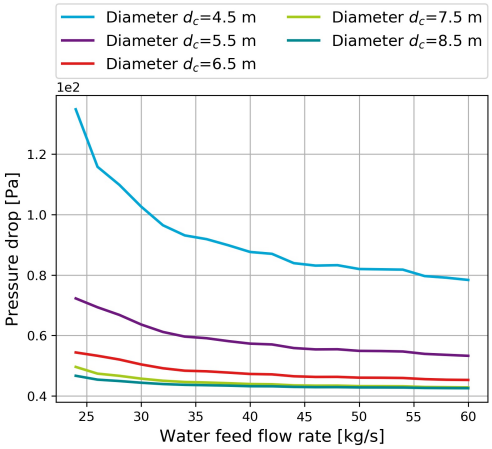

(a) Pressure drop in the air flow

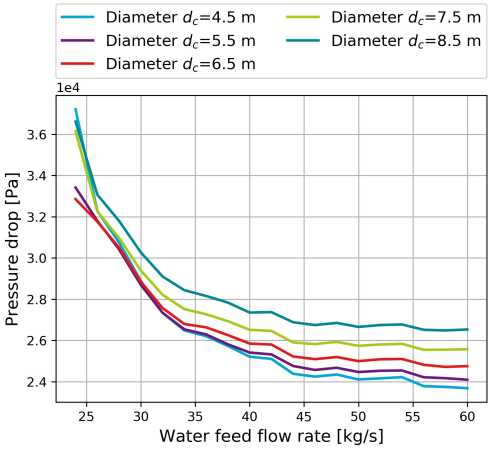

(b) Pressure drop in the fresh water flow

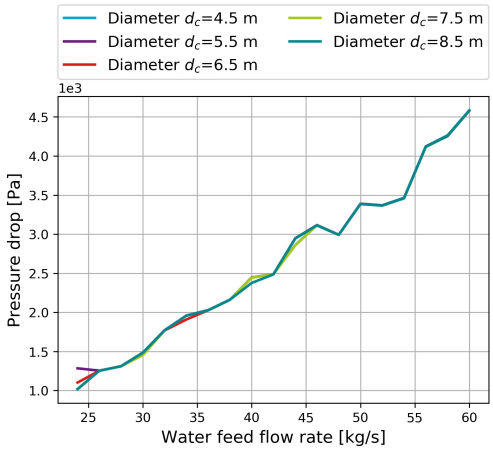

(c) Pressure drop in the sea water flow

Figure H.1: Pressure drops in the OTWP pilot-plant over water flow-rate and for varying column diameters

H.2. POWER REQUIREMENTS

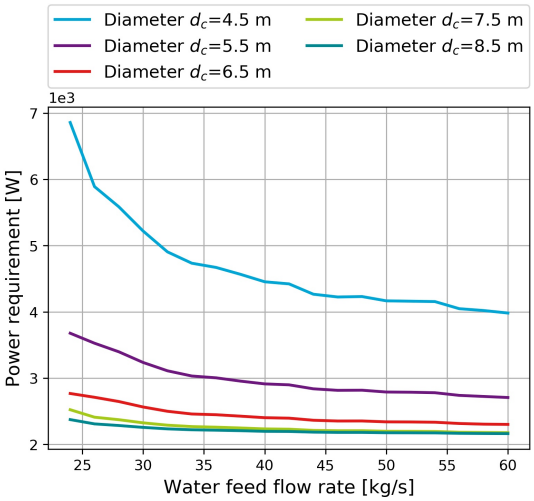

(a) Power requirement of the fan units

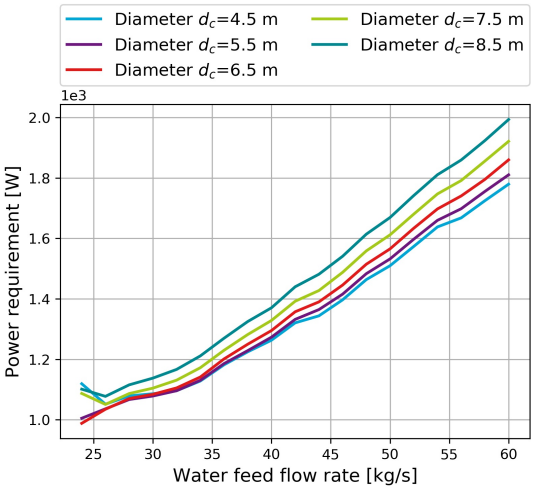

(b) Power requirement of the fresh water pump

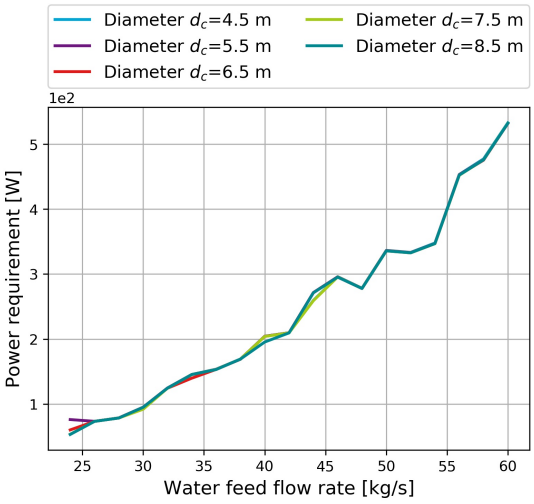

(c) Power requirement of the sea water pump

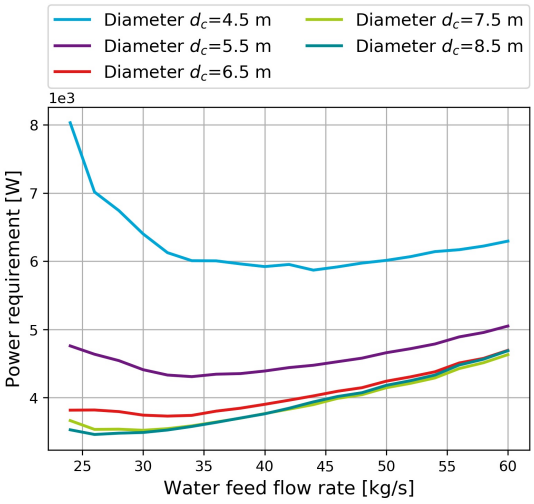

(d) Total OTWP pilot-plant power requirement

Figure H.2: Power requirement of the OTWP pilot-plant over water flow-rate and for varying column diameters

H.3. ENERGY CONSUMPTION

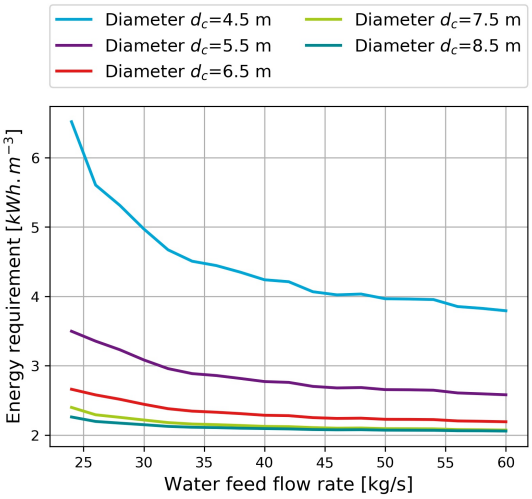

(a) Energy consumption of the fan units

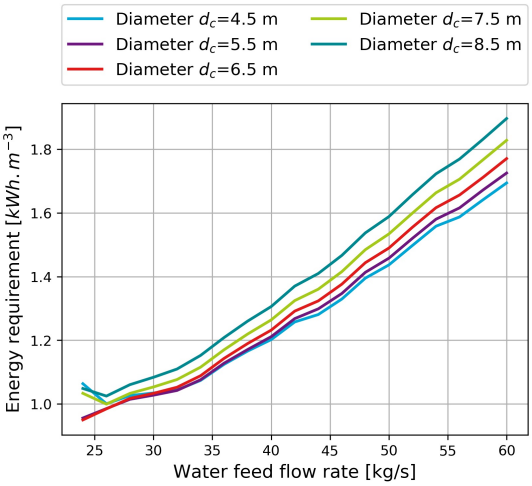

(b) Energy consumption of the fresh water pump

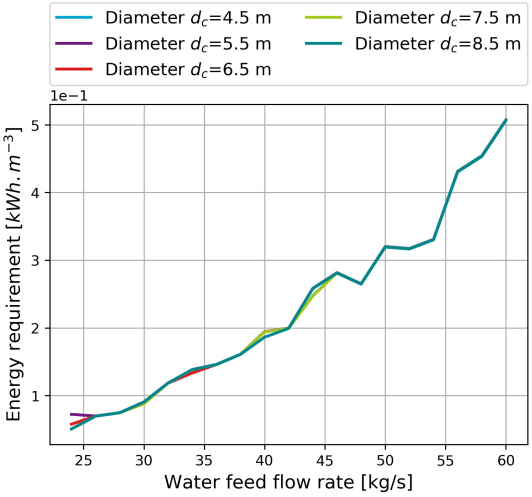

(c) Energy consumption of the sea water pump

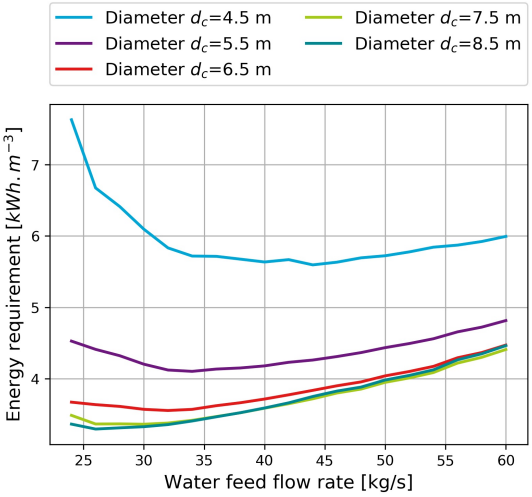

(d) Total OTWP pilot-plant Energy consumption

Figure H.3: Power requirement of the OTWP pilot-plant over water flow-rate and for varying column diameters

I

CAPEX OF THE OTWP PILOT-PLANT

For this preliminary estimation of the capital costs of the OTWP system, the major process equipments are considered. These include: the fresh water and sea water pump, the fan, the HEX, the packing and the column.

The cost of the packing FlexiPac 350X is given by Koch-Glitsch as 1315 € m^{-3} (~ 1620 \$ m^{-3}). Koch-Glitsch stated that the price of the packing is approximately scalable with its volume. The equipment costs, C_{Eq}, of the pumps and the HEX are calculated according to cost correlations of the form [10]:

$$C_{Eq} = K_a + K_b s^n \tag{I.1}$$

with s the size parameter, K_a and K_b the cost constants, and n the equipment dependent exponent.

For the construction of the condenser column and the (axial) fans, Towler and Sinnott [10] and the cost booklet did not provide a satisfactory cost estimation. Couper *et al.* [70] provides a more detailed correlation of the form,

$$C_{Eq} = 1.218 \exp\left[K_a + K_b(\ln s) + K_c(\ln s)^2\right] \tag{I.2}$$

where K_c is a cost constant. A viable material for the construction of the column would be concrete. Concrete can be insulated, is cheap and easy to transport. Transportation is an important factor, since the column should be constructed on an island (field erected). For a concrete, field erected storage vessel the size parameter is volume in gallons and the resulting equipment cost is given in \$. For an axial propeller fan including the motor, the size parameter is the volumetric flowrate (in thousand standard cubic feet per minute, KSCFM, at 0 °C and 1 atm) and the resulting cost is in unit \$1000. This expression is valid for volumetric flow rates up to 300 KSCFM. For this system two fan units are assumed. Table I.1 gives an overview of the parameters used in the equipment cost calculations.

When available, the outcomes of this cost correlations are compared to cost price estimations based on listed equipment costs from 2005 (cost booklet) [71]. To account for inflation the prices that are used are updated with published cost indexes according to [10],

$$\text{Cost in year A} = \text{Cost in year B} * \frac{\text{cost index in year A}}{\text{cost index in year B}} \tag{I.3}$$

Table I.1: Estimated parameters for the purchase costs (on a U.S. Gulf Coast basis, Jan. 2010 [10])

	Towler and Sinnott [10] cost correlation			Couper *et al.* [70] cost correlation		Quotation
	HEX	Pump_{fw}	Pump_{sw}	Axial fan	Column	Packing
cost constant K_a	1600	8000	8000	−0.4456	11.662	
cost constant K_b	210	240	240	0.2211	−0.6104	
cost constant K_c				0.0820	0.04536	
size parameter s	332 m^2	variable[$l\,s^{-1}$]	variable [$l\,s^{-1}$]	47.9 KSCFM	variable [gal]	
equipment exponent n	0.95	0.9	0.9			
installation factor[10]	3.5	4	4	2.5		
installation factor[70]	1.5	1.4	1.4	2.2	0.55	
cost booklet price	8400 $	6200 $	6200 $			
quotation						1620 $\$\,m^{-3}$

Table I.2 shows the Chemical Engineering Cost indexes used to update the cost booklet prices (2005) and the cost correlation outcomes (2010). This allows for comparison between price estimations and cost booklet prices. For various equipments the costs differed by more than a factor 2; the average is taken for the calculation of the levelized cost of water production. Figure I.1a shows the estimated equipment cost of the OTWP system. The individual equipment costs can be found in section I.1.

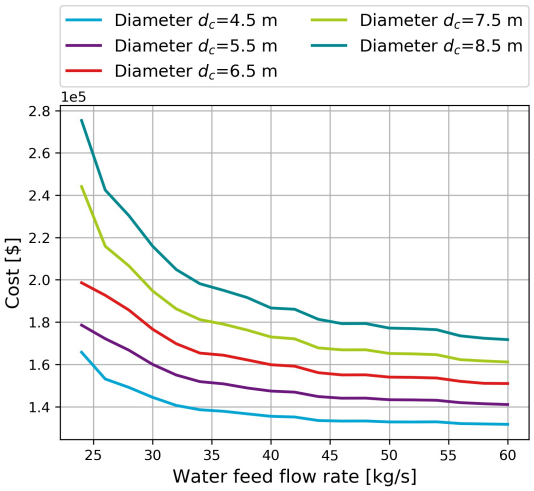

(a) Combined equipment cost

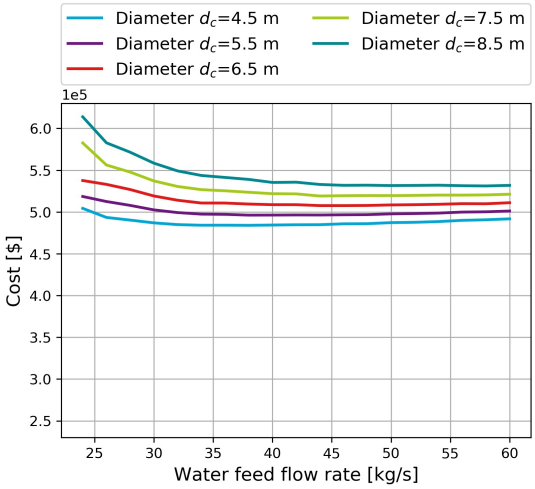

(b) CAPEX according to the installation factors suggested by Towler and Sinnott [10]

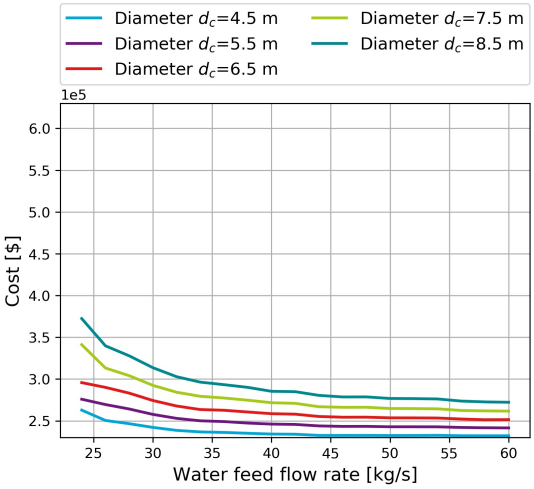

(c) CAPEX according to the installation factors suggested by Couper *et al.* [70]

Figure I.1: The investment cost for a 25 $m^3\,day^{-1}$ OTWP system with a lifetime of 10 years

The capital cost of the system include the installation cost of the equipment. These express the additional labor costs, transportation costs and any other additional costs that come with the OTWP installation. To obtain this, the purchase costs are multiplied wit an installation factor F_i (for this rough economic analysis: CAPEX = $F_i * \sum C_{Eq}$, see table I.1). The installation factors that are proposed by Towler and Sinnott [10] and Couper *et al.* [70] differ significantly. The CAPEX of the OTWP system is calculated with both installation factors and compared.

Table I.2: Chemical Engineering Cost index

	Sep 2005	Jan 2010	Nov 2017
CE INDEX	467.2	532.9	573.2
HEX	509.2	571.9	692.5
Pumps and compressors	756.3	903.0	995.9

The total CAPEX of the system for the different installation factors over a varying fresh water flow feed and column diameter according to the above estimations is shown in figure I.1. There is a relatively small increase in cost with column diameter, but the costs mainly increase with a decrease in water feed flow rate. This is caused by the higher column height for those flow rates. To make an estimation of the levelized cost of water production the OPEX should be determined.

I.1. EQUIPMENT COST

This section includes the graphs with the individual component cost over varying water feed flow rate and column diameter for the 25 $m^3\ day^{-1}$ OTWP system. Since the air feed flow is fixed, the price of the fan units stays constant for the different water feeds and columns. This is similar for the HEX (fig. I.2a and I.2b). The fresh and sea water pump increase with flowrates. The seawater flowrate is calculated as the minimum flowrate needed to cool down the fresh water flow to 12 °C and depends both on the fresh water flow rate and the incoming water temperature. With in increase in water feed flow rate, the water exit flow temperature of the condenser is lower. The cost of the packing and column scale with an increase in volume.

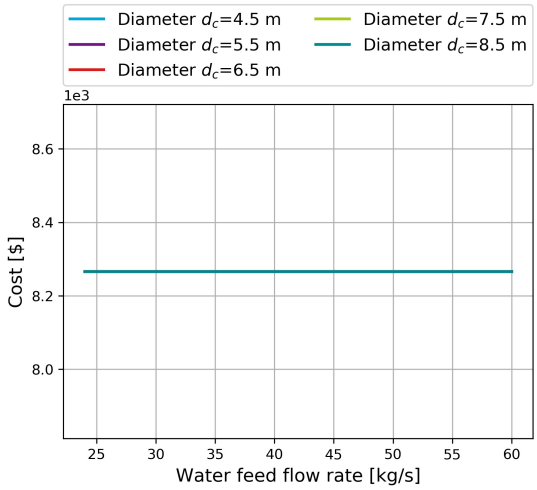

(a) Equipment cost of the fan

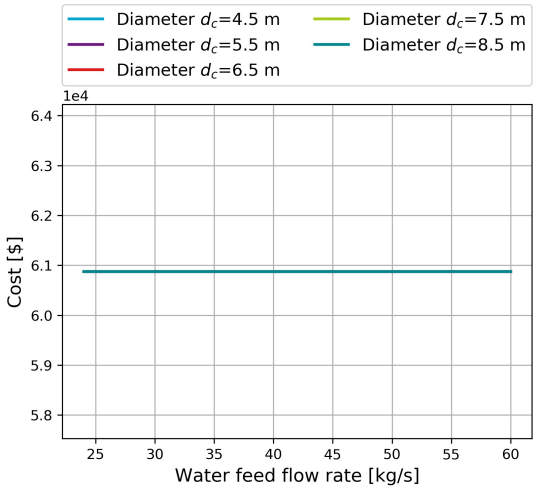

(b) Energy consumption of the fresh water pump

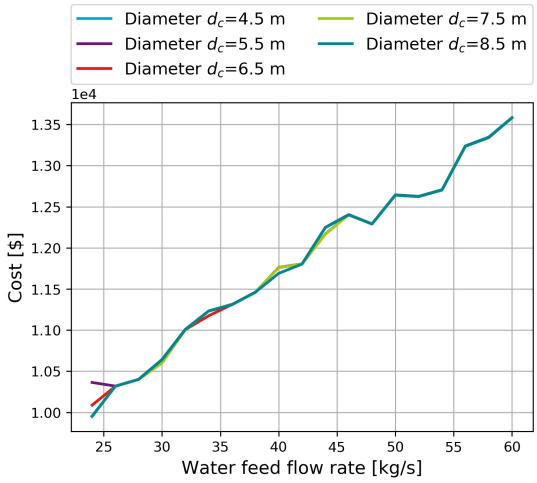

(c) Energy consumption of the sea water pump

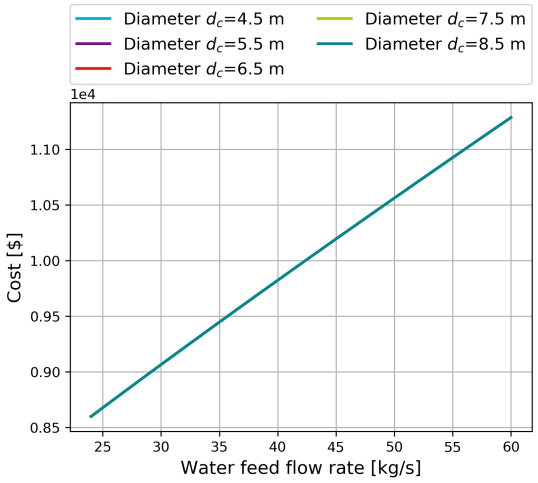

(d) Total OTWP pilot-plant Energy consumption

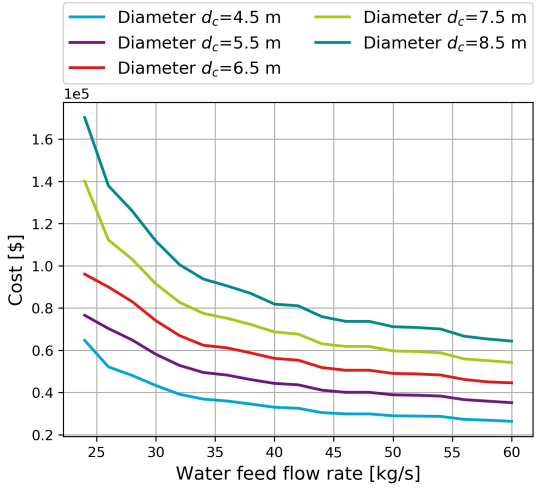

(e) Energy consumption of the sea water pump

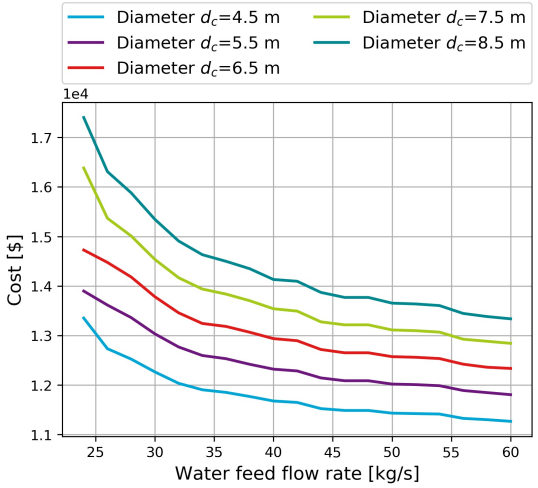

(f) Total OTWP pilot-plant Energy consumption

Figure I.2: Power requirement of the OTWP pilot-plant over water flow-rate and for varying column diameters

J

COSTS PILOT-PLANT DESIGN

This appendix present an overview of the cost devision of the preliminary pilot plant design. The energy requirement division is equal to the OPEX cost division (energy costs are the same).

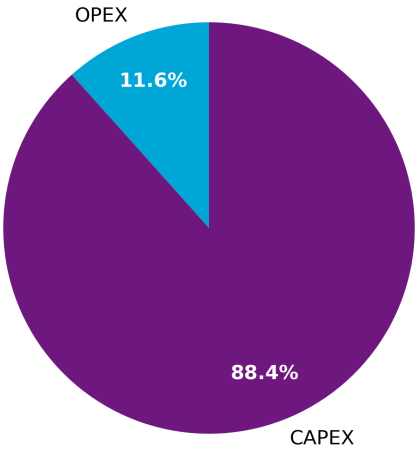

(a) The OPEX and CAPEX cost division according to installation factors by Towler and Sinnott [10]

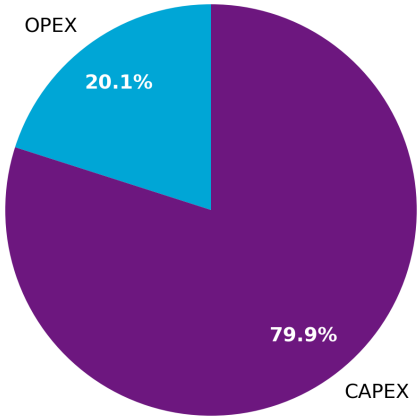

(b) The OPEX and CAPEX cost division according to installation factors by Couper *et al.* [70]

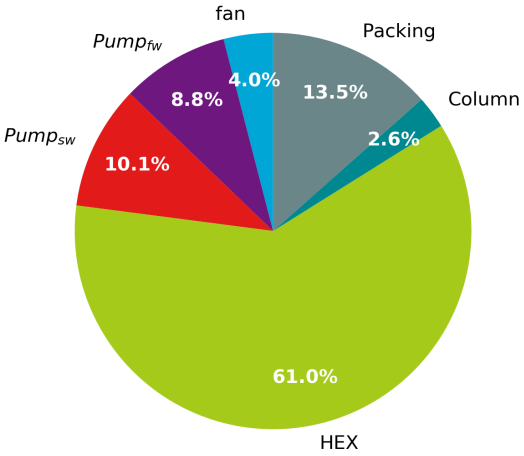

(c) The CAPEX cost division according to installation factors by Towler and Sinnott [10]

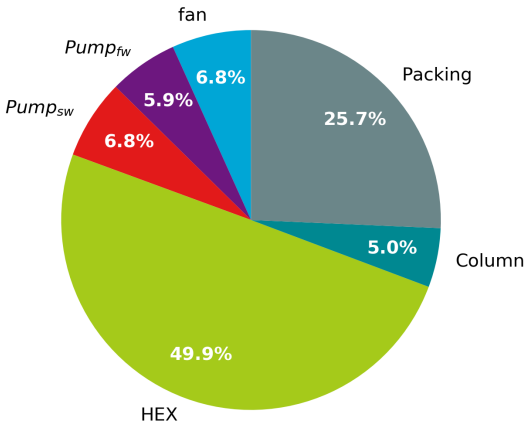

(d) The CAPEX cost division according to installation factors by Couper *et al.* [70]

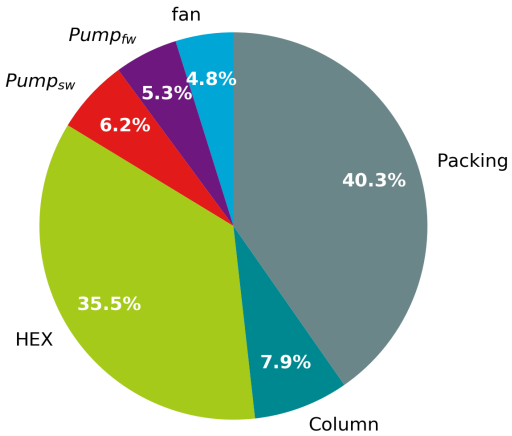

(e) The equipment cost division

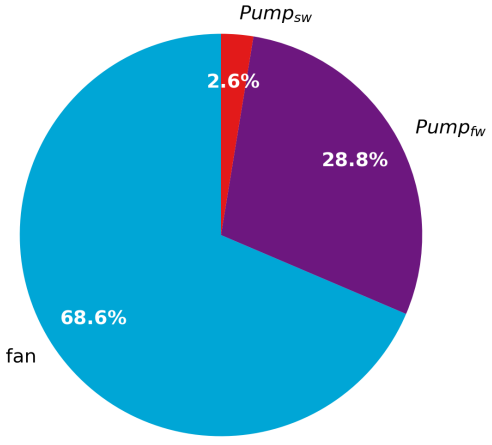

(f) The OPEX cost divisions

Figure J.1: Cost division of OTWP pilot-plant